Universiteit Utrecht

Master Thesis Robin Geitenbeek

Incorporation of Trivalent Lanthanide Ions in CdSe Semiconductor Nanocrystals

Supervisors:
Joren Eilers
Rosa Martín-Rodríguez
Andries Meijerink

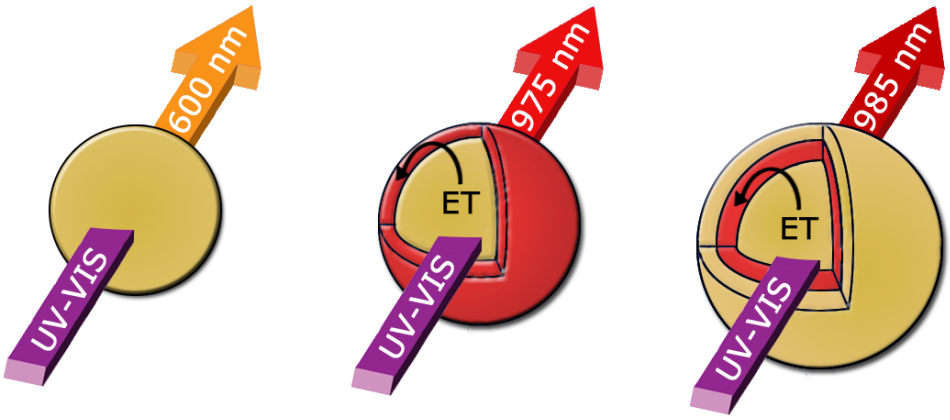

3253384
15th of June 2014
R.G.Geitenbeek@students.uu.nl
Condensed Matter and Interfaces

Contents

Chapter 1

Introduction

1.1 Nanomaterials

Nanoscience has been on the rise to a promising future since the scientific report of Michael Faraday on colloidal gold particles in 1857[1]. In 1959 well-known physicist Richard Feynman stated at a meeting of the American Physical Society: "There's plenty of room at the bottom". He was proven right since a lot of work has been performed to create creating novel and smart materials based on the manipulation of materials at the nanoscale and a lot is still being done. The quantum confinement effects and the higher surface to volume ratio result in the unique properties of nanomaterials. The advanced technology and knowledge of the present time is not only sufficient to create these materials but also to manipulate them at an atomic or molecular level making them suitable for a wide range of different applications. These range from (opto)electronics (*e.g.* nanophosphors and conducting nanoceramics), magnetic materials (*e.g.* materials with high coercivity for magnetic memories), energy storage and solar cells, medical applications to catalysis.

1.2 Doping

One of many different methods to modify these nanomaterials is by introducing impurities in a controlled fashion. Doping (semiconductors) bulk materials is well-established and very important. This results in the doping of bulk materials to be the inspiration to also dope nanomaterials. In this section the doping of both bulk and nanomaterials will be discussed. Due to the large effect doping can have on the properties of materials several examples will be given where the electronic, optical and magnetic properties were altered.

1.2.1 Altering the electronic properties

In solid state physics band theory states that the wave functions of electrons in a large periodic lattice causes certain ranges of energies to be allowed (bands) and certain energies to be forbidden (bandgaps) for electrons. From band theory the electric conductivity of a material can be predicted. If the highest occupied molecular orbital (HOMO) is only partially filled the electrons can move in a continuous range of energies, resulting in a high electron mobility and a high electric conductivity. However, if the HOMO is completely filled, there is a lack of electron mobility and these materials show low electric conductivities. The first material is defined as a metal while the latter is defined as an insulator. A semiconductor is a material with properties which lie in between that of a metal and an insulator. It has intermediate conductivity and this conductivity increases with increasing temperature. These properties originate in a completely filled valence band although a partially filled conduction band is achieved by having either a small bandgap (lower than 200 meV) or an impurity. Figure 1.1 (a) shows a band diagram of an intrinsic semiconductor in which the bandgap is lower than 200 meV. This bandgap can be overcome by thermal, optical or electrical excitation, resulting in a partially filled conduction band and metallic behaviour. Figure 1.1 (b) shows a band diagram of an extrensic semiconductor. In this material either an electron deficient dopant is introduced to create energy levels just above the valence band (p-type doping) or an electron rich dopant to create energy levels just below the conduction band (n-type doping). In the first case, electrons can migrate towards the electron deficient energy states of the dopant. In the latter case

the electrons of the dopant can be thermally excited to the conduction band. In both cases a partially filled conduction band is created resulting in metallic behaviour[2].

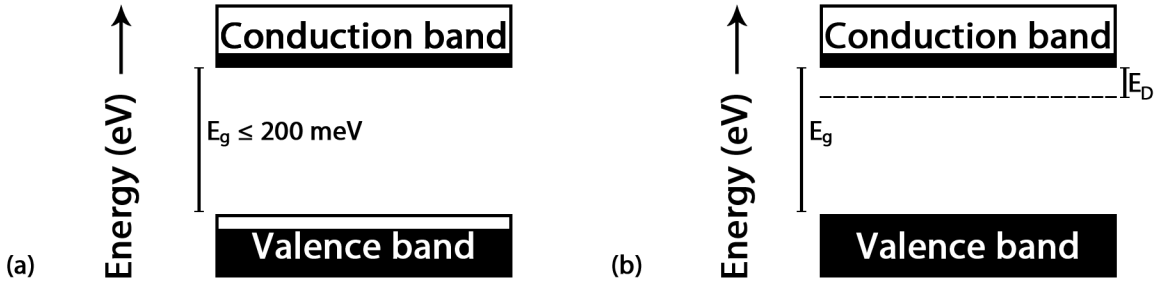

Figure 1.1: The two different kinds of semiconductors. On the left side, an intrinsic semiconductor is shown. On the right side, a n-type extrinsic semiconductor is shown.

1.2.2 Altering the optical properties

One of the most important properties of materials for (modern day) life is the way it interacts with light. The first thing God created after the Earth according to the Bible is light[3]. The doping of materials can have a significant effect on the optical properties of materials. Although the incorporation of impurity atoms in materials is a man-made invention, this phenomenon also occurs in nature, for instance in rubies. Rubies are minerals made from aluminium oxide (α-Al_2O_3) with 0.05% of chromium (Cr^{3+}) impurity. Even though the amount of Cr^{3+} is minute, the well known red colour of a ruby originates solely from this impurity[4].

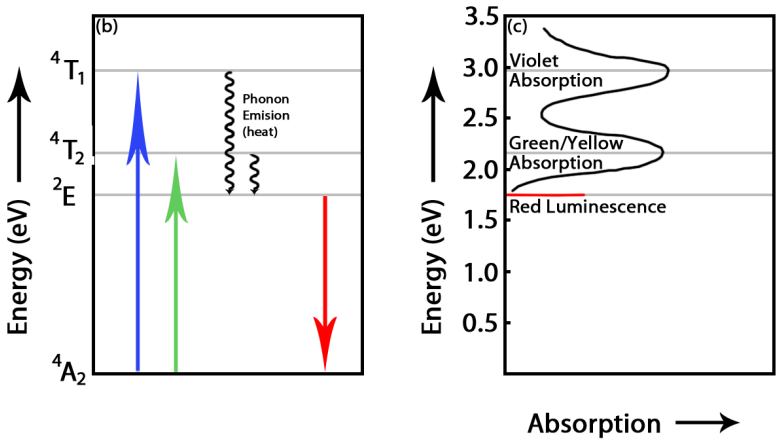

Figure 1.2: (a) The lowest four energy levels of Cr^{3+} in α-Al_2O_3. The ground state $^4A_2$ and 3 excited states at ca. 1.7 eV (^2E), 2.2 eV ($^4T_2$) and 3.0 eV ($^4T_1$). Due to these four energy levels absorption (blue $^4A_2 \rightarrow {}^4T_2$ and green $^4A_2 \rightarrow {}^4T_1$) can occur resulting in spin forbidden and parity forbidden red emission ($^2E \rightarrow {}^4A_2$).

Figure 1.2 shows the four lowest energy levels of a ruby on the left. From the $^4A_2$ ground state excitation is possible to two excited states ($^4T_2$) and ($^4T_1$), with transitions of of 2.2 eV and 3.0 eV respectively since the transition to the ^2E excited state is forbidden and weak (Figure 1.2b). From these states a fast non-radiative relaxation pathway is dominant towards the ^2E excited state by multi-phonon relaxation. From this energy level the dominant relaxation pathway is the long-lived emission of a photon with 1.7 eV. Figure 1.2 shows that the absorption of violet, green and yellow and the emission of red cause the ruby to appear bright red on the right. Due to the forbidden character of the $^2E \rightarrow {}^4A_2$ transition the system can be used to obtain population inversion and lasing[4].

1.2.3 Altering the magnetic properties

The magnetic properties of materials can be altered by adding paramagnetic dopants. In the case of CdTe nanocrystals doped with Mn^{2+}[5], a special phenomenon is observed. Figure 1.3 shows the scheme of light induced spontaneous magnetization of Mn^{2+}-doped nanocrystals.

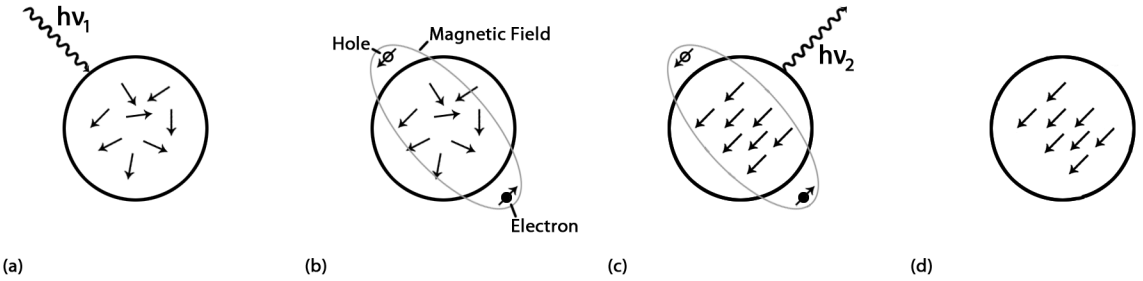

Figure 1.3: The light induced sponteneous magnetization of Mn^{2+} doped CdTe nanocrystals. First a photon creates an electron-hole pair (a), the electron and the hole have a certain spin creating a magnetic field in the quantum dot (b). The paramagnetic Mn^{2+} dopants react to the magnetic field, creating a excitonic magnetic polaron (c) resulting in the magnetization of the nanoparticle (d).

In this process of light induced spontaneous magnetization, a photon creates an exciton. This creates a local magnetic field which influences the Mn^{2+} dopants due to their paramagnetic properties. The magnetization effect is dominated by the hole, due to the localisation of the electron as a result of trap states. As a result of the spontaneous alignment of the paramagnetic ions the exciton can lower it's energy consequently, the emitted photon will have a lower energy than the photon used to excite the system ($h\nu_1 > h\nu_2$).

1.3 Applications of doped semiconductor nanocrystals

By exploiting the combination of the size-dependent and doping-dependent properties good properties control is achieved. The combination of doping and size-dependent properties gives rise to a whole new range of possibilities. A small selection of these applications will be discussed below.

1.3.1 Photovoltaics

Over the years a lot of research has been done on optimizing silicon based photovoltaic modules. Although a lot of improvements are still being developed, there is a intrinsic problem which must be solved using other materials than silicon. Figure 1.4 shows the solar emission spectrum and the (double) silicon band gap. Since silicon can only absorb light of certain energies (up to ca. 1100 nm) all light with a lower energy ($>$ 1100 nm) will pass through the solar panels without being absorbed and converted into usable energy. On the other hand all light with energies higher than the double silicon band gap ($<$ 550 nm) have sufficient energy to provide two excitons for charge separation in the solar cell. This extra energy will be lost as heat if no material is present that can 'cut' the photon in two photons of lower energy[6].

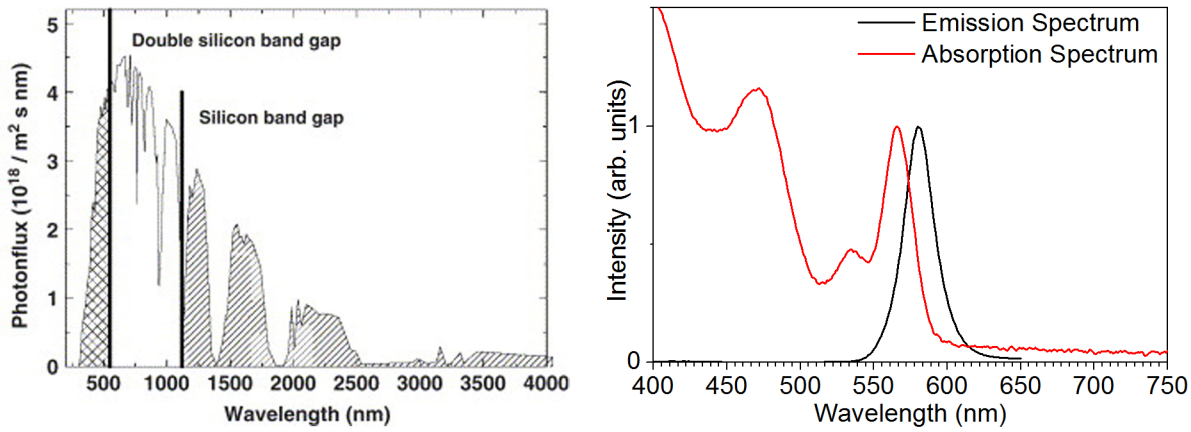

Figure 1.4: The solar emission spectrum and the position of the silicon band gap (left) and the typical emission (black) and absorption (red) spectra of CdSe nanocrystals (right).

By converting multiple lower energy photons into sufficient energy photons (upconversion) or by converting higher energy photons in multiple lower energy photons (downconversion), a higher efficiency of solar panels can be obtained.

Due to the ability of these so called 'quantum dots' (QDs) to absorb a wide range of energies and emitting this absorbed energy in a relatively narrow range (Figure 1.4, right), doped QDs can be used as efficient methods for the manipulation of light.

1.3.2 Bio-imaging

Since manipulation of light is an important part of this thesis the second example will also treat this phenomenon. A lot of different techniques to image (in vivo) cells and biological processes are available. The unique optical properties of QDs and the versatility of the different ligands able to passivate and functionalize the surface of the QDs make these materials highly promising for optical imaging techniques. Figure 1.5 shows a schematic of the current surface coating techniques that allow QDs to be incorporated in biological systems and allow for biorecognition[7].

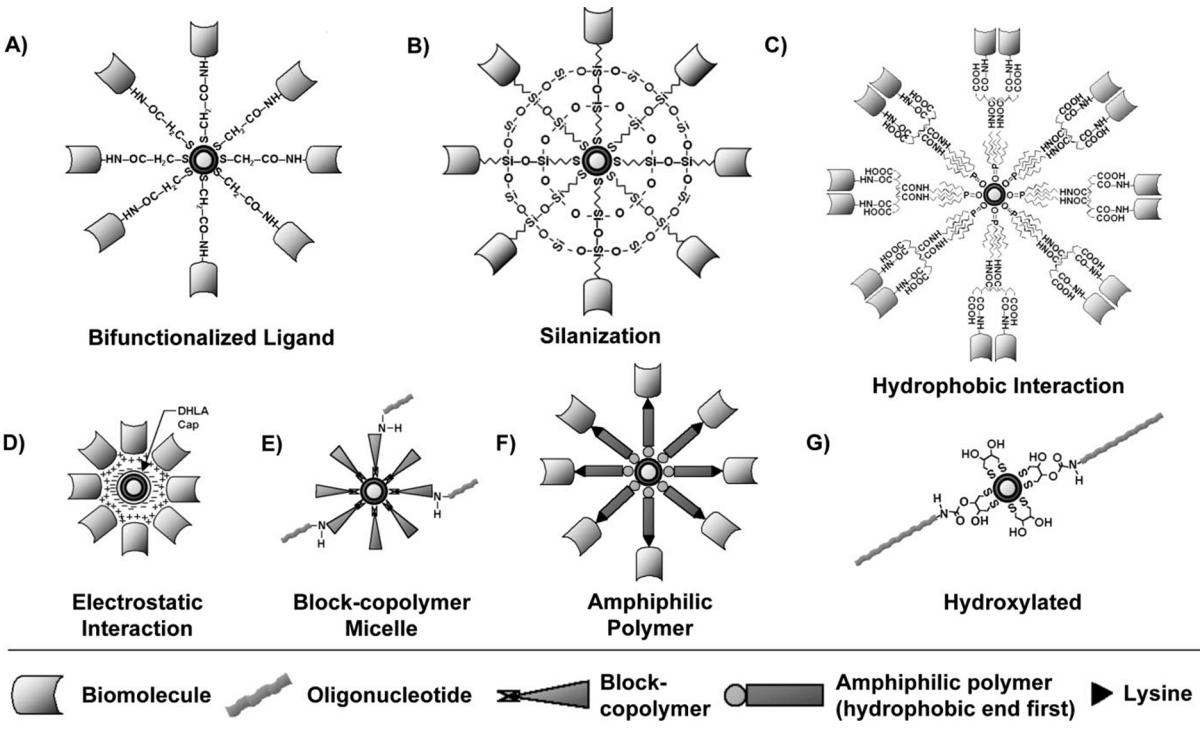

Figure 1.5: Overview of the available ligands for compatability of QDs in biological systems and biorecognition.

The semiconductor bandgap increases with decreasing particle size due to quantum confinement effects, thus, the optical properties of the quantum dots, *i.e.* absorption and emission wavelength, can be controlled by modifying the size of the quantum dots. Quantum dots have a strong potential as fluorophores due to the broad absorption spectrum which overlaps for different sizes of quantum dots, resulting in different emission maxima[8].

1.4 Goal of thesis

Lanthanide ions are usually incorporated into insulator nanocrystals, especially fluorides and phosphates, where Ln^{3+} ions substitute for chemically related rare earth ions. In these insulator nanocrystals the functionalities are solely determined by the lanthanide dopants. For optical applications the efficient line emission of lanthanide ions can be utilized, but a drawback is the weak and narrow band absorption lines, due to the parity forbidden character of the 4f-4f transitions. This limits applications where strong absorption is required.

Incorporation of lanthanide ions in QDs offers the possibility to combine the strong and size-tunable absorption of QDs with the efficient narrow line emission of lanthanide ions in the visible or infrared. It has however been a challenge to incorporate lanthanide ions in II-VI QDs. Although work has been published it is not clear whether the rare earths are incorporated and no energy transfer has been observed.

The scope of this thesis is to synthesize lanthanide doped II-VI nanocrystals and investigate and optimize the energy transfer in these systems. Due to the extensive work performed on CdSe QDs a lot is know about these nanocrystals and the synthesis is well understood. For this reason CdSe QDs will be used in this thesis. To synthesize the Ln^{3+}-doped CdSe QDs, a three step growth doping method was developed. In the first step the quantum dots are synthesized. In the second step the lanthanide is adsorbed on the quantum dot surface followed by the growth of a selenium shell incorporating the Ln^{3+} into the CdSe quantum dot.

The choice of dopant is made by considering the energy level schemes of the lanthanides. Due to the simplicity of the Yb^{3+} electron configuration only two energy levels are present for Yb^{3+} which have a spacing of ca. 1000 nm. Transitions with this energy are sufficiently red-shifted from the excitonic transitions of the CdSe nanocrystals which ranges from 500-650 nm depending on the size of the nanocrystals. Due to the simplicity and separation of the energy levels this system will be ideal for investigating energy transfer behaviour.

To investigate these systems a large variety of analytical tools will be used. Using (high resolution) transmission electron micropscopy ((HR)TEM) and electron diffractive X-ray spectroscopy (EDX) the size, shape and polydispersity can be investigated as well as the composition of the nanocrystals. Using absorption spectroscopy and photoluminescence spectroscopy the optical properties of the materials can be investigated, including the emission of the quantum dots in the visible and infrared section of the spectrum and the lifetime of these emissions. Using the data acquired with these techniques a model will be constructed to explain the system and the observed phenomena.

Chapter 2

Theory

Nanocrystals have been investigated extensively in the past decades and a lot is know about the doping of these materials. However, semiconductor nanocrystals are usually doped with 3d transition metals like Mn^{2+} or Co^{2+}. Although many reports have shown to incorporate lanthanide dopants into insulator nanocrystals like fluorides and phospates, it remains challenging to incorporate lanthanides in semiconductor nanocrystals. In this chapter a more in-depth explanation of relevant concepts will be treated. An explanation of what quantum dots are and how they are made will be given, followed by an explanation of lanthanides. Due to the energy levels associated with both nanocrystal host and lanthanide dopant, energy transfer can occur. This phenomenon will also be discussed in this chapter.

2.1 Quantum dots

Semiconductor nanoparticles show quantum confinement effects when the size approaches the Bohr radius of the exciton, as a result of spatial confinement of the electron and hole in the nanoparticles. As a result, the bandgap increases and the energy bands transform into discrete energy levels. When there is no quantum confinement the 3D material has bulk properties. If a system is confined in 1 dimension the resulting particles (platelets or sheets[9]) are a 2D material. If a system is confined in 2 dimensions the resulting particles (rods[10],[11]) are a 1D material. This thesis will use 0D materials, quantum dots, which are confined in all three dimensions. These materials can be synthesized with many different chemical compounds (*e.g.* CdSe, CdTe, CdS, ZnS and GaAs). More complex structures are possible as will be discussed later. Also more complex structures are possible to prepare, as will be discussed later.

2.1.1 Quantum confinement

Nanocrystals, materials which are confined in one, two or three dimensions, display different properties than bulk materials. To explain the different behaviour due to quantum confinement two different approaches will be discussed, the more chemical bottom-up approach and the more physical top-down approach.

Top-down approach

When a materials gets smaller and smaller the electron-hole pair (exciton) will become spatially confined. This can be understood by evaluating the de Broglie wave-particle duality for electrons and holes (equation 2.1) and by using the relation between the linear momentum, p, and the kinetic energy, E.

$$\lambda_e = \frac{h}{p} = \frac{h}{\sqrt{2m_e^* E}} \tag{2.1}$$

Due to the confinement of the wavefunction in smaller particles the system behaves analogously to the particle-in-a-box model. In this model the general solution of the wavefunction is determined by the boundary conditions as shown in equation 2.2. These are that the intensity of the wavefunction should be 0 at the boundaries of the box ($x = 0$ and $x = \mathrm{a}$) due to standing waves.

$$\Phi(x) = \mathrm{A}sin(kx) + \mathrm{B}cos(k) \qquad \Phi_n(x) = \mathrm{A}sin(k_n x), \text{where } K_n = \frac{n\pi}{\mathrm{a}} \tag{2.2}$$

Using the relation between the energy and the wavevector k_n (equation 2.3) we find that the system is quantized, giving rise to discrete energy levels. Furthermore, by decreasing the size of the box, or in this case the particle radius, the energy level difference increases.

$$E = \frac{\hbar^2 k^2}{2m} = \frac{n^2 h^2}{8ma^2} \tag{2.3}$$

More accurately, the group of Brus[12],[13] has performed ground breaking work on the investigation of these quantum confinement effects in CdS, ZnO, GaAs and InSb. By investigating the size dependent properties Brus has proposed a model based on the particle in a sphere model, which is similar to the particle in a box model shown above. This proposed model approximates the lowest excited state energy E as shown in equation 2.4.

$$E = E_g + \frac{\hbar^2 \pi^2}{2r^2}\left[\frac{1}{m_e} + \frac{1}{m_h}\right] - \frac{1.8e^2}{\epsilon_2 r} + \text{smaller terms} \tag{2.4}$$

In this equation the first term (E_g) is the bulk band gap at 0 °C, r is the radius of the box (in this case the particle radius), ϵ_2 is the semiconductor high frequency dielectric coefficient and the m_e and m_h are the effective masses of the electron and hole respectively. The second term originates from the spatial localization of the electron and hole, varying with r^{-2}. The third term originates from the size dependent Coulomb attraction, varying with r^{-1}. For sufficient low r (*i.e.* the quantum confinement regime), the spatial localization term dominates the offset from the bulk band gap.

These results also explain the strong quantum confinement effects for the semiconductors. Since the materials have strong chemical bonds between individual molecular units, the materials have a strong tendency to delocalize electrons involved in the bonding. This delocalization results in a very small effective mass, which in turn results in high offsets from the E_g.

The tunability of the bandgap by varying the size of the particles is a large advantage in the control of the optical properties. In semiconductor nanocrystals the bandgap is in the order of several eV, resulting in an energy difference which leads to absorption and emission of visible light. A well known example of the tunability of the colours of semiconductor nanocrystals is CdSe, which is shown in Figure 2.1[14]. A rule of thumb is that quantum confinement in the semiconductors occurs if the particle size is less than four times the exciton bohr radius.

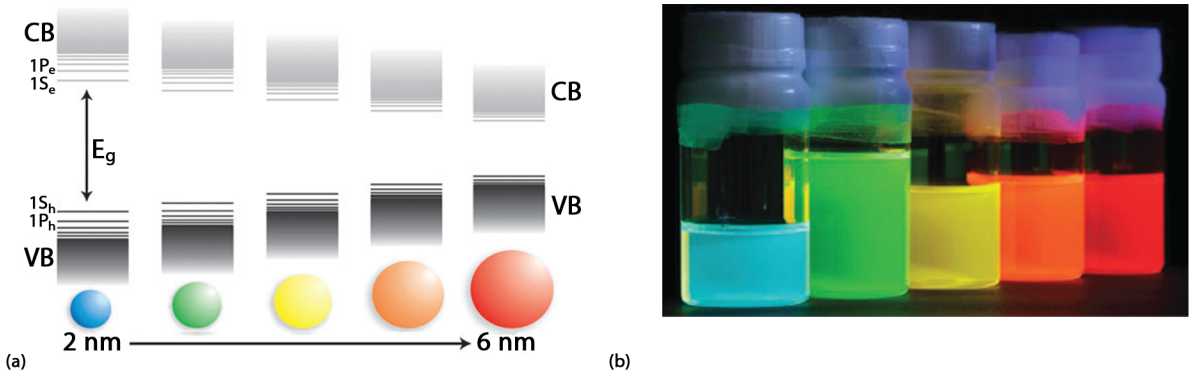

Figure 2.1: The effect of quantum confinement on the bandgap of CdSe (left) and the resulting colours of the dispersions (right).

When the spatial confinement of materials becomes comparable to the length scales of certain physical phenomena the properties can drastically change, but quantum confinement is not limited to the optical properties of materials. For instance, when the size of bulk gold is decreased (1-2 nm) a whole range of properties are altered; the melting temperature decreases, the material loses it's noble character, becomes red and turns magnetic[15].

Bottom-up approach

The phenomenon of bands and bandgaps in solids can also be explained by the bottom-up approach. The basis of this approach is molecular orbital theory. When two atoms approach each other they can reduce the internal energy by forming a bond and create a more stable molecule. This is shown in Figure 2.2 on the left for two hydrogen atoms and a hydrogen molecule.

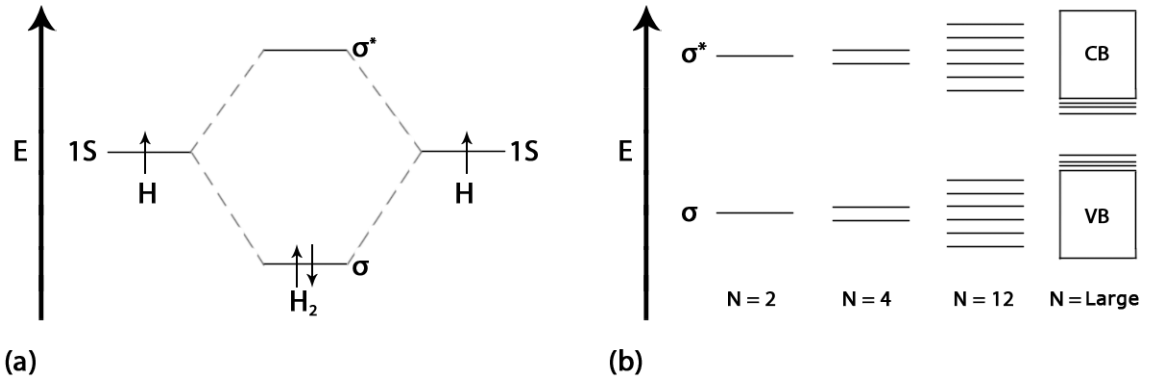

Figure 2.2: The molecular orbital diagram of hydrogen (a) and the bottom-up approach to bands (b).

More generally, quantum physics dictates that N atomic orbitals will form N molecular orbitals (MOs). In this case two sigma bonds will be created (one bonding σ and one antibonding σ^*) and the electrons will be go to the lowest energy orbital: the bonding MO (*i.e.* a bond is formed). In the case of Helium, four electrons need to be divided into the same molecular orbitals. The two bonding electrons reduce the energy of the system, resulting in a more stable particle. However the two antibonding electrons have a higher energy, resulting in a molecule with more energy than the separate atoms. This means that no bond is formed (unlike H, which forms H_2, He is stable).

In the case of larger molecules (larger N) more molecular orbitals are formed. This results in more energy levels and at a certain point these molecular orbitals will grow into two quasi-continuous bands with several discrete energy levels in between as shown in Figure 2.2 on the right. These bands are called the valence band (VB) and the conduction band (CB) and they find their origin in the (highest occupied and lowest unoccupied) bonding and antibonding atomic orbitals. When more atoms are incorporated in the material the CB and the VB will become larger and the gap between these two bands will decrease, resulting in the same confinement effects as described in Figure 2.1.

2.1.2 Size dependence of E_g

Due to the correlation between the size of the nanoparticles and the energy difference between the CB and VB (E_g) the size of the particles can be extracted from the position of the first excitonic peak in the absorption spectrum. In the photoluminscence measurements an ensemble of quantum dots is measured. Different sizes of nanoparticles give rise to emission at different wavelengths, resulting in a broader emission peak for more polydisperse samples.

By analysing data reported in literature Yu and coworkers[16] have made a calibration curve for the relation between the particle size and the absorption maximum of the first excitonic transition. This has been done for CdSe, CdS and CdTe. The formula for the calibration curve in the case of CdSe QDs is shown in equation 2.5

$$D = 1.6122 * 10^{-9} * \lambda^4 - 2.6575 * 10^{-6} * \lambda^3 + 1.6242 * 10^{-3}\lambda^2 - 0.4277 * \lambda + 41.57 \tag{2.5}$$

Where D and λ are in nm and λ is the wavelength of the maximum of the first excitonic absorption peak of the corresponding sample. By using atomic absorption measurements to find the amount of cadmium ions, the amount of nanocrystals could be obtained by dividing the amount of cadmium ions in the sample by the amount of cadmium ions in one nanoparticle. By combining the concentration of the sample, the absorbance of the sample and Lambert-Beer's law the extinction coefficient can be obtained, which is dependent on the diameter of the particles as shown in equation 2.6.

$$\epsilon = 5857 D^{2.65} \tag{2.6}$$

Using the extinction coefficient and the intensity from the absorption spectrum the concentration of the nanoparticles can be calculated. The concentrations and diameters can later be used for further experimentation.

2.1.3 Crystal structure

The size of an atom or ion is determined by the Coulombic interactions between the positive nucleus and the electron cloud. Since electrons can screen the positive charge of the nucleus elements the radius will decrease with increasing group number. In the case of cations a more positive charge has a stronger Coulombic interaction with the electrons, pulling the electrons to the nucleus, decreasing the size. Due to the larger size of anions, the lattice structure is dominated by the anions. The cations will be located at interstitial positions between the anions in the lattice. It is found that II-VI semiconductors crystallize in either the zinc blende or wurtzite crystal structure. The chemical compounds used in the semiconductor determine which lattice is thermodynamically more stable. For instance CdSe has the Wurtzite lattice as the most thermodynamic stable phase at 300 K[17], while Zinc Blende is the most stable lattice for CdTe at 300 K. Although these lattices are the most thermodynamically stable, certain approaches during synthesis may result in the alternative lattice[18].

2.1.4 Complex nanomaterials

Extensive research in past few decades have led to control over the synthesis of spherical quantum dots, but also many more shapes of semiconductor nanocrystals, like platelets (or sheets), rods (or wires), tetrapods and dumbbells[19],[20],[21]. By varying the shape, size or composition of nanoparticles the properties of materials can be changed significantly. Another method of varying the properties of these particles is to create heteronanoparticles.

Heteronanocrystals, nanocrystals made of two, or more different crystals can alter the properties of nanomaterials drastically. This can be done by either a (homogeneous/gradient) alloy or core/shell system[22] of quantum dots with a uniform shell, but also dots in rods[20],[23] or even core/shell/shell particles[24]. Due to the multiple constituents in the heteronanocrystals there are also multiple bands (and E_g) present in the system. Figure 2.3 (left) shows the energy of the electronic band edges relative to the vacuum level of several bulk materials.

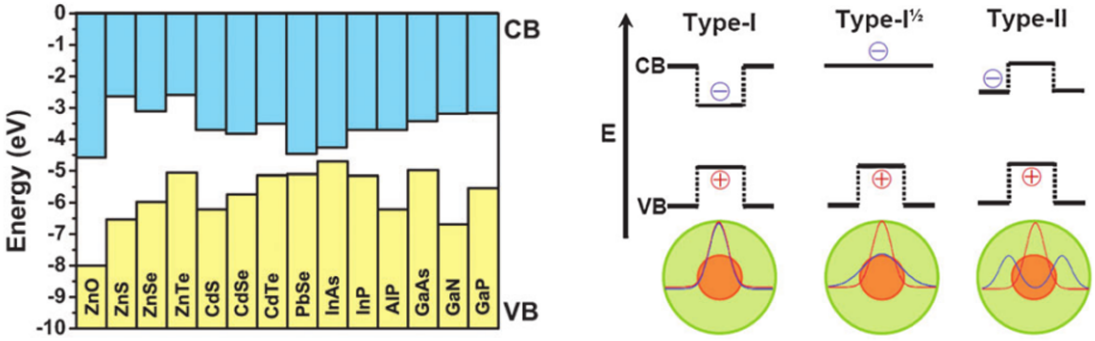

Figure 2.3: The energy of the electronic band edges relative to the vacuum level (a) and the different types of heteronanocrystals (b).

Due to the different bandgaps different combinations of constituents can result in three different types of nanocrystals. Figure 2.3 (right) shows the three different cases for heteronanocrystals. Type-I (left) QDs have a localized exciton, both electron and hole are confined in the same part of the heteronanocrystal (core or shell). Type-$I^{1/2}$ (middle) QDs have a localized carrier (either electron or hole) and a delocalized carrier. Type-II (right) QDs have a localized carrier in either the core or the shell and the other carrier is located in the opposite part of the heteronanocrystal. Even though the carriers can be confined to a certain part of the heteronanocrystal, the energy difference between the different parts is finite and thus there will be some exciton leakage into the other parts of the heteronanocrystal.

2.2 Synthesis of nanocrystals

A multitude of different methods to create nanocrystals have been developed. These techniques can be divided into two different types of approaches. The first method of creating nanoparticles is by starting with a bulkmaterial and reduce the size in a controlled fashion (*e.g.* lithography). Another method is to start from molecular or atomic building blocks and create ordered structures via colloidal chemistry methods.

2.2.1 Wet synthesis

By starting from atomic or molecular level, a whole range of different nanoparticles can be obtained. Due to the large control over synthesis using coordinating and stabilizing ligands it is possible to synthesize nanomaterials from atomic/molecular precursors in a solution. This can be done by adding all materials used for the synthesis (precursors, coordinating and stabilizing ligands) to a (coordinating) solvent and slowly heating up the mixture (heating up method) or by adding one (or both) of the precursors to a heated mixture of the other precursor in coordinating and stabilizing ligands (hot injection method). Both methods are designed to have a small burst of nucleation and a subsequent growth phase.

2.2.2 Nucleation and Growth

Nucleation occurs when a new stable phase is started inside an existing phase (for instance crystalline solids inside a liquid or condensation in a saturated gas phase)[25]. In most cases the newly created phase needs to have a certain size before it is stable. This is due to two opposing energies which are linked to this phenomenon (Equation 2.7).

$$\Delta G = \Delta G_{surface} + \Delta G_{bulk} \tag{2.7}$$

The creation of crystals is energetically favourable due to the enthalpic energy win (Equation 2.8). In this formula ΔG_{Bulk} is the Gibbs free energy for creating a crystalline material, r is the radius of the particle and $\frac{S}{S_0}$ is the saturation ratio. The saturation ratio is the concentration of monomer molecules divided by the concentration of monomer molecules at saturation equilibrium.

$$\Delta G_{bulk} = -\frac{\frac{4}{3}\pi r^3}{v_0} kTln(\frac{S}{S_0}) \tag{2.8}$$

However, the creation of a surface between the particles and the solvent is energetically unfavourable (Equation 2.9). Here, the $\Delta G_{surface}$ is the Gibbs free energy for the creation of a surface and γ is the surface tension.

$$\Delta G_{surface} = 4\pi r^2 \gamma \tag{2.9}$$

When these two formula are combined (Equation 2.10) the Gibbs free energy at low r will be dominated by the surface term ($\Delta G \propto r^2$) and will be dominated by the bulk term at higher r ($\Delta G \propto r^3$). At a certain point the energy barrier will be highest and both terms will contribute equally to the total Gibbs free energy ($\frac{dG}{dr} = 0$). This is called the critical point and it is the smallest size needed for the new phase to become stable (Figure 2.4).

$$\Delta G = 4\pi r^2 \gamma - \frac{\frac{4}{3}\pi r^3}{v_0} kTln(\frac{S}{S_0}) \tag{2.10}$$

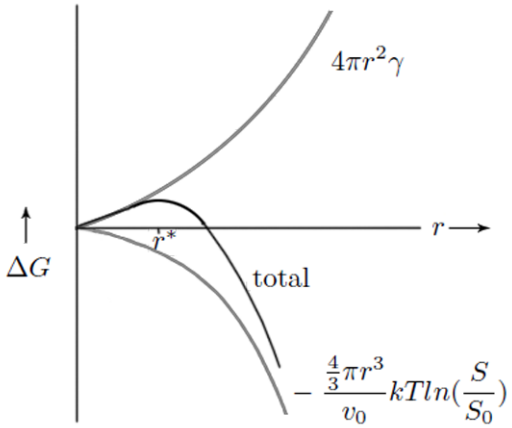

Figure 2.4: The Gibbs free energy plotted versus the radius of the new phase, the critical radius is denoted as r*.

When nucleation and growth occur simultaneously, particles will be in different stages of the growth resulting in a polydisperse sample. To create monodisperse quantum dots nucleation and growth should take place in two separate steps. In the hot injection method, a precursor is added to create a short burst of super saturation and high temperature in which nuclei with a critical radius or larger will be formed. Due to an immediate temperature drop and the quick drop in concentration the saturation level is no longer maintained and the growth phase will occur. Due to the short interval of nucleation all nuclei will be in the same size regime since the growth during the nucleation phase is minimized resulting in monodisperse particles.

2.2.3 Ligands

Research has shown that a key aspect of the nanocrystals with respect to the optical properties and the colloidal stability is the surface. A stabilizing force (*e.g.* Coulombic repulsion or steric repulsion) is needed to keep the particles from aggregating due to attractive van der Waals forces. To optimize the optical properties of quantum dots the particle surface should be passivated to reduce the number of surface states which reduce the quantum efficieny of the nanoparticles.

Both the surface passivation and the stabilization of the particles can be obtained by combining inorganic quantum dots with organic ligands. The organic ligands combine a polar headgroup (*e.g.* amines, thiols, phosphines) with an apolar hydrocarbon tail. 1-octadecene (ODE) is a non-coordinating solvent but the capping ligands trioctylphosphine (TOP) and trioctylphosphine oxide (TOPO) and the oleate of the cadmium precursor do play an important role[26] in the control over the synthesis. By binding to the nanocrystals the ligands hinder particle-particle aggregation and may also influence monomer deposition, resulting in control over the size and shape of the nanoparticles by the choice of ligands.

2.3 Lanthanides

Extensive research has yielded a wide selection of dopants for the incorporation into nanocrystals. Recent studies have shown to succesfully dope nanocrystals with Mn^{2+}[27], Co^{2+}[28], Sn^{2+} and In^{3+}[29] among others and also a new set of dopants is getting more and more attention: the lanthanides. By combining insulator nanoparticles with lanthanides a low-phonon energy lattice is created which protects the lanthanides from multip-phonon coupling. Due to this large advantage the incorporation of lanthanides in insulator nanoparticles has been studied extensively, although the low extinction cross section of the lanthanides remains a major disadvantage. By combining the lanthanides with semiconductor nanoparticles the quantum dots can not only act as a low-phonon protective environment but also as an indirect excitation source via energy transfer. In this fashion the advantages of the quantum dots (high excitation cross section, size tunable absorption) can be combined with sharp emission peaks with long lifetimes characteristic for the lanthanides. Although recent reports have shown the incorporation of Eu^{3+} and Tb^{3+}[30][31][32] into II-IV semiconductor nanocrystals, the incorporation remains problematic due to the higher coordination number and charge compensation required for the trivalent lanthanides. In this work it was chosen to use ytterbium, since trivalent ytterbium only has two energy states at low energies and the transition is sufficiently red-shifted from the CdSe QD bandgap energy.

2.3.1 Lanthanides

Trivalent lanthanides are ions with a partially filled f-orbital and the main characteristics of these materials are derived from this fact. For instance the f-orbitals are well shielded from the environment due to the fact that the 5s and 5p orbitals extend further outside than the 4f-orbitals. They are chemically similar because the interacting orbitals are the same. The occupation of the f-shell changes but the f-electrons do not, as stated, interact (significantly) with the other ions and do not form bonds. This results in similar f-f transitions of lanthanides for different host materials (as opposed to f-d transitions in lanthanides and d-d transitions in transition metals). From a spectroscopic point of view the f-f transitions are Laporte forbidden resulting in materials with a low excitation crosssection with (relatively) long lifetime emissions.

2.3.2 Energy levels of lanthanides

Configuring the electrons of atoms or ions, including the lanthanides, in the available orbitals gives rise to different energy levels. These energy levels are defined with term symbols. In general, term symbols used for the different energy levels are defined as $^{2S+1}$L. Where S is the spin quantum number and L is the azimuthal quantum number (S,P,D,F... for $L = 1, 2, 3, 4...$). The configuration which is lowest in energy can be found by applying Hund's rules, where first S is maximized and then L. For instance the ground state of a molecule with the electron configuration $1s^2 2s^2 2p^2$ (carbon) is the configuration where the two electrons of the p-orbital are parallel (maximized S) and where the azimuthal quantum number equals +1. This means that the term symbol for this electron configuration is ^{3}P ($=^{(2*(\frac{1}{2}+\frac{1}{2})+1}$L and $L = 1$ equals P).

The term symbols for the heavier elements, like the lanthanides, are less straightforward due to spin-orbit coupling. For these elements a new quantum number needs to be introduced, J. The total angular momentum quantum number J is defined as all the integers between |L+S| and |L-S|. The new notation in term symbols is $^{2S+1}$L$_J$ and Hund's rules still apply to determine the ground state but now also J needs to be maximized for configurations in which the orbitals are filled with less than 7 electrons. In the case of 7 or more electrons the J-value needs to be maximized.

In the case of Yb^{3+} ($1s^2 2s^2 2p^6 3s^2 3p^6 4s^2 3d^{10} 5p^6 4f^{13}$) the f-orbital is filled with 13 electrons, which means that the maximum spin quantum number is $\frac{1}{2}$ (7 up spins and 6 down spins) and the maximum azimuthal quantum number is 3 ($= 3+3+2+2+1+1+0+0-1-1-2-2-3$). From these values the different values of J can be calculated, which are 7/2 and 5/2. If the lanthanide has 7 or more electrons in the f-orbital the ground state is the term symbol with the lowest J-value. Since ytterbium has more then 7 (13) electrons, the ground state is ^{2}F$_{7/2}$ and the first excited state is ^{2}F$_{5/2}$. For cerium, which has 1 electron, the energy states are the same although the ground state has a maximized J-value, resulting in the ^{2}F$_{5/2}$ ground state and the ^{2}F$_{7/2}$ excited state.

The case of Er^{3+} is less straightforward. Er^{3+} has eleven electrons which can be distributed between the 7 f-orbitals in 364 ($= \binom{14}{11}$) different manners. All different distributions can be written down for these electrons, but a lot of the corresponding energies will be degenerate. To confirm the different term symbols for the energy states, all these configurations should be evaluated and tabulated according to the m$_l$ and m$_s$ values as shown in Table 2.1 for Er^{3+}.

m$_s$\m$_l$	-8	-7	-6	-5	-4	-3	-2	-1	0	1	2	3	4	5	6	7	8
$+\frac{3}{2}$	0	0	1	1	2	3	4	4	5	4	4	3	2	1	1	0	0
$+\frac{1}{2}$	1	2	4	6	9	12	15	16	17	16	15	12	9	6	4	2	1
$-\frac{1}{2}$	1	2	4	6	9	12	15	16	17	16	15	12	9	6	4	2	1
$-\frac{3}{2}$	0	0	1	1	2	3	4	4	5	4	4	3	2	1	1	0	0

Table 2.1: A table with all different combinations of m$_l$ and m$_s$ for the electron configurations of Er^{3+}.

Note that the total amount of combinations in Table 2.1 is 364. Due to the high degree of degeneracy of the energy states, the table can be written as the summation of tables where all values are equal to 1. In this fashion new tables arise which have varying m$_l$ and m$_s$ values. These values represent the different term symbols for the energy states. In this case the term symbols become ^{2}L$_J$ (m$_s = \frac{1}{2}$ and m$_l = 8$), ^{4}G$_J$ (m$_s = \frac{3}{2}$ and m$_l = 4$), ^{2}K$_J$, ^{4}L$_J$, ^{4}I$_J$, ^{4}F$_J$, ^{4}D$_J$, ^{4}S$_J$, ^{2}I$_J$, ^{2}H$_J$, ^{2}G$_J$, ^{2}F$_J$, ^{2}D$_J$ and ^{2}P$_J$. The ground state can be determined again by applying Hund's rules and in this case the ^{4}I$_{15/2}$ will be lowest energy state. Following the same procedure the energy levels for thulium, europium and all other lanthanides can be found. Figure 2.5 shows the energy levels (up to 40,000 cm^{-1}) of all different lanthanides with respect to the ground state in $LaCl_3$.

The fact that the 5s and 5p orbitals extend further outwards than the 4f orbitals gives rise to a minimal response of the energy states of the lanthanide to the environment. This results in narrow absorption/emission lines for the f-f transitions which are lattice-independent. The crystal field splitting is also much lower than the spin-orbit coupling, which is indicated by the width of the energy states. Comparing cerium and ytterbium it is clear that the spin-orbit coupling increases with the atomic number.

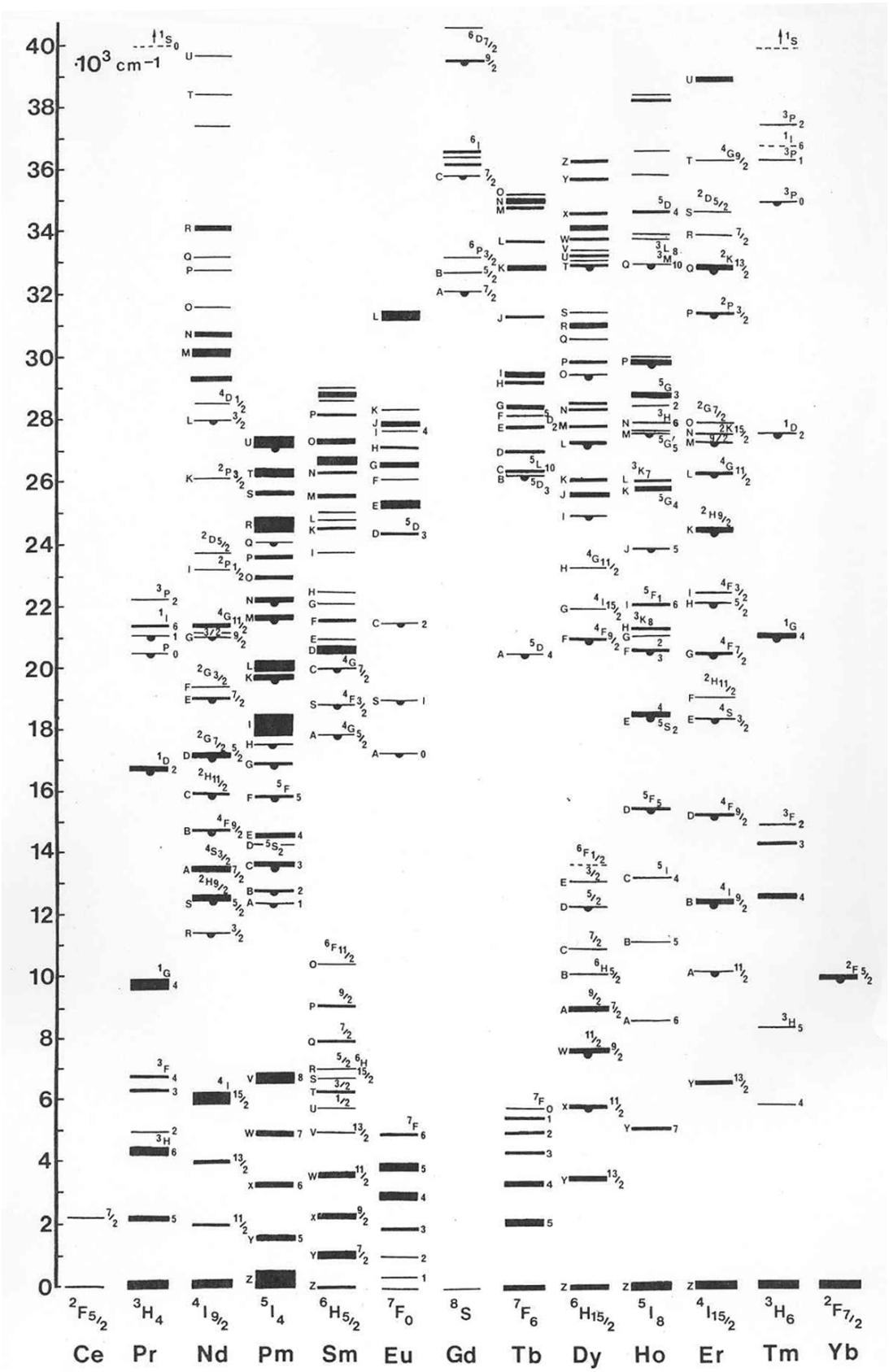

Figure 2.5: The Dieke diagram with all different energy levels (up to 40,000 cm^{-1}) of the lanthanides in $LaCl_3$.

2.4 Nanocrystal doping

As already mentioned in the introduction of this thesis, doping can have a large effect by introducing new properties of (nano)materials. Several different methods are known to successfully incorporate impurity ions into nanostructures as will be explained below.

2.4.1 Doping strategies

A new method for doping which is acquiring a lot of attention nowadays is cation exchange[33]. Due to the large anions a lattice consists of rigid anions with more mobile cations which can migrate through the crystal. By exploiting this mobility, the cation exchange method is mostly used as a strategy to change the nature of the nanocrystal completely. By partial cation exchange it is possible to incorporate impurity ions in (nano)crystals. However, to exchange the cations only partially is not trivial.

A first intuitively logical factor of successful doping is the size of the cations. If the cation sites inside the anion lattice are too small for a cation to reside, it will distort the crystal lattice and the exchange becomes thermodynamically and kinetically limited. Another factor is the valency of the impurity ion. If there is a surplus or deficiency of charge this needs to be compensated in the crystal by surface ligands, empty cation sites or a codopant. The favoured coordination of the cations also plays an important role in the successful cation exchange. If a newly introduced dopant prefers a coordination number of 6 (octahedral sites) but the only available cation sites in the lattice are tetrahedral sites this will also be energetically unfavourable. A lot of different factors determine the success of cation exchange and it might not be the right approach for many systems where the dopant has different properties than the host cations.

A different method of introducing a certain element to a nanocrystal is by already having the doping material present during the synthesis of the nanocrystals. In this method the success of doping is dependent the Gibbs energy as mentioned in section 2.2.2. The Gibbs energy is dependent on both the affinity for the crystal lattice (ΔG_{bulk}) and the interfacial tension ($\Delta G_{surface}$), which are dependent on the dopant materials. During the growth phase monomers with more affinity for the crystal will be incorporated in the nanocrystal. If there is no affinity of the dopant for the nanocrystal, there will be no incorporation of the dopant. At the nucleation stage of the synthesis the dopant also plays an important role[34]. In this case the dopant is lowering the lattice stabilization, meaning that the clusters with dopant are less stable resulting in larger clusters needed to reach the critical size. This means that under normal conditions the population is dominated by the undoped clusters as nuclei.

Yet another method of introducing impurities into a host lattice is by growth doping[35], also known as isocrystalline core/shell procedure. In this case the nanocrystals are first synthesized, then a certain dopant is adsorbed on the surface of these nanocrystals and subsequently anchored in place by growing (an) extra layer(s) of nanocrystal material or another shell material to create either a doped nanocrystal or a core/shell nanocrystal with the dopants at the interface between the core and the shell.

2.4.2 Location of the impurity ions

As explained in the section Complex nanostructures, different types of nanocrystals give rise to different materials (type-I, type-I$\frac{1}{2}$ and type-II). The charge carriers can be localized in different parts of the heteronanocrystals. It can be intuitively understood that the position of an impurity ion can play a crucial role in the behaviour of the particles[36]. A multitude of reasons can explain this phenomenon, for instance the interaction between dopants[37], the difference in chemical environment at the surface and the inside of nanocrystals[38] and the (lack of) overlap between the exciton wave function and the dopant atoms. The location of the dopant with respect to the exciton can be controlled to a certain extent by using a Successive Ionic Layer Adsorption and Reaction (SILAR)[39] method. By using the SILAR method, additional layers of the host material can be deposited on the nanocrystals layer by layer. By introducing additional layers of host material the nanocrystal grows, resulting in a broader exciton wavefunction and more overlap with the dopant.

2.5 Energy transfer

If two parts of a system or two different systems are in close proximity, energy transfer can occur. For instance, in the case of multiphonon relaxation, energy is transferred from an excited state and released in the form of phonons. Another example is between difference systems, Förster resonance energy transfer (FRET)[40]. In this case one system can transfer energy to another system which is in close proximity (ca. < 10 nm). Another example of energy transfer is upconversion. By combining different lanthanides in insulator materials, energy transfer between different lanthanides can occur[41]. If via energy transfer multiple energies are combined, this can lead to a higher excited state and subsequent high energy photons, which is called upconversion[42].

2.5.1 Radiative vs non-radiative

In the case of this thesis there are two general ways in which energy can be transferred to different energy levels. Usually there is an energy difference between the original energy level and the energy level after the energy transfer. Due to conservation of energy this energy difference needs to be dissipated as either heat (non-radiative energy transfer) or an ejected photon (radiative energy transfer). In most cases a useful rule of thumb can be applied, which states that no non-radiative energy transfer will occur when the gap to bridge during energy transfer is larger than 5 phonons (a lattice vibration).

In this work, ytterbium is incorporated in a low phonon energy medium, CdSe nanocrystals. To completely gap the energy difference of the Yb^{3+} $^2F_{5/2}$ and $^2F_{7/2}$ state, a lot of phonons are required. In this case the five phonon rule dictates that the ytterbium emission will not be quenched due to non-radiative processes.

However, if the ytterbium is in close proximity to solvents, ligands or impurities, energy transfer can occur towards these organic molecules. These organic molecules have much larger phonon energies (high energy vibrations of C-H (3000 cm^{-1}) and O-H (3300 cm^{-1})) and these organic ligands only require 3-4 phonons to bridge the energy gap of ca. 10000 cm^{-1} for ytterbium $^2F_{5/2} \rightarrow {}^2F_{7/2}$.

2.6 Lanthanide-doped nanomaterials

In the case of trivalent lanthanides it will be hard to perform a cation exchange reaction with the cadmium within the CdSe quantum dots due to the difference in valency and the preferred coordination number. It is therefore unlikely that CdSe quantum dots can easily be doped with trivalent lanthanides. It will therefore be more realistic to try a growth doping approach in combination with SILAR or by incorporating the lanthanides during a fast nucleation of single source cluster precursors.

In the case of successful incorporation of a lanthanide in the CdSe quantum dots there will be an interesting combination of the high excitation cross section of the quantum dots with the sharp lanthanide emission. As discussed above one of the main disadvantages of lanthanides is the quenching due to solvent/ligand vibrations. If the lanthanide is incorporated into the CdSe quantum dot or adsorbed on the surface with a protective selenium layer, the environment of the lanthanide will change and the vibrations of ligands and solvents will no longer be able to couple to the f-f transitions. A second advantage of the combination of CdSe quantum dots and lanthanides is the fact that the CdSe quantum dots, which have a high excitation cross section, can transfer the energy to the lanthanides, resulting in an effective excitation pathway for the lanthanides. In this case the CdSe quantum dots will act as an exciton donor (with a wide excitation range) as well as provide a lattice with low phonon energies, providing protection from multiphonon relaxation with high energy vibrations.

Chapter 3

Experimental Section

In this chapter the synthesis procedures used to prepare the CdSe quantum dots and to incorporate the trivalent lanthanide ions to the quantum dot surface will be discussed. The experimental techniques employed to characterize the prepared samples will also be discussed.

Selenium (99.999%) was purchased from Alfa, oleic acid (99%) was purchased from Fluka and methanol (99.9%) was purchased from Sial. Acetone (99.9%), cadmiumacetate ($\geq$ 99.99%), trioctylphosphine (TOP; 90%), trioctylphosphine oxide (TOPO; 90%), octadecylamine (ODA; 97%), ytterbium acetate (99.9%), erbium acetate (99.9%), thulium acetate (99.9%), europium acetate (99.9%) and oleylamine (OLAM; 70%) were purchased from Sigma-Aldrich. The solvents hexane ($\geq$99%), 1-octadecene (ODE; 90%) and toluene (99.8%) were also purchased at Sigma-Aldrich. All chemicals were used as provided with the exceptions of ODE, ODA, OLAM, which were degassed under vacuum using a Schlenk line.

A multistep approach was used to synthesize lanthanide-doped quantum dots. The first step in creating these nanocrystals is to synthesise CdSe quantum dots. This was done using a hot injection method based on the method described by Qu and Peng[17]. The synthesis was further optimized by Mello Donegá *et al.*[43]. The second part of the experimental work was to dope these newly synthesised quantum dots with a lanthanide (Yb^{3+}, Er^{3+}, Eu^{3+} or Tm^{3+}). This was done using a method based on the work of Yang *et al.*[27] in which they doped CdS/ZnS Core/Shell nanocrystals with Mn^{2+}. After the addition of the lanthanide during the doping procedure, an extra amount of selenium is added to grow an additional monolayer to ensure the incorporation of the lanthanide. To further incorporate the lanthanide inside the nanocrystals the doped quantum dots were treated with a SILAR method[39].

After the synthesis of the quantum dots and after the treatment of the quantum dots with ytterbium and selenium the prepared samples were washed thrice. The first two washing steps are with methanol as an antisolvent and the colourless layer is removed after phase separation. The third washing step involved precipation by adding acetone and centrifuging. The supernatant was removed and the CdSe quantum dots were redispersed in 2 mL of hexane while the doped nanocrystals were redispersed in 2 mL of toluene.

Transmission electron microscopy (TEM) was performed using a FEI Tecnai microscope operating at 120 kV. Energy dispersive x-ray (EDX) spectra were obtained on an aberration-corrected high-resolution Titan microscope operating at 300 kV. Samples for analysis were obtained by depositing a droplet of sample on a carbon coated copper TEM grid and evaporating the supernatant. TEM image statistics were performed on more than 100 particles. Absorption spectra were recorded using a Perkin-Elmer Lambda 950 absorption spectrophotometer. Emission and excitation measurements were performed using an Edinburgh Instruments FLS 920 spectrofluorometer equipped with two photomultiplier tube (PMT) detectors, the Hamamatsu R928 and the Nitrogen-cooled R5509-72, for detection in the visible and infrared range respectively. A 450 W Xe lamp and an optical parametric oscillator (OPO) laser system (Opotek HE 355 II) were used as excitation sources. The lifetimes of the CdSe emission were measured using the Hamamatsu H7422-02 PMT, an Edinburgh Instruments picoscecond pulsed diode laser operating at 376.8 nm with a pulse width of 64.8 ps and a double monochromator, Bentham DTMS300 1200 lines/mm grating blazed at 300 nm.

All experiments are performed inside a glovebox under nitrogen atmosphere employing oxygen and water free conditions unless stated otherwise ($\leq$5 ppm O_2 and H_2O).

3.1 Quantum dot synthesis

To synthesize CdSe quantum dots a hot injection method was chosen to prepare high quality monodisperse particles. The reaction can be divided in the preparation of the precursors, the actual synthesis and the washing of the samples as mentioned above. An excess of selenium is used in this synthesis to achieve high quality particles (high photoluminescent quantum yield) based on the findings of Qu and Peng[17].

3.1.1 Selenium precursor

In the Selenium precursor 0.35 g of selenium (4.4 mmol) was added to 1.9 g of TOP to dissolve the selenium and form the complex TOPSe. The Se was dissolved under heating (ca. 150 °C) and stirring. 3.0 g of ODE was added to the solution, resulting in a clear colourless solution.

3.1.2 Cadmium precursor

To create the Cadmium precursor a mixture of 0.32 g of cadmiumacetate (1.4 mmol), an excess of 1.84 g of oleic acid (OA) and 13 g of ODE was degassed under vacuum using a Schlenk line. This was done while stirring and heating (ca. 150 °C) to evaporate the acetic acid. The resulting cadmium oleate in ODE and OA was either a colourless clear solution or a clear brown solution, most likely due to a little bit of impurity which was seen more often in the cadmium precursors.

3.1.3 Hot injection

The hot injection synthesis was performed using a 50 mL three necked round bottom flask with a mixture of 1.11 g of TOPO (2.8 mmol), 3.2 g of ODA (11.9 mmol) and 5.2 g of Se precursor. The mixture was heated to 290 °C and a needleless syringe was used to quickly add 4.9 g of Cadmium precursor to the mixture. Immediately after the injection the colour of the mixture changes to bright yellow and during the reaction the colour shifts to orange/red or further to black. Also the temperature decreases to ca. 270 °C due to the injection of the cold Cadmium precursor.

The reaction has been performed with both taking small aliquots after different reaction times (30 seconds, 1 minute, 2 minutes, 3 minutes and 5 minutes) or without taking aliquots and just cooling the reaction mixture down after 5 or 10 minutes of reaction time. In both cases the volume of the samples was tripled with hexane before washing as described above.

3.2 Doping of CdSe quantum dots

During the second part of the separated doping method the lanthanide is adsorbed on the quantum dot surface by addition of a lanthanide precursor. A selenium precursor was added afterwards to facilitate the incorporation of the lanthanide.

Concentrated solutions of the different precursors were made, these were diluted to yield the precursor concentrations required for the different reactions.

3.2.1 Concentrated dopant precursors

Different ytterbium precursors were used in order to optimize the synthesis of CdSe:Yb^{3+}. Besides, the optimized synthesis procedure was employed to incorporate other trivalent lanthanide ions such as Eu^{3+}, Er^{3+} or Tm^{3+}.

Ytterbium acetate

The first tested ytterbium precursor was ytterbium acetate. This precursor was made by adding 0.9 g (2.1 mmol) of ytterbium acetate to 4.0 mL of OLAM. The reaction mixture was heated to 150 °C under vacuum while stirring to remove the hydrates. During heating the ytterbium acetate was a clear solution, but after cooling down to room temperature it was observed that the precursor was a white turbid dispersion. It might be that the elevated temperature results in a fully dissolved ytterbium acetate in OLAM or that the ytterbium acetate has melted. Although the solubility is too low at room temperature the precursor can still be used due to the reaction temperature of 265 °C during the doping.

Ytterbium oleate

It is known that oleic acid has an effect on the growth kinetics of CdSe quantum dots[26] due to it's coordinating nature. It might be that the oleic acid also plays an important role in the doping kinetics. To see if the ytterbium oleate was a more soluble precursor and to check the role of oleic acid a second precursor was made. The second ytterbium precursor was made by adding 0.46 g (1.1 mmol) of ytterbium acetate hexahydrate to 1.88 g of oleic acid and 13 g of ODE (the same ratios as with the cadmium precursor for the quantum dot synthesis). The mixture was stirred and heated at 150 °C under vacuum using a Schlenk line. The result was a clear, faintly yellowish solution indicating a well soluble ytterbium oleate precursor.

Other lanthanide oleates

The erbium oleate, europium oleate and thulium oleate were made by adding 0.4 g (1.2 mmol) of the corresponding lanthanide acetate hydrate to 1.88 g of oleic acid and 13 g of ODE. The mixture was stirred and heated at 150 °C under vacuum using a Schlenk line. The europium oleate and thulium oleate resulted in a clear colourless solution while the erbium oleate was clear and faintly pink.

3.2.2 Concentrated selenium precursors

TOP is a reactive coordinating ligand which can bind to a multitude of different materials and form complexes, especially with the chalcogenides (*e.g.* Se, S, Te). It is plausible that TOP can have a large effect on the doping, for instance by stabilizing the selenium too much. If the stability of the TOP-Se complex is too high, more activation energy is needed to separate the Se from the TOP and to incorporate it into the surface and the deposition of the selenium on the ytterbium rich surface is halted. It is therefore useful to investigate the doping synthesis both with and without TOP.

Se precursor

A Se precursor without TOP was made by adding 0.8 g of selenium powder (10 mmol) to 20.0 mL of ODE. The resulting mixture was black and turbid as expected. Even though the selenium did not dissolve, the solubility will increase with increasing temperature, making the selenium a viable precursor at doping temperatures of 265 °C.

TOPSe precursor

A TOPSe precursor in which the TOP-selenium complex is fully dissolved was made by adding 0.8 g (10 mmol) of selenium powder to 6 mL of TOP and adding 14 mL of ODE while heating (150 °C) and stirring to create a colourless, clear solution (even after cooling down to room temperature).

3.2.3 Precursors

To optimise the doping synthesis a whole variety of different precursors were made using the concentrated precursors described above. In most cases the selenium precursors were matched to have the same amounts as the dopant precursors. Table A.1 in the chapter Appendices shows the different samples made with the different amount of precursors. The different concentrations of precursors were made by diluting the concentrated precursors with ODE.

3.2.4 Doping method

The method used for the doping is an adapted version of the Mn^{2+} doping performed by Yang *et al.*[27]. Either 140 or 100 nmol of CdSe quantum dots dispersed in hexane were added to a vial with 9 mL of ODE and 3 mL of OLAM. Although different amounts of solvents have been used, the ratio between the ODE and OLAM always was 3:1.

The samples were homogeneously heated to 265 °C using a metal block on a heating plate and the samples were kept at these temperatures for at least 30 minutes to remove the remaining hexane from the quantum dot dispersions.

Next the dopant precursor was slowly added to the vial. This was done by adding 1 mL of precursor solution in roughly 3 minutes in a dropwise fashion using a Finn pipette or Pasteur pipette. The reaction was then kept at 265 °C for 30 minutes to allow the adsorption of the dopant on the quantum dot surface.

Subsequently the selenium precursor was added in the same way (1 mL of precursor in roughly 3 minutes in a dropwise fashion). The temperature was kept at 265 °C for another 30 minutes to allow the growth of the nanocrystals before the reaction mixture was cooled down to RT and washed.

3.3 Successive ionic layer adsorption and reaction (SILAR)

The SILAR method[39] is a method in which extra monolayers of cadmium and selenium (or other chalcogenides) are controllably grown around quantum dots. An adapted SILAR method has been used in this thesis where the ODA has been replaced with OLAM. Using the known lattice parameters (a = 0.43 nm, c = 0.702 nm and Z = 2)[44] and the radius and concentration of the quantum dots an estimate can be made of the amounts of cadmium and selenium precursors needed for the growth of 1 monolayer. In the case of CdSe quantum dots with a starting diameter of 3.5 nm the resulting particles will have a diameter of 3.930 nm (by adding up the lattice parameter a). The difference in volume can be calculated and translated into number of unit cells (since 1 unit cell has a volume of 0.1124 nm^3) as shown in Equation 3.1.

$$\frac{\frac{4}{3}\pi\left(\frac{3.93*10^{-9}\text{ m}}{2}-\frac{3.5*10^{-9}\text{ m}}{2}\right)}{1.124*10^{-28}\text{ m}} = 83.02 \text{ unit cells} \tag{3.1}$$

So increasing the size of a 3.5 nm quantum dot with 1 monolayer is equal to 83.02 unit cells. Taken into account the amount of quantum dots (100 nmol) and the fact that we need 2 cadmium and selenium atoms per unit cell (Z=2), we need a total of $(83.02 * 2 * 100 * 10^{-9}\text{mol} =) 1.66 * 10^{-5}$ mol of cadmium and selenium. Using 0.1 M precursors, this would be equivalent to 0.166 mL of precursor per ion.

These calculations were performed automatically using an excel sheet created by Wiel Evers which gives the amount of mL needed to be added of a 0.1 M solution of the corresponding ion per monolayer as an output. This is shown in Table 3.1.

3.3.1 Selenium precursor (0.1 M)

Both selenium precursors with and without TOP have been created for the addition of monolayers to lanthanide doped quantum dots.

TOP-Selenium precursor

To prepare a 0.5 M solution of TOP-Selenium precursor 0.71 g of selenium was added to 5 mL of TOP. After heating (T = 130 °C) and stirring the selenium was dissolved, resulting in a clear colourless solution. This solution was diluted with ODE to create 0.1 M precursors.

Selenium precursor

To prepare a 0.1 M dispersion of Selenium precursor 0.08 g of selenium was added to 10 mL of ODE. The dispersion remained black and turbid.

3.3.2 Cadmium precursor (0.1 M)

To prepare a 0.1 M solution of Cadmium precursor 0.57 g of cadmium acetate was added to 6.19 g of oleic acid. After adding 18 mL of ODE the mixture was stirred and heated to 120 °C under vacuum

using a Schlenk line. The result was a clear brown solution, most likely due to a little bit of impurity which was seen more often in the cadmium precursors.

3.3.3 Adding extra layers of cadmium and selenium

Adding extra layers of cadmium and selenium using the SILAR method is quite similar to the doping method described above. 100 nmol of quantum dots were added to 6 mL of ODE and 2 mL of OLAM. The mixture was homogeneously heated to 240 °C for 30 minutes to remove the toluene from the quantum dot dispersion. Keeping the temperature at 240 °C, the calculated amount of cadmium or selenium was slowly added in a dropwise fashion. After a delay of a few minutes the other precursor solution was added and the mixture was then left at 240 °C for 30 minutes to ensure that the growth is complete. The addition of selenium and cadmium could then be repeated with an increased amount of precursor solution due to the increased size of the quantum dots and the more precursor needed to create an additional shell. An example of the amount of precursors needed per monolayer is shown below in Table 3.1.

Monolayer	Cadmium precursor (mL)	Selenium precursor (mL)
1	0.166	0.166
2	0.207	0.207
3	0.252	0.252
4	0.301	0.301
5	0.355	0.355
6	0.414	0.414
7	0.476	0.476
8	0.544	0.544
9	0.615	0.615
10	0.692	0.692
11	0.772	0.772
12	0.857	0.857
13	0.947	0.947
14	1.04	1.04
15	1.14	1.14
16	1.24	1.24
17	1.35	1.35
18	1.46	1.46
19	1.58	1.58
20	1.70	1.70

Table 3.1: An example of the amount of precursors needed for a 100 nmol dispersion of CdSe quantum dots with a starting diameter of 3.5 nm.

3.4 Combined versus separated doping and SILAR

Due to the similar reaction parameters of the doping synthesis and the SILAR method a new synthesis method was designed to combine the doping and the subsequent growth of CdSe monolayers around the incorporated lanthanide ion. When the syntheses are combined the extra layer of selenium was not added because of the extra layers added using SILAR. Table B.1 in the appendices shows the samples made using SILAR, both directly combined with doping (DS1-12) and with separated doping and SILAR (DS13-14 and RS1-4).

3.5 Single source precursor method

Although the separation of reactions is a common method for doping syntheses [27],[32],[36],[45] there is an alternative. Another common reaction method is to use a single source precursor and a dopant [28],[29],[31],[46]. This method was tested as well at the start of the thesis.

At the start of the thesis two different approaches to doping CdSe quantum dots were tried. Next to the sequence of experiments mentioned above it was also investigated if doping was possible with a single source precursor of cadmium and selenium with a dopant. The single source precursor used is $Li_4[Cd_{10}Se_4(SPh)_{16})]$ and was provided by Yiming Zhao. The dopant precursor was made by dissolving 0.56 g of anhydrous $YbCl_3$ in 2.0 mL of HDA.

Two different methods were tried using these clusters. In the first method a solution of precursor and dopant precursor was slowly heated while in the other case the solvent and dopant precursor were heated and the clusters were added via a hot injection.

3.5.1 Heating up single source precursor method

In the heating up single source precursor method 180 µL of dopant precursor and 0.55 g of the $Li_4[Cd_{10}Se_4(SPh)_{16})]$ were added to 10.8 g of HDA in a round bottom flask. The mixture was heated to 130 °C for 3 hours before increasing the temperature to 230 °C. While increasing the temperature aliquots were taken after 1.30 minutes (T = 180 °C), 3.20 minutes (T = 190 °C), 5.30 minutes (T = 225 °C), 7.15 minutes (T = 228 °C) and 12.40 minutes (T = 231 °C).

3.5.2 Hot injection single source precursor method

In the hot injection single source precursor method an injection solution was prepared by adding 0.55 g of $Li_4[Cd_{10}Se_4(SPh)_{16})]$ to 6 mL of OLAM. 180 µL of dopant precursor was added to 6 mL of HDA in a round bottom flask and the mixture was heated to 300 °C. Next, the injection solution was quickly injected using a needleless syringe. Aliquots were taken after 15 and 40 seconds and after 1 and 5 minutes. The colour of these samples ranges from yellow/orange to (dark) red.

Chapter 4

Ytterbium doped quantum dots

The main aim of this work was to develop a synthesis procedure to incorporate lanthanide ions in CdSe quantum dots and to demonstrate energy transfer from the quantum dot host to the lanthanide dopant. For this purpose, the Yb^{3+} ion was chosen because of the few energy states of the Yb^{3+} ions resulting in only one transition. Because of the large redshift of the Yb^{3+} transition with respect to the the CdSe bandgap transition, the interpretation of the experiments is straightforward. Before the doping procedure was investigated, the CdSe quantum dots were synthesized and characterized.

The incorporation of the lanthanide ion is investigated and optimized by adjusting the ratio between the dopant and the quantum dot and by varying the dopant precursor. Furthermore the role of the extra amount of selenium added after the synthesis and the role of TOP during the doping is investigated. After investigation of the doping process, the possibility of growing extra CdSe monolayers around the system and the relation between the location of the dopant ion and the lifetime of the dopant and CdSe emissions was investigated.

The investigation of the energy transfer and the successful incorporation of the dopant was investigated using a variety of techniques. The luminescent properties of the CdSe quantum dots, both with and without the incorporation of Yb^{3+}, have been investigated using steady state (absorption, excitation and emission) and time-resolved spectroscopy.

4.1 Analysing the quantum dots

After the synthesis, the first priority is to check whether the synthesis was successful and to investigate the size, polydispersity and concentration of the quantum dots. This can be done using absorption and fluorescence spectroscopy and TEM. The bright orange to red colour of the dispersions after the synthesis and the fluorescence upon illumination with UV light is a first indication of the successful synthesis of QDs, but more detailed analysis is needed. Figure 4.1 shows the absorption spectra of samples extracted after different reaction times (30 seconds, 1 minute, 3 minutes and 5 minutes; left). On the right, the typical emission (black) and absorption (red) spectra (right) of the final sample are shown.

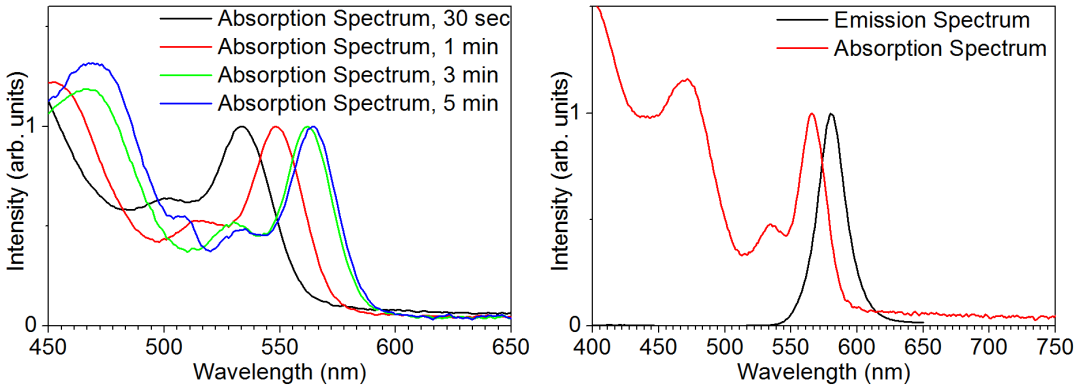

Figure 4.1: The absorption spectra of CdSe QDs (left) for different growth times; 30 seconds (black, λ_{max} = 533 nm), 1 minute (red, λ_{max} = 548 nm), 3 minutes (green, λ_{max} = 562 nm) and 5 minutes (blue, λ_{max} = 564 nm) and the typical emission (black) and absorption (red) spectra of the final sample (right).

A redshift can be observed in these absorption spectra due to the growth over time for the samples, resulting in larger particles and thus a smaller band gap as discussed in the theory section of this thesis. The spectra are similar to spectra shown in literature for CdSe quantum dots[26], suggesting a successful synthesis. The narrow emission peak indicates monodisperse CdSe quantum dots.

A second method used to confirm the success of the synthesis was TEM combined with EDX. Figure 4.2 shows a TEM image of a typical CdSe QD sample. On the right side an EDX spectrum of this sample is shown.

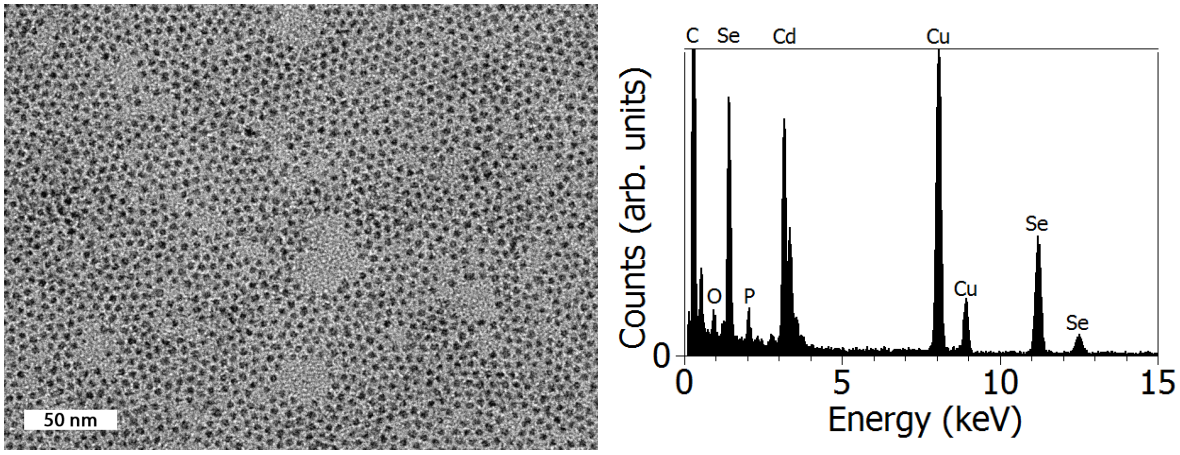

Figure 4.2: TEM image of a typical CdSe quantum dot sample (left) and the matching EDX spectrum of this section of the same sample. The copper peak is due to the TEM grid, phosphor and oxide are due to the ligands (TOP/TOPO).

The TEM image shows spherical particles and from the integrated intensity of the L-shell absorption edges (Se = 1.3 keV and Cd = 3.2 keV) an elemental ratio of 52:48 was found. This is well within the ranges (50:50) expected for CdSe quantum dots.

The sizes found in TEM images can be compared with the sizes found by analysing the absorption spectra. Table 4.1 shows the sizes found of different quantum dot samples using both TEM images and analysing the absorption spectra. The concentration is calculated using the absorption spectra.

Sample	λ_{max} (nm)	c (mmol L^{-1})	D Abs (nm)	D TEM (nm)
CdSe3.1	575	0.140	3.7	3.7 ± 0.4
CdSe3.2	574	0.114	3.6	3.7 ± 0.3
CdSe3.3	575	0.151	3.7	3.7 ± 0.4
CdSe3.4	574	0.194	3.6	3.7 ± 0.4
CdSe3.5	575	0.224	3.7	3.8 ± 0.4

Table 4.1: The concentrations and diameters of quantum dots made with a typical hot injection synthesis.

Even though the particle size is hard to obtain using TEM analysis due to the poorresolution, the diameter obtained by TEM analysis and analysis of the absorption spectra match very well.

A final proof of the successful synthesis of quantum dots is given by the emission and excitation spectra of the samples in the visible region as shown in Figure 4.3.

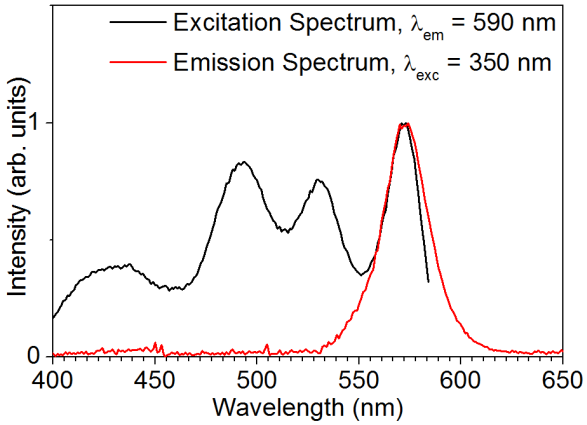

Figure 4.3: An excitation (black) and emission spectrum (red) of sample CdSe3.4.

The maximum for the first exciton peak is comparable to the maximum found with absorption spectroscopy. The emission spectrum shows one symmetrical peak, which is expected for high quality CdSe quantum dots. This peak originates from the transition of the $1S_e$ to $1S_h$ state.

4.2 Separated doping method versus single source precursor method

As mentioned in the Experimental Section multiple approaches were developed to perform the incorporation of the lanthanide ion in the CdSe quantum dots. Several pilot experiments have been carried out to determine whether the possible approaches yield success. Three different experiments have been performed as described in the Experimental Section. The first approach was the separated production of CdSe quantum dots and the subsequent addition of the dopant and selenium overgrowth. The second approach was to heat up a mixture of dopant and single source precursors. The third approach was the hot injection of the single source precursor in a mixture with the dopant ion.

To check the success of the incorporation of ytterbium, the energy transfer process was investigated. This was done by analysing the ytterbium emission peak, which is expected from the Dieke Diagram to be around 1000 nm (10^5 cm^{-1}). This was investigated by first measuring the emission spectrum of the CdSe QDs. Subsequently the ideal excitation wavelength (λ_{exc}) was obtained by consideration of the excitation spectrum of the CdSe QD emission. The first excitonic absorption peak, which has the highest intensity, was chosen as the excitation peak for the ytterbium emission spectra.

Figure 4.4 shows the emission spectra of the CdSe QDs treated with the separated doping method (left, sample R3, λ_{exc} = 470 nm). Figure 4.5 shows the emission spectrum of a sample (ClusterHI4, λ_{exc} = 516 nm) prepared by the hot injection single source precursor method. The spectra range from 950 - 1050 nm in which the ytterbium emission peak is expected.

If ytterbium emission is observed, energy transfer processes occur indicating the close proximity of ytterbium ions to CdSe quantum dots. In the case of the heating up single source precursor method no signal was observed in the expected range.

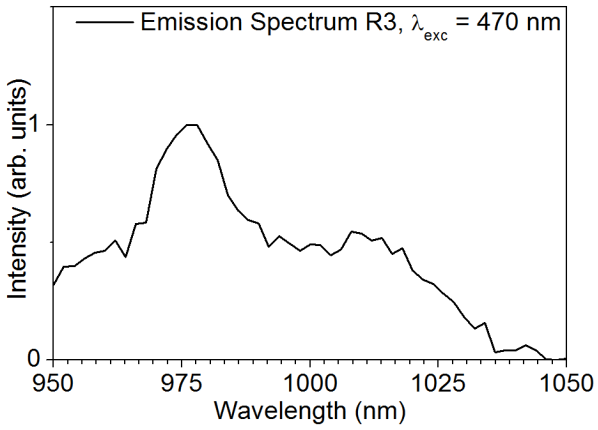

Figure 4.4: The ytterbium emission of a sample prepared using the separated doping method, provided by Rosa Martín-Rodríguez.

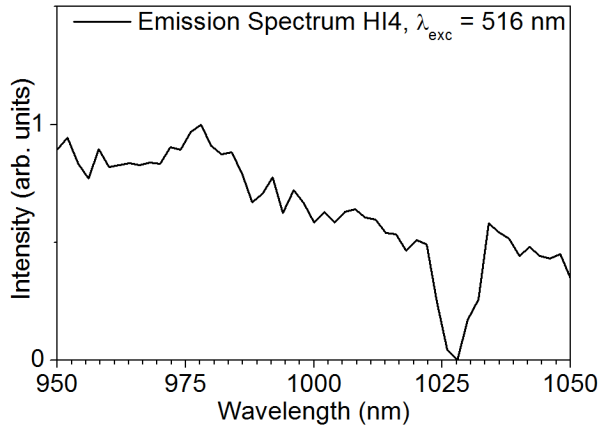

Figure 4.5: The ytterbium emission of a sample prepared using the single source precursor in a hot injection method.

As can be seen in Figure 4.4, there are two samples for which the spectra display some intensity at 975 nm. One sample was synthesized using the separated doping method (Sample R3) and one sample was synthesized using the hot injection single source precursor method (Sample HI4). Figure 4.6 shows the excitation spectra from the ytterbium emission observed for the samples R3 (separated doping method, left) and Cluster HI4 (hot injection single precursor method, right). Even though the intensity of the ytterbium emission of the samples is weak, the excitation spectra of this emission shows that the emission originates from the CdSe quantum dots. Note that the Yb^{3+} ions have no transitions in the UV-VIS range.

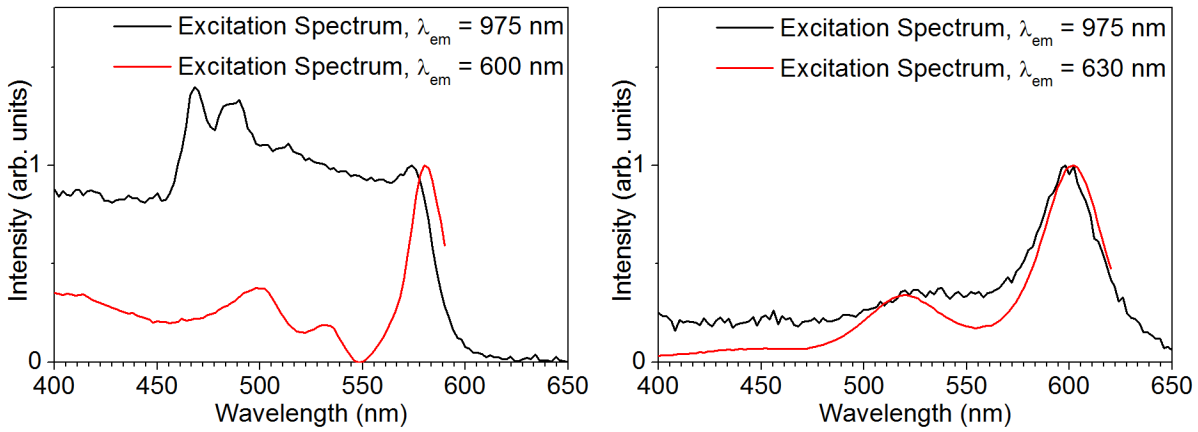

Figure 4.6: Excitation spectra of a sample prepared with the separated doping method (left, sample R3) and with the hot injection single source precursor method (right, Cluster HI4). The black excitation spectra correspond to λ_{em} = 975 nm and the red spectra correspond to λ_{em} = 600 nm and λ_{em} = 630 nm respectively.

Next to the optical properties also the size and polydispersity of the samples were compared. Figure 4.7 shows a representative TEM image of both samples. From these images the average size and polydispersity were calculated and compared.

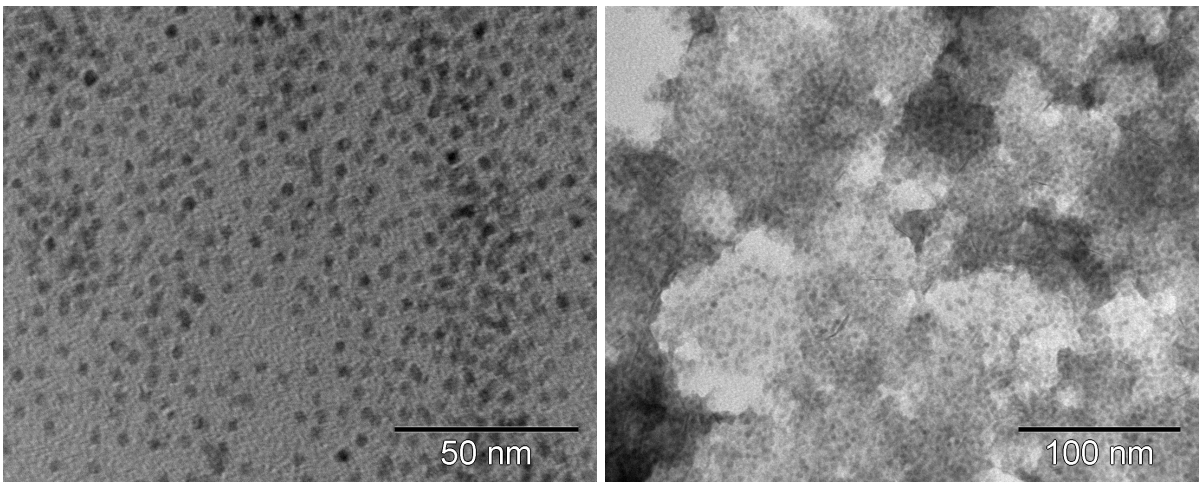

Figure 4.7: TEM images of a sample made with the separated doping method (left; D = 3.5 ± 0.37 nm) and a sample made with the hot injection single source precursor method (right; D = 4.0 ± 0.51 nm).

From this data it can be concluded that the separated doping method yields particles with a polydispersity of 10.6 %. The hot injection single source precursor method, yielded particles with a polydispersity of 12.8 %. From the images it can be observed that the custer sample is much harder to wash, since there is still a lot of amorphous material (most likely precursor material) present.

The data shown implies that the separated doping method yields cleaner samples. Combined with a more pronounced ytterbium emission peak and matching excitation spectra the preferred method of synthesis is the separated doping method (although optimisation is needed). Even though the hot injection single source precursor method is faster and a more facile method, the separated doping method has more versatility. With one batch of CdSe quantum dots several different doped samples can be made with different dopants. Furthermore, the separated doping method allows for experimentation on different II-VI quantum dots (*e.g.* CdTe).

Based on the advantages of the separated doping method and the results shown above, it was decided to optimise the incorporation of lanthanides in CdSe quantum dots with this method.

4.3 Optimising the doping method

The observation of ytterbium emission which originates from the CdSe QDs is a first indication of energy transfer. However, the observed ytterbium emission intensity was very weak and so optimisation is necessary. Several different parameters were modified to improve the quality of the ytterbium doped nanocrystals and these are discussed below.

4.3.1 Optimising the ratio between ytterbium acetate and CdSe quantum dots

The first optimisation process revolved around the ratio between the dopant and the CdSe QDs. In these experiments a constant amount of 140 nmol of quantum dots and a varying amount of ytterbium precursor was used, resulting in ratios ranging from 1875:1 to 38:1. Table 4.2 shows the prepared samples for the ratio optimisation. Note that the amount of selenium was equal to the amount of Yb^{3+} precursor in order to have sufficient selenium to fully cover the ytterbium.

Sample	QDs (nmol)	$Yb(Ac)_3$ (mmol)	Se (mmol)	Ratio Yb^{3+}:QDs
DOP1	140	0.26	0.25	1875:1
DOP2	140	0.18	0.18	1313:1
DOP3	140	0.11	0.1	750:1
DOP4	140	0.026	0.025	188:1
DOP5	140	0.026	0.025	188:1
DOP6	140	0.053	0.05	375:1
DOP7	140	0.026	0.025	188:1
DOP8	140	0.053	0.05	375:1
DOP9	140	0.013	0.025	94:1
DOP10	140	0.0053	0.005	38:1

Table 4.2: A summary of the samples prepared for the optimization of the ratio between the ytterbium acetate dopant and the CdSe QDs.

Samples with large excess of ytterbium dopant

The first four samples made (DOP1-4) already showed a large difference in optical properties. Figure 4.8 shows thep hotos of samples DOP1-4. The typical bright orange colour of CdSe quantum dots of around 3-4 nm was not observed for these samples (DOP1 and DOP2). However, the orange colour started to appear with lower amount of ytterbium added (DOP3 and DOP4).

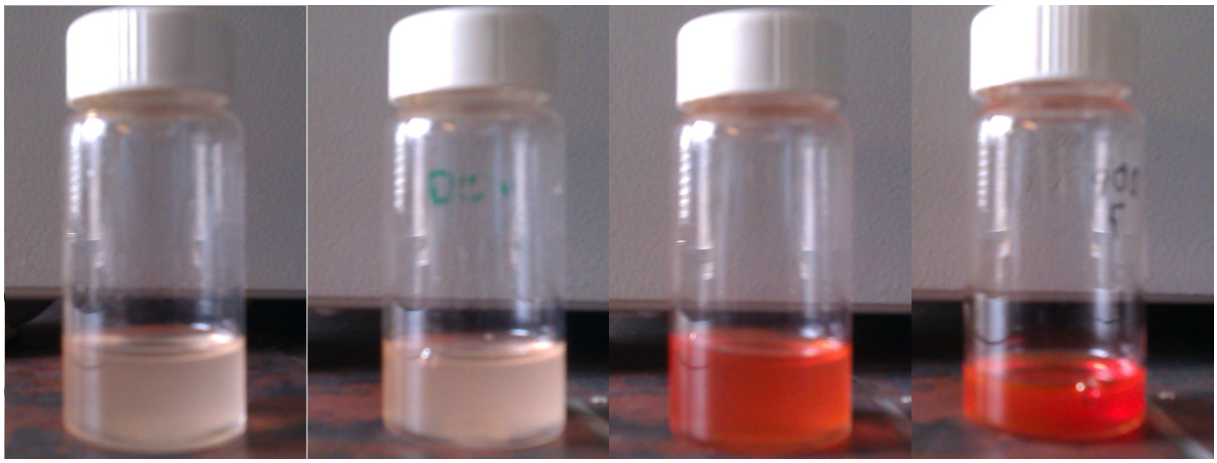

Figure 4.8: Images of the first four samples, from left to right: DOP1 (ratio = 1875:1), DOP2 (ratio = 1313:1), DOP3 (ratio = 750:1) and DOP4 (ratio = 188:1) made in the optimisation process of the doping method.

Figure 4.9 shows the absorption spectra of Samples DOP1-4. It is observed that the typical CdSe QDs absorption spectrum is not found in the samples with the high excess of ytterbium dopant. Upon lowering the ratio, the CdSe spectrum is restored. However, a long and intense tail is present in the absorption spectrum, most likely due to scattering.

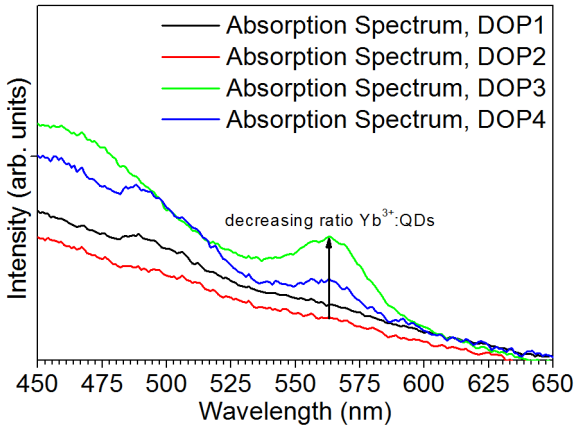

Figure 4.9: The absorption spectra of DOP1 (black; ratio = 1875:1), DOP2 (red; ratio = 1313:1), DOP3 (green; ratio = 750:1) and DOP4 (blue; ratio = 188:1).

Figure 4.10 shows the TEM images of samples DOP1-4. Clearly, all samples contain large clusters of unknown material. This is in agreement with the observed absorption spectra where scattering is observed in all four samples. Although no EDX has been performed on these samples, the large clusters are most probably the result of the large excess of ytterbium precursor. It can be observed that in samples with smaller ratios (DOP3 and DOP4) less cluster were found and single CdSe nanoparticles were observed.

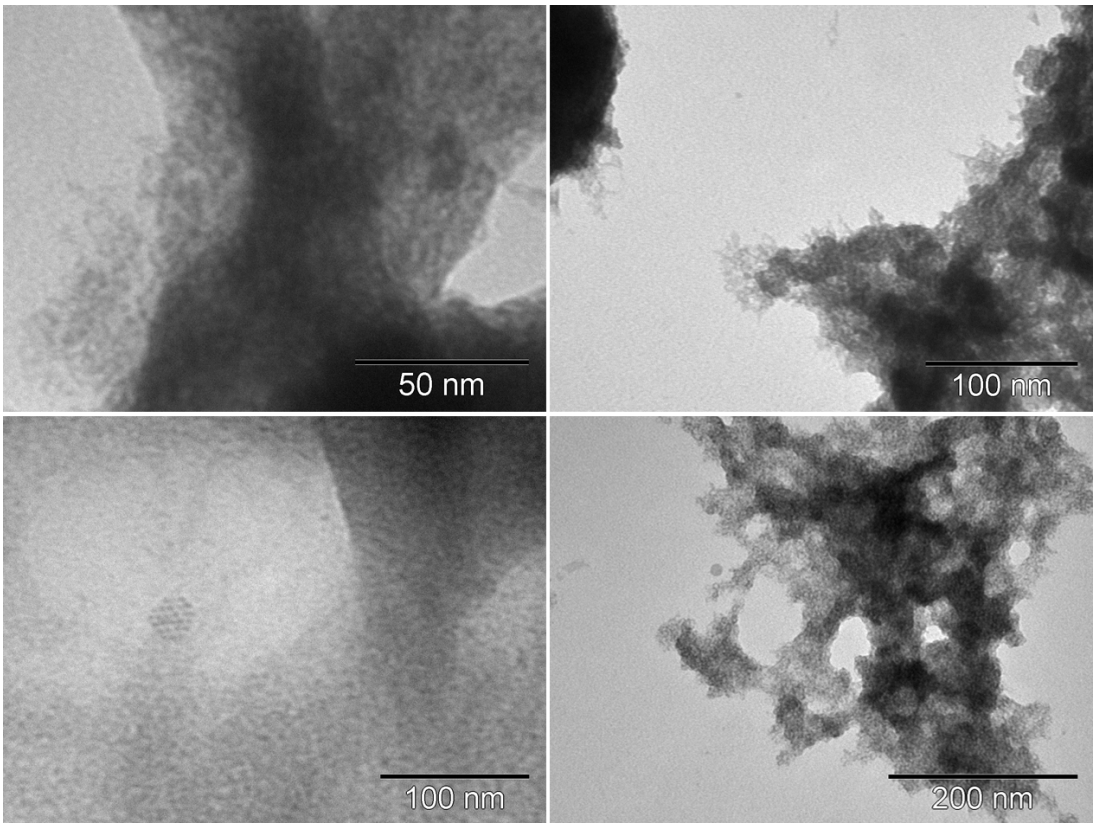

Figure 4.10: TEM images of sample DOP1 (top left; ratio = 1875:1), DOP2 (top right; ratio = 1313:1), DOP3 (bottom left; ratio = 750:1) and DOP4 (bottom right; ratio = 188:1).

The other factor in optimising the doping procedure, the efficiency of the energy transfer has also been investigated for these samples. In the case of samples with ratios of 1875:1, 1313:1 and 750:1, no ytterbium emission was observed. However, Figure 4.11 shows ytterbium emission upon CdSe QD excitation from sample DOP4, which has a ratio of 188:1. The low quality of the spectra is due to the low signal to noise ratio of the ytterbium emission (975 nm) and the CdSe emission (600 nm).

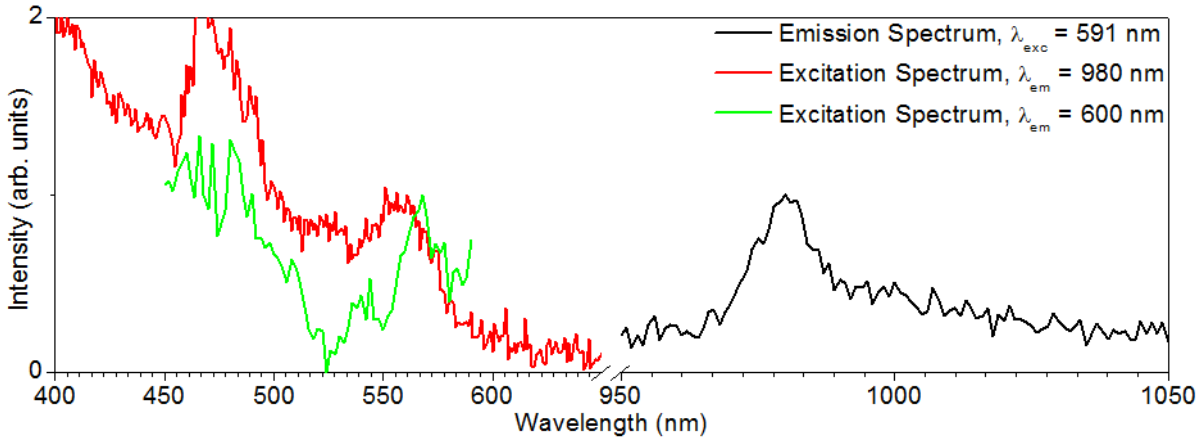

Figure 4.11: Emission spectrum (black) of sample DOP4 (ratio = 188:1) while exciting at 591 nm. The corresponding excitation spectra of the emission of ytterbium (red; λ_{em} = 980 nm) and CdSe (green; λ_{em} = 600 nm) are also shown.

In these spectra a relatively broad peak of low intensity is observed at 980 nm and the excitation spectrum of this emission shows features similar to the excitation spectrum of the CdSe quantum dot emission (λ_{em} = 600 nm).

For the samples with a large excess of ytterbium dopant, a weak ytterbium emission peak was found which can be related to the CdSe QD host, indicating energy transfer. The CdSe quantum dot nature of the sample has been largely lost however by the large excess of dopant precursor. More samples with lower excess of ytterbium dopant were made and analysed.

Samples with small excess of ytterbium dopant

Since the characteristic absorption spectrum of CdSe was not yet observed without the large tail resulting from scattering, an extra set of samples was made for which the ratio of dopant and quantum dot was lowered even further to range from 375:1 to 38:1 (samples DOP5-DOP10 in Table 4.2. All samples showed the expected, bright orange colour. Figure 4.12 shows the absorption spectra of these samples. A trend in the spectra can be observed where the CdSe quantum dot character becomes more apparent with lower ratios between the dopant and the quantum dots. Furthermore, the tail in the absorption spectra is still present in samples with lower ratios but the intensity is very low.

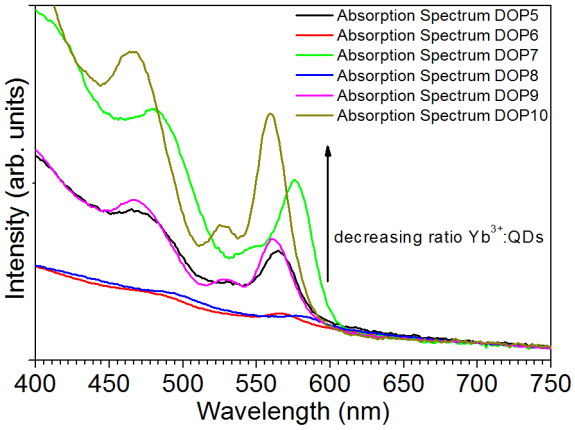

Figure 4.12: Absorption spectra of samples DOP5 (black; ratio = 188:1), DOP6 (red; ratio = 375:1), DOP7 (green; ratio = 188:1), DOP8 (blue; ratio = 375:1), DOP9 (magenta; ratio = 94:1) and DOP10 (dark yellow; ratio = 38:1).

The TEM images further confirm that the clustering effect, caused by the large excess of ytterbium is no longer present at smaller excesses. Figure 4.13 shows TEM images of samples DOP7 (ratio = 188:1), DOP9 (ratio = 94:1) and DOP10 (ratio = 38:1). The images show single particles without the large clusters of ytterbium dopant, indicating that an excess of 50-200 times of ytterbium acetate can be successfully washed out to produce intact CdSe nanocrystals.

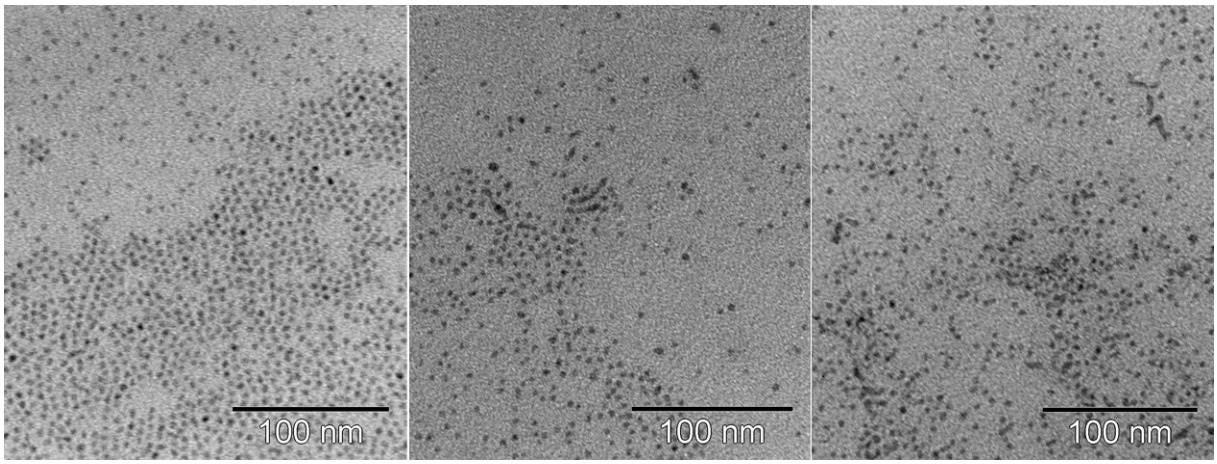

Figure 4.13: TEM images of samples DOP7 (left; ratio = 188:1), DOP9 (middle; ratio = 94:1) and DOP10 (right; 38:1).

Now that a range of acceptable ratios for doping resulting in intact CdSe quantum dots has been found the ytterbium emission can be investigated to see which ratio results in the most efficient energy transfer. Figure 4.14 shows the emission spectra of samples DOP7 (black, ratio = 188:1, λ_{exc} = 581 nm), DOP9 (red, ratio = 94:1, λ_{exc} = 530 nm) and DOP10 (green, ratio = 38:1, λ_{exc} = 530 nm) in the IR range upon CdSe QD excitation. The inset of Figure 4.14 shows the normalized intensities with respect to the ytterbium emission intensity of sample DOP7.

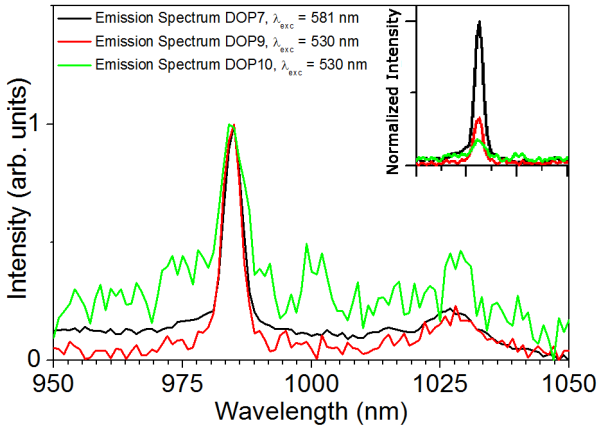

Figure 4.14: The ytterbium emission spectra of DOP7 (black; ratio = 188:1), DOP9 (red; ratio = 94:1) and DOP10 (green; ratio = 38:1) upon excitation of the CdSe quantum dots. The inset shows the relative ytterbium emission intensities of the samples.

All three spectra show a sharp peak at 985 nm and a weaker, broader peak 1030 nm, which can be assigned to the $^2F_{5/2}$ - $^2F_{7/2}$ transition. Clearly, the signal to noise ratios of the different samples are different. The emission spectrum of sample DOP7 (ratio = 188:1) shows to be the most intense peak while the signal to noise ratio worsens with lower dopant to QD ratios, which can be clearly seen for sample DOP10 (ratio = 38:1).

To double-check the origin of the ytterbium emission of sample DOP7 an excitation spectrum was recorded. Figure 4.15 shows the emission spectrum of sample DOP7 (red, $\lambda_{exc} = 581$ nm), the excitation spectrum of the CdSe QD emission (blue, $\lambda_{em} = 620$ nm) and ytterbium emission (green, $\lambda_{em} = 985$ nm) and the absorption spectrum (black).

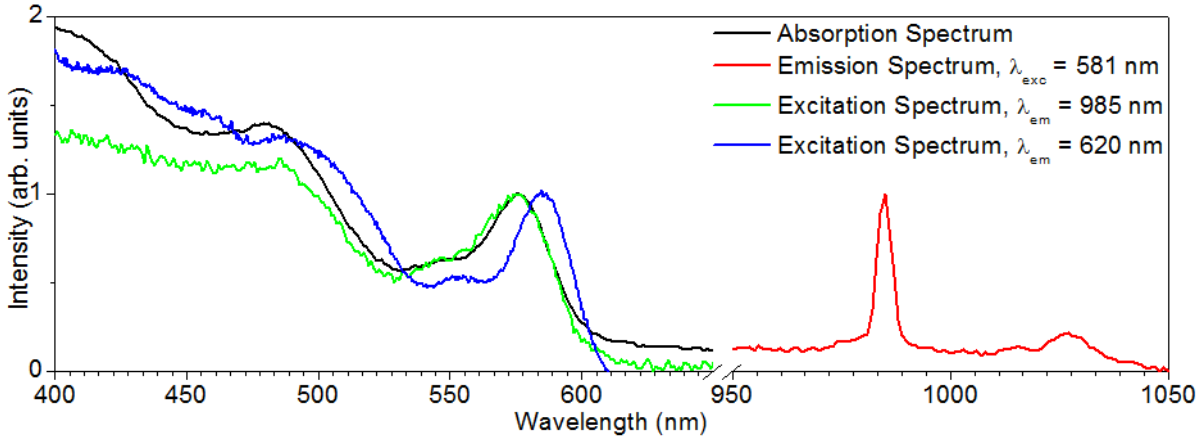

Figure 4.15: Sample DOP7 (ratio = 188:1). The emission spectrum (red, $\lambda_{exc} = 581$ nm) of ytterbium, the excitation spectra (green, $\lambda_{em} = 985$ nm and blue, $\lambda_{em} = 620$ nm) and the absorption spectrum (black) are shown. The redshift in the excitation spectrum of the CdSe emission is due to the choice of λ_{em}. Due to the large value for λ_{em} only the larger nanoparticles of the ensemble are probed, resulting in a red shift.

The excitation spectrum was compared to the excitation spectrum of the CdSe quantum dot emission and the absorption spectrum of the sample. As can be seen, the spectra match very well and it can be safely assumed that the CdSe quantum dot excitation is the origin of the ytterbium emission. Although no literature is available for the ytterbium emission in bulk CdSe the results shown here compare well with the literature of ytterbium emission in bulk CdS[47],[48].

To get more information about the amount of dopant ions and the location of the dopant, EDX and time-resolved spectroscopy were performed respectively. Figure 4.16 shows the EDX spectrum recorded.

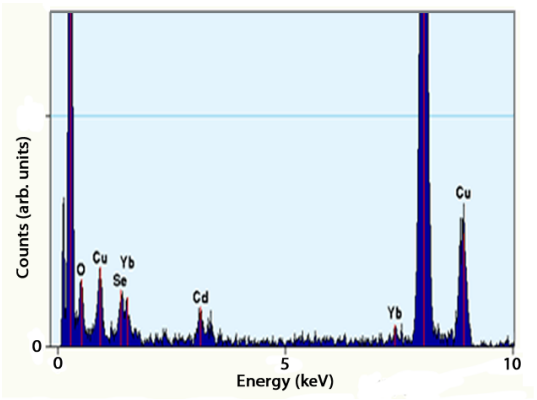

Figure 4.16: The EDX spectrum of sample DOP7 (ratio = 188:1).

In the EDX spectrum peaks for Cd, Se and Yb are observed. When analysing the results carefully, atomic ratios of 33%, 58% and 8% respectively are found. The dopant concentration is in the correct order for a monolayer of Yb and Se for a particle of 4.2 nm since these small particles have a relative large surface with respect to the volume.

Figure 4.17 shows the the lifetime measurement (black) including the exponential fit (red).

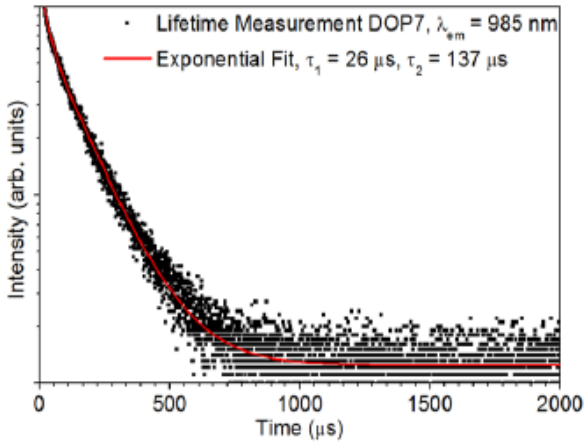

Figure 4.17: The lifetime measurement (black) of sample DOP7 (ratio = 188:1) and the exponential fit (red).

The data points of the decay curve were fitted to a biexponential fit, resulting in a lifetime of 26 µs and 137 µs. These lifetimes most likely originate from the ytterbium on the surface of the quantum dot (short lifetime) and the ytterbium incorporated in the quantum dot (longer lifetime). The radiative lifetime of the $^2F_{5/2} \rightarrow {}^2F_{7/2}$ emission is typically 0.5-1 ms[49], which decreases drastically to ca. 10 µs[50],[51],[52] in the presence of organic ligands and solvents. The observed 137 µs indicates the successful (partial) protection of the ytterbium from organic solvents and ligands, indicating successful incorporation into the quantum dots.

Another experiment performed on sample DOP7 was the comparison of the CdSe QD emission with that of the undoped QD emission under same conditions (λ_{exc}, concentration, etc.). Figure 4.18 shows the comparison between the quantum dot emission of sample DOP7 (red) and the original undoped quantum dots of sample CdSe2.6 (black).

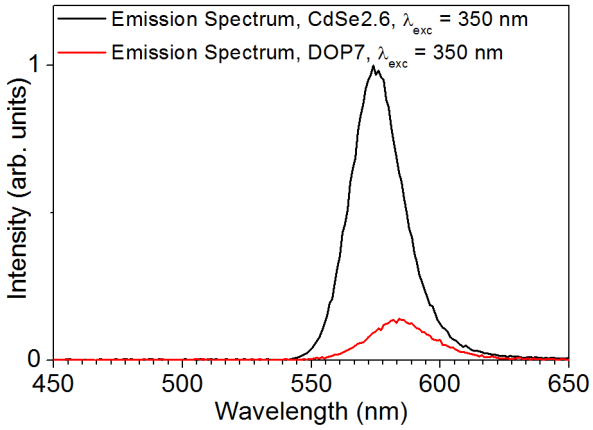

Figure 4.18: The CdSe emission for sample DOP7 (doped, red) and CdSe2.6 (undoped, black). The integrated intensity of the red curve is 16% of the original black curve.

As can be observed in the figure, the CdSe intensity decreases significantly after ytterbium incorporation. From the integrated areas the intensity of emission was calculated and it was found that the CdSe emission intensity of sample DOP7 is 16% of the original CdSe emission. The decrease in intensity is most likely due to the extra relaxation pathway via the ytterbium ion, although the ytterbium doping procedure might also give rise to surface defects resulting in extra quenching due to trap states.

From all the samples and experiments mentioned above, an optimised ratio between the ytterbium dopant and the CdSe quantum dots has been achieved. The ratio of ca. 175:1 was found to be optimal both in terms of energy transfer (ytterbium emission) as well as keeping the CdSe QDs intact during the doping and washing procedure.

4.3.2 Ytterbium acetate versus ytterbium oleate

As mentioned in the Experimental Section, multiple ytterbium precursors were used during the course of this thesis. It was already observed that ytterbium acetate did not dissolve in ODE, resulting in a dispersion. Because of the low solubility of the ytterbium acetate, an alternative precursor was tested for doping. Based on the hot injection synthesis, in which cadmium oleate was used as precursor by treating the cadmium acetate with oleic acid, a similar precursor solution was made with the ytterbium acetate. Ytterbium oleate was made by adding ytterbium acetate to a mixture of oleic acid and ODE and heating the solution under vacuum using a Schlenk line.

Figure 4.19 shows one of the samples (DOP11) made using the separated doping method using ytterbium oleate as a dopant precursor. Both the absorption spectrum and a TEM image of the sample are shown.

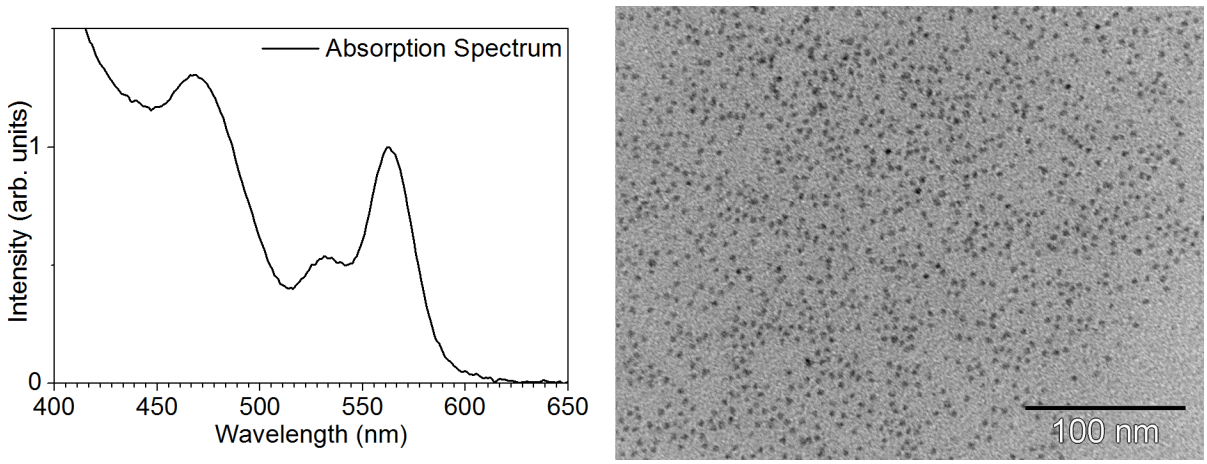

Figure 4.19: The absorption spectrum (left) and a TEM image (right; D = 3.95 ± 0.42 nm) of a sample made with ytterbium oleate as a precursor (DOP11).

Sample DOP11 was made using a ratio (ratio = 136:1) similar to the optimal ratio between the ytterbium acetate and quantum dots. Figure 4.19 shows a well defined absorption spectrum with a sharp first exciton absorption peak. The TEM image show monodisperse particles which are not aggregated. The data suggests that the extra coordinating ligand, oleic acid, does not inhibit the stability of the CdSe QDs.

The next step in evaluating the precursor is to check the ytterbium emission and lifetime and compare these to the optimised sample that was doped with ytterbium acetate. Figure 4.20 shows the emission spectrum and the lifetime measurement of sample DOP11.

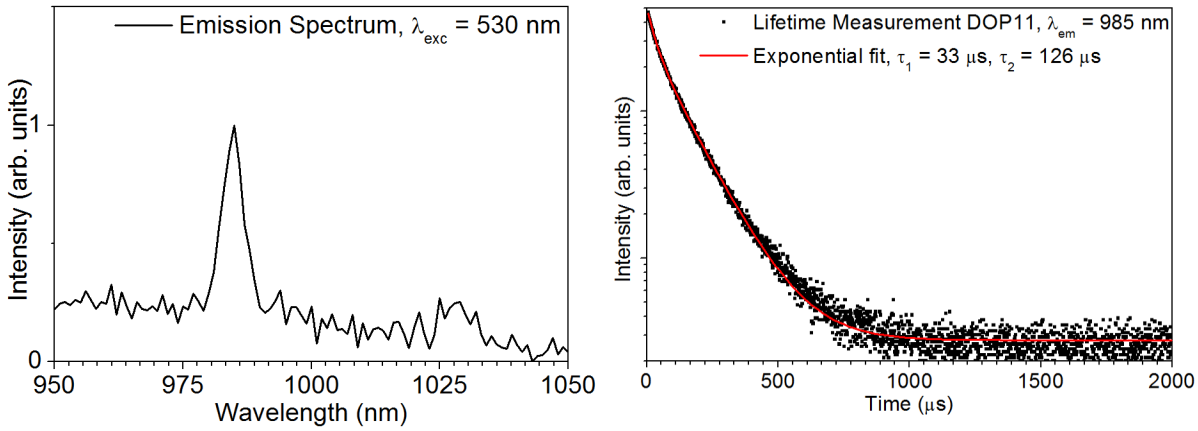

Figure 4.20: The ytterbium emission spectrum upon excitation of the CdSe (left) and the lifetime measurement of the ytterbium emission (right).

The emission spectrum shows a sharp and distinct peak at 985 nm with a smaller peak at 1030 nm, similar to the optimised ytterbium acetate sample (DOP7). The fitted lifetimes are 33 µs and 126 µs, which are similar to the sample doped with ytterbium acetate. From this data it can be concluded that the oleic acid has no negative effect on the incorporation of the ytterbium in the CdSe quantum dots. Due to the better solubility of the ytterbium oleate, this precursor will be used for the subsequent experiments.

4.3.3 The role of selenium after doping

All the samples prepared as described above have an extra amount of selenium added after the ytterbium doping similar to the method of Yang and co-workers[27]. A control sample (DOP12) was made in which no extra selenium was added after the reaction with ytterbium. From this sample an aliquot was taken before washing (DOP12UW). Ytterbium emission spectra have been acquired for both the washed and unwashed sample.

Figure 4.21 shows the spectra without selenium overgrowth, before and after washing. The emission peak is centered at 975 nm. On the right of Figure 4.21 the lifetime measurement of the unwashed sample is shown in comparison with the sample doped with ytterbium acetate (sample DOP7).

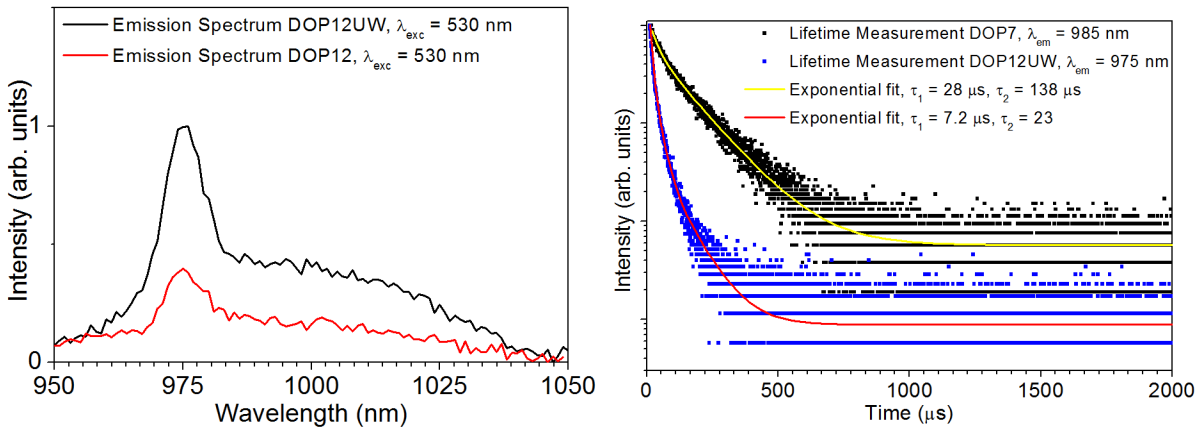

Figure 4.21: The ytterbium emission spectra of sample DOP12, unwashed (left; black) and washed (left; red). On the right, the lifetime measurement of the unwashed sample (blue/red; ratio = 188:1) compared to sample DOP7 (black/yellow; ratio = 188:1).

Clearly, the intensity of the ytterbium emission decreases after washing, indicating a weakly bound ytterbium species at the surface of the quantum dots. Because of the washing treatment ytterbium is partially removed from the nanocrystal surface. Not only the decrease in intensity after washing is apparent, also the initial intensity of the unwashed sample is low compared to the other samples. The emission wavelength is 975 nm and the spectrum shows a broad peak unlike the samples showing emission at 985 nm. The longest lifetime observed for sample DOP12UW is 23 µs, which is much lower than the lifetime of ytterbium emission found at 985 nm (138 µs) and comparable to the short lifetime of sample DOP7, attributed to ytterbium at the surface of the QDs.

Because of the extra layer of selenium the ytterbium is kept in place, resulting in more intense ytterbium emission and a longer lifetime, especially after washing. Due to the difference in chemical environment, the wavelength of the ytterbium emission is shifted 10 nm, which is possible for the lanthanides with either a high or a low amount of electrons in the f-orbitals. As a result of the more homogeneous lattice around the lanthanides of the sample with selenium overgrowth, the emission peak is more narrow as expected for lanthanide emission.

4.3.4 The rol of TOP during the doping

The selenium precursor used up to now was not a stable solution, because selenium does not dissolve in ODE. An alternative selenium precursor solution was prepared in which the selenium did dissolve. In this alternative precursor the selenium was first added to TOP to create a TOP-Selenium complex which is soluble in ODE. With this precursor 12 samples were made. Figure 4.22 shows the ytterbium emission peaks of two samples prepared (green, blue) which show a broad peak at 975 nm with low intensity. The samples depicted at the bottom of Figure 4.22 were made afterwards using the Se-precursor without TOP to confirm the spectral shift of the ytterbium emission towards 975 nm because of the TOP-Se precursor.

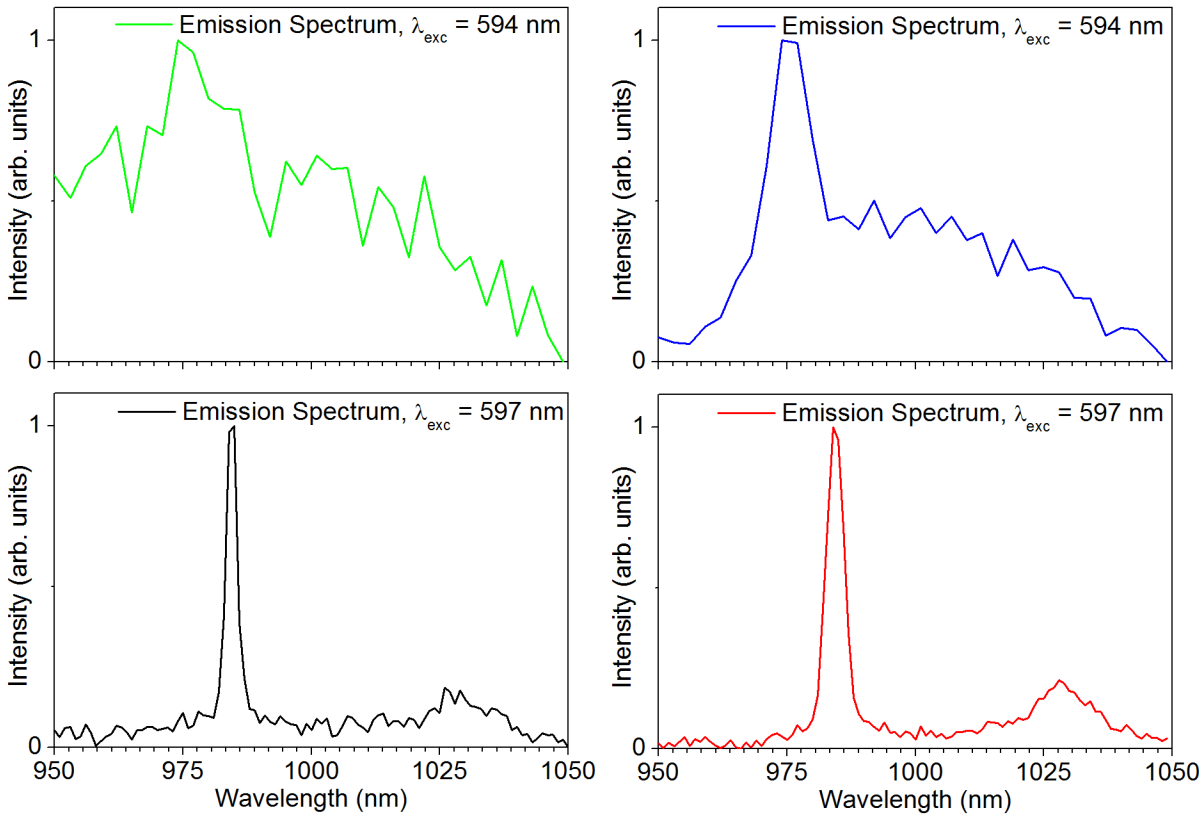

Figure 4.22: The ytterbium emission spectra of samples prepared with a TOP-Se precursor (top; green and blue) and with a Se precursor (bottom; black and red).

These experiments suggest that the TOP has some role in the doping procedure and with TOP present during the doping, the samples will show wide ytterbium emission at 975 nm. The spectra shown for the samples made in the absence of TOP show narrow peaks as found earlier. Figure 4.23 shows the lifetime measurements of this emission.

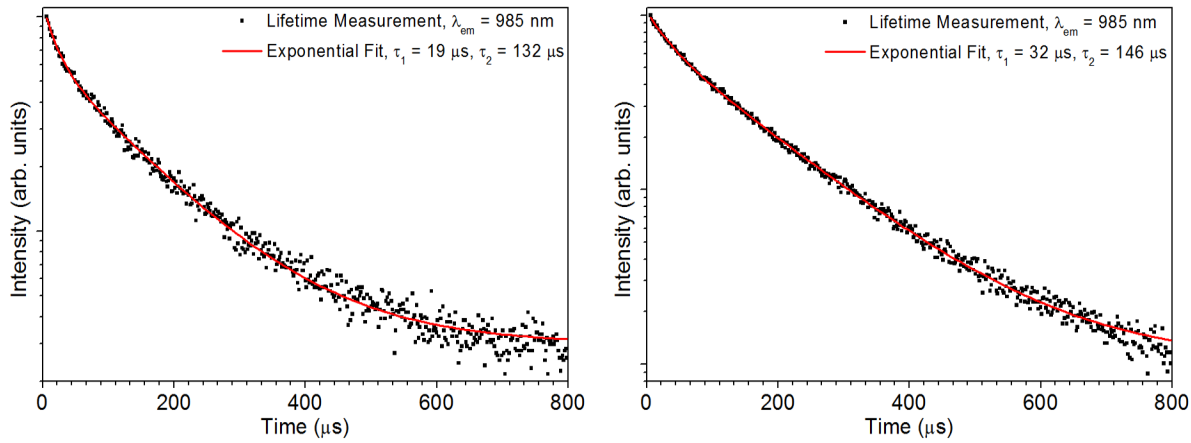

Figure 4.23: The lifetime measurements of the ytterbium emission of samples RG13 (left) and RG14 (right).

The lifetimes which correspond to the emission of the incorporated ytterbium ions are similar to values found in comparable experiments shown earlier in this work. From these experiments it can be concluded that the TOP has an important effect on the ability to incorporate ytterbium into CdSe quantum dots. This might be because of the stabilizing effect the TOP has on the selenium monomers. The selenium overgrowth is dependent on the adsorption of the selenium monomers on the ytterbium rich surface. It might be that the TOP-Se is thermodynamically favoured over the adsorption on the surface. In the absence of TOP, the selenium is not stabilized and the adsorption of selenium on the ytterbium rich surface is favoured.

4.3.5 Temperature dependence of the synthesis

Although the synthesis procedure described in the Experimental Section of this thesis was used throughout this work, experiments using different temperatures have been performed. Using different temperatures both above and below 265 °C the influence on the incorporation of ytterbium has been investigated. Figure 4.24 shows the ytterbium emission of different samples with either 255 °C (left) or 275 °C (right) as doping temperature .

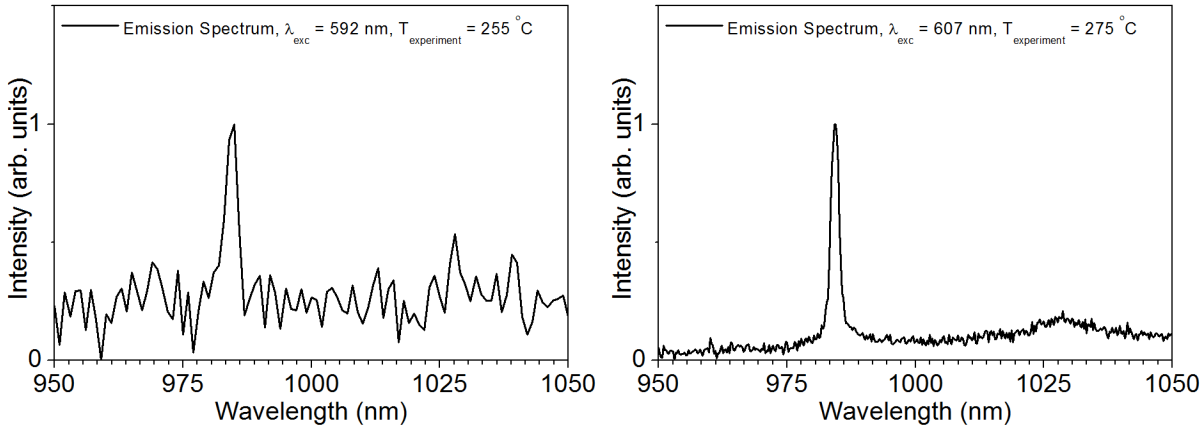

Figure 4.24: Emission spectra of CdSe quantum dots with ytterbium incorporation prepared at different temperatures. The spectrum on the left was a sample prepared at 255 °C, the spectrum on the right was of a sample prepared at 275 °C.

No EDX data has been acquired for these samples so the amount of dopant cannot be determined quantitatively. However, the quality of the spectra above suggest that the incorporation of the ytterbium was more successful for the higher temperature. The sample prepared at 255 °C barely rises above the noise and although a sharp peak at the expected wavelength is observed the intensity is low. The sample prepared at 275 °C however shows an intense peak with the distinctive second peak around 1030 nm present. From these spectra it can be concluded that the higher temperature has a positive effect on the incorporation of the ytterbium in the CdSe. This effect might arise from the fact that the higher temperature can result in the incorporation of more material or the diffusion of the material inside the quantum dot.

4.4 SILAR

To further incorporate the lanthanide dopant inside the nanocrystal a shell of CdSe was grown around the doped quantum dots using the SILAR method. Several different parameters have been varied to optimize the effectiveness of the nanoparticle growth.

4.4.1 Combined versus separated doping and SILAR

The reaction parameters for the doping procedure and the SILAR method are similar (temperature, solvent, etc.). Therefore, it was tried to prepare samples by combining both methods without intermediate washing of the samples. The resulting samples were investigated and the quality of the sample was compared to samples prepared by the separated doping and SILAR procedures. Figure 4.25 shows the emission spectra of sample DS1 (red) and DS14 (black). Sample DS1 was made with the combined

method while sample DS14 was prepared using separate steps of first doping the material, subsequent washing and after a few weeks performing SILAR.

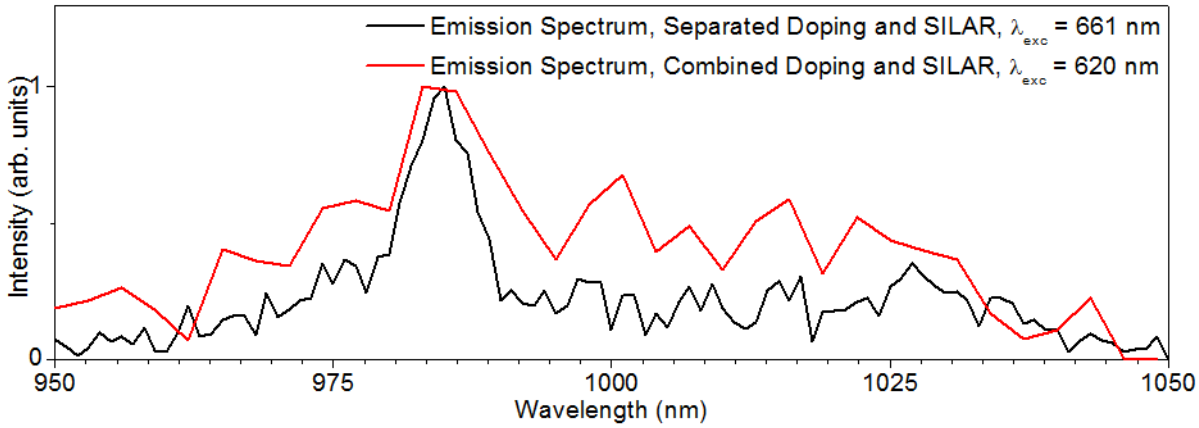

Figure 4.25: The ytterbium emission spectra of samples prepared with subsequent doping and SILAR (red) and separated doping and SILAR (black).

The ytterbium emission peak at 985 nm was much more pronounced for sample DS14, compared to sample DS1. Although optimization is still required to increase the emission intensity, the results suggests that the preparation of samples via a separated doping and SILAR method yields particles with a higher quality of ytterbium emission.

4.4.2 Starting Ion

Another parameter that was investigated is the effect of the choise of starting ion (Se or Cd) on the intensity of the Yb-emission from the final sample. To check this, different samples were made and compared. Figure 4.26 shows sample DS8 (black), which had cadmium as a starting ion and DS10 (red), which had selenium as a starting ion.

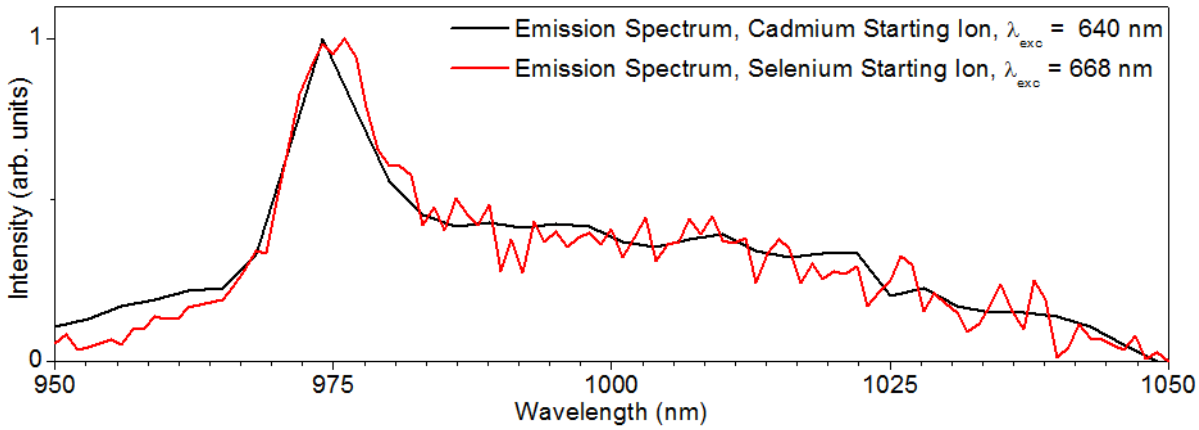

Figure 4.26: The ytterbium emission spectra of samples prepared with cadmium (black) and selenium (red) as starting ion during the SILAR treatment.

The black spectrum, which shows the sample with the cadmium starting ion, shows a much higher signal to noise ratio. The signal to noise ratio suggests a more well defined ytterbium emission, which is the result of higher quality particles.

4.4.3 TOPSe versus Se

For the doping methods it was observed that TOP plays an important role in the successful incorporation of the lanthanide ion. For this reason, the role of TOP was also investigated during the SILAR method after the already successful incorporation of the lanthanide. Figure 4.27 shows the ytterbium emission spectra of different samples produced using precursors either with (black) or without (red, green) TOP.

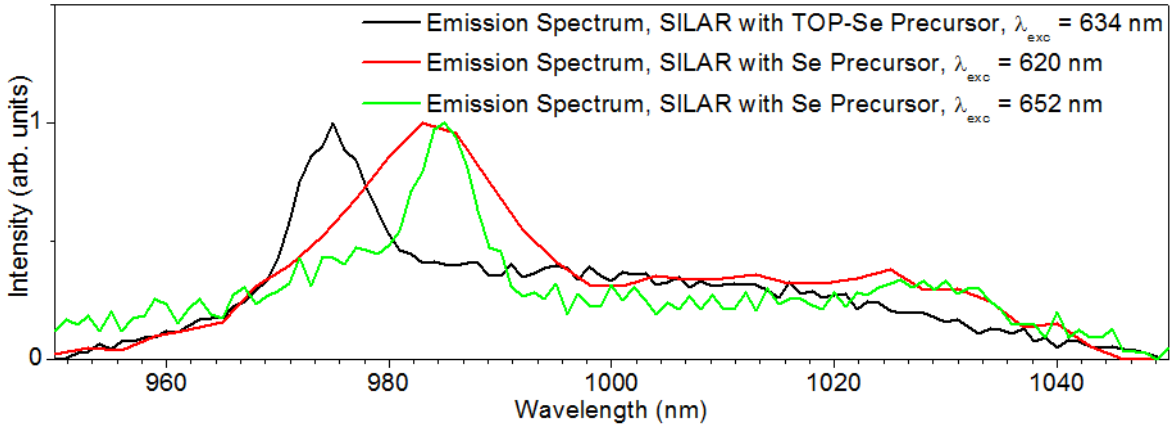

Figure 4.27: The ytterbium emission spectra of samples prepared with TOPSe precursor (black) and with Se precursor (red, green). The sample with the green emission spectrum was made using the separated doping and SILAR method.

From these spectra it can be observed that the location of the ytterbium emission peak shifts from 975 nm if TOP is used to 985 nm if a precursor without TOP is used, similar to the doping process. Even though the lanthanide is already incorporated in the material after the doping method, using a TOP-based selenium precursor destabilizes the loosely bound ytterbium and the peak shifts towards 975 nm. TOP results in selenium stripped from the surface and subsequent competition between the cadmium and the ytterbium. Another important observation here is the difference between the quality of the green and red spectrum. Sample DS7 (red) was produced by adding two extra layers of CdSe after the incorporation of the lanthanide while sample DS13 (green) was produced by adding three extra layers of CdSe after the incorporation of the lanthanide. The more sharp peak of sample DS13 suggests that the influence of the environment on the ytterbium is still present in the range of several monolayers of CdSe. The environment is more uniform in a system where the lanthanide is incorporated further away from the quantum dot surface.

4.4.4 # of CdSe layers vs Lifetime

As mentioned above, the extra layers added by the SILAR method strongly affects the ytterbium emission quality. Figure 4.28 shows the lifetime of samples with different amounts of CdSe layers. In the left part, the exponential fits of the lifetime measurements are shown and on the right side, the lifetime has been plotted versus the amount of monolayers.

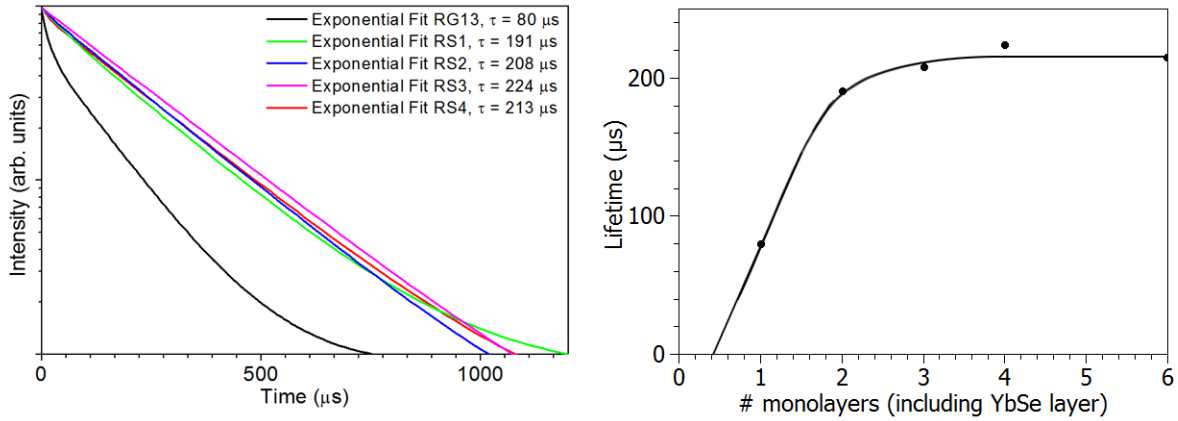

Figure 4.28: The exponential fits (left) of the different samples with varying amounts of CdSe layers added by the SILAR method for the ytterbium. The lifetimes plotted versus the amount of protective monolayers added (right).

From the figure it can be observed that the lifetime of the ytterbium emission increases drastically by addition of a monolayer and then reaches a plateau quite fast. The maximum observed lifetime was around 210 µs and the lifetimes of sample RS2 with 2 monolayers of CdSe added by SILAR (red) and sample RS4 with 5 monolayers of CdSe added by SILAR (dark blue) show no significant difference. In the plot of monolayers versus lifetime the initial selenium layer deposited during the doping method is counted as the first layer. Although the difference between two and three CdSe monolayers is not apperent in the lifetime measurements, it does affect the ytterbium emission intensity strongly (Figure 4.27).

4.5 Optimal sample

During this thesis the incorporation of ytterbium in CdSe nanocrystals has been investigated and optimized. Different methods of doping have been investigated and the most promising method has been chosen for further development. The concentration of dopant precursor has been optimized. Different dopant and selenium precursors as well as the role of the selenium addition after the ytterbium addition has been investigated. By combining the method with SILAR, extra layers of protective CdSe have been grown on top of the ytterbium-doped nanocrystals.

The SILAR method has been investigated with respect to the choice of starting ion and the use of selenium precursors (both with and without TOP). Furthermore, the possibility of combining the SILAR method and the doping method in one experiment has been evaluated. From these experiments it has been shown that the optimal ratio between quantum dots and dopant precursor is 1:30 for the ytterbium oleate precursor and the best results were obtained for the separated syntheses of doping and SILAR. The optimal selenium precursors for both the doping and the SILAR experiments did not contain TOP. The extra CdSe layers grown using the SILAR method had a large influence on the lifetime of the ytterbium emission. However, the effect of the extra layers decreased rapidly after several monolayers.

Figure 4.29 shows the absorption spectra of the samples made with the conditions described above. The black spectrum is the sample of undoped quantum dots, the red spectrum is the sample of doped quantum dots and the green, blue, magenta and dark blue spectra are the absorption spectra of samples with 1,2,3 and 5 extra CdSe layers respectively.

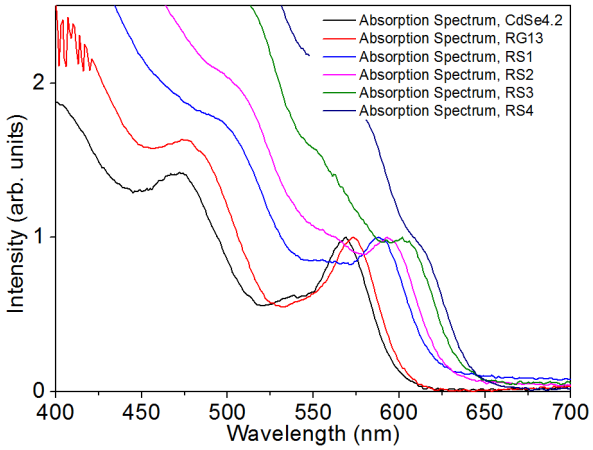

Figure 4.29: The absorption spectra of the samples made using the optimized conditions (black = undoped; red = Yb^{3+} doped; green = 1 layer SILAR; blue = 2 layers; magenta = 3 layers; dark blue = 5 layers).

The redshift in these spectra can be explained by the addition of a YbSe layer (from black to red spectrum) and addition of extra CdSe layers (from red to dark blue spectrum). The loss of distinctive features in the spectra can be explained in terms of particle size and size dispersion. Specifically, when the number of extra CdSe layers increases the size of the quantum dots increases and the particles are less monodisperse. No selective precipitation steps have been performed during the synthesis of the final sample and the ensemble is expected to be less monodisperse than the initial samples. The polydispersity of the sample gives rise to broader peaks in the absorption spectra.

Figure 4.30 (left) compares the excitation spectra (black, red) of sample RS4, the sample with 5 extra CdSe layers, with the absorption spectrum (green). Figure 4.30 (right) shows the ytterbium emission before (black) and after (red) the SILAR treatment.

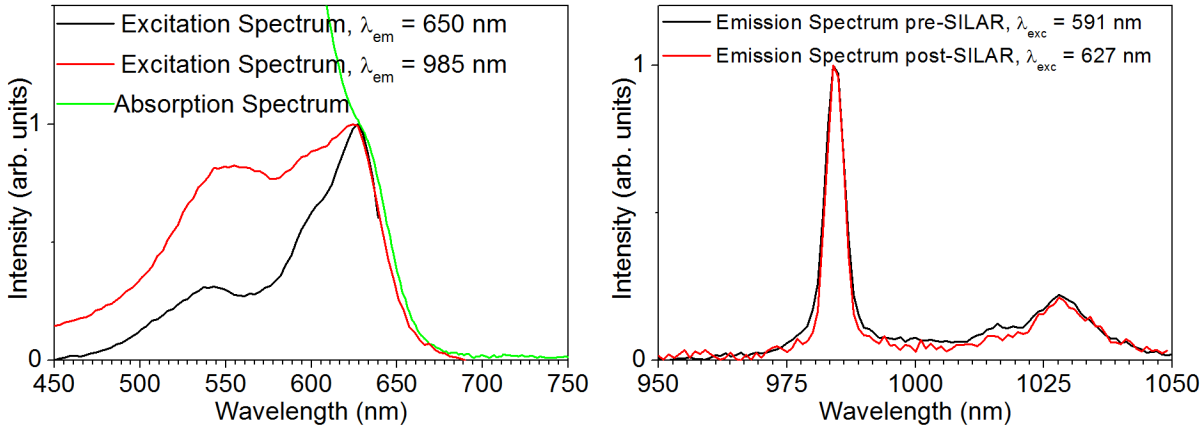

Figure 4.30: The excitation spectra (black, λ_{em} = 650 nm and red, λ_{em} = 985 nm) and absorption spectrum (green) of sample RS4 (left) and the ytterbium emission spectra before (black) and after (red) treatment with SILAR (right).

In the figure on the left, the excitation spectrum of CdSe emission (black), the excitation spectrum of ytterbium emission (red) and the absorption spectrum (green) match with respect to the first exciton peak, although this was harder to determine for the absorption spectrum since the characteristic features are less pronounced here. The figure on the right shows that the peak position and width reamin unchanged after the addition of extra CdSe monolayers via the SILAR method. However, the lifetime of the ytterbium emission is influenced by the extra monolayers of CdSe.

Due to the low intensity of the ytterbium emission, the measurements were performed using a large emission slit and a large step width to acquire a proper signal from the ytterbium. To determine the full width at half maximum (FWHM) of the lanthanide emission, the measurement was performed using smaller slit widths and longer measurement times. Figure 4.31 shows the results of these measurements. The image on the left shows the spectrum (black) and Gaussian fit (red) of the short measurement with a large slit width while the right image shows the spectrum (black) and Gaussian fit (red) of the long measurement with a small slit width.

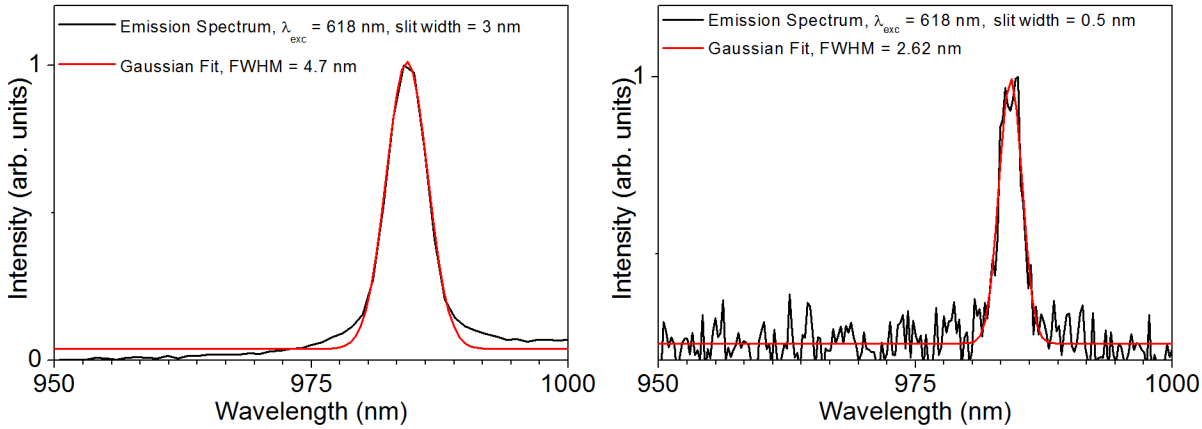

Figure 4.31: The ytterbium emission spectra and corresponding FWHM of sample RS4 with a slit width of 3.0 nm (left; FWHM = 4.7 nm) and a slit width of 0.5 nm (right; FWHM = 2.6 nm).

To determine the FWHM, the emission spectra were plotted using Origin 8.6. A Gaussian fit was applied to these excitonic emission spectra and were optimized using a simplex. The FWHM was then obtained by carefull inspection of the Gaussian fit. The FWHM of these two emission peaks are 4.7 nm and 2.6 nm respectively. This experiment shows that the larger slit width causes broadening of the measured emission peak. The FWHM of the ytterbium emission peak is around 2.5 nm which is as expected of a lanthanide emission peak at room temperature. Measurements of the FWHM of the ytterbium emission measured with a slit width of 0.24 nm yielded a FWHM of 2.32 nm (not shown here).

4.6 Emission at low temperature

We study the temperature dependence of the ytterbium emission, because low temperature emission spectra provide information about the temperature dependance of the energy transfer process and the ytterbium crystal field splitting[49]. Figure 4.32 shows spectra measured at different temperatures, ranging from 5 K to room temperature.

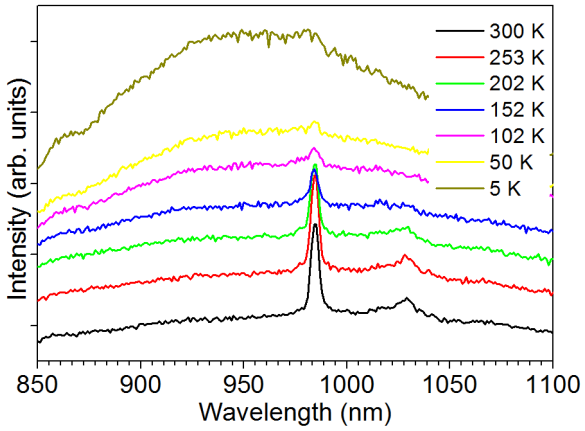

Figure 4.32: The ytterbium emission spectra at different temperatures, ranging from 5K to room temperature.

As can be observed from the spectra, a large broad band increases with decreasing temperature. Due to the width of the band it is not likely that this band originates from the Yb^{3+} $^2F_{5/2} \rightarrow {}^2F_{7/2}$ transition. The band is most likely caused by emission from trap states in the CdSe quantum dots. At lower temperatures trap states can no longer relax in a non-radiative fashion and the large broad band rises. Due to this broad band the information of the ytterbium emission is lost and no usefull data concerning the ytterbium emission can be obtained.

4.7 Fraction of particles doped

The spectroscopic data shown here suggests that the incorporation of the ytterbium in CdSe quantum dots was successful. However, from the shown data it can not be determined whether the whole ensemble of quantum dots or only a fraction of the quantum dots have successfully incorporated ytterbium ions. To investigate this, the lifetime of the excitonic CdSe emission has been investigated. Two different samples have been prepared and measured. Figure 4.33 shows these samples in which the black curve corresponds to undoped quantum dots and the dark blue curve corresponds to the doped quantum dots.

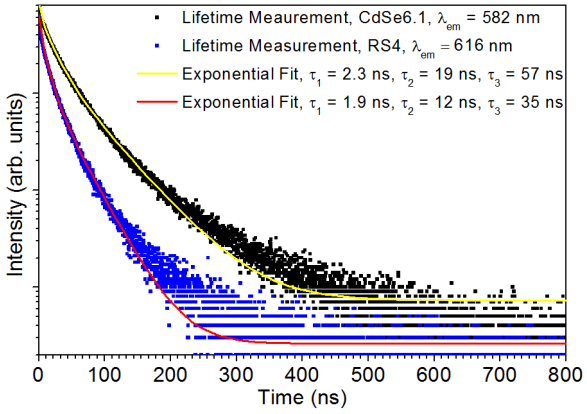

Figure 4.33: The lifetime measurements of the CdSe emission and the exponential fits before (black/yellow) and after (blue/red) doping with ytterbium.

The measured samples were quite concentrated and this results in energy transfer between the different quantum dots. Due to this energy transfer, the exponential decay of the measured samples was not monodisperse. A multi-expontial resulted in the best fit (lowest χ). However, more information can be extracted from the data by calculating the average decay time. This can be done using equation 4.1.

$$\tau_{av} = \frac{\sum \tau_i * \mathrm{I}_i}{\sum \mathrm{I}_i} \tag{4.1}$$

In which, τ_{av} is the average lifetime, I_i is the intensity at point i and τ_i is the lifetime at point i. For sample CdSe6.1 this equation yields an average lifetime of 50.6 ns and for sample RS4 an average lifetime of 30.8 ns. The data shows a decrease of the average lifetime in the doped sample with respect to the undoped sample, which reflects the presence of an additional pathway for the relaxation of the excited CdSe state via the ytterbium. Another important thing that can be observed, is the fact that the incorporation of ytterbium affects the whole decay curve. If only a fraction of the quantum dots was doped with ytterbium it would be expected to find a decay curve in which first a steep slope was present, while a longer decay tail similar to the curve of the undoped sample would be present. Since this is not the case we expect that all the quantum dots are doped with ytterbium rather than just a portion of the quantum dots.

Chapter 5

Varying the lanthanide dopant

After the successful incorporation of ytterbium in CdSe quantum dots, the posibility to incorporate several other lanthanide ions has been investigated. Due to the similarities between trivalent lanthanides (radius, valence, etc.), it is expected that the incorporation as performed in this thesis is a general approach. The optimized parameters, based on the ytterbium incorporation experiments, were used to investigate the incorporation of europium, erbium and thulium in CdSe quantum dots. In particular, using erbium, europium and thulium acetate salts in combination with oleic acid three different concentrated oleate precursor solutions have been prepared.

To investigate the incorporation of the lanthanides spectroscopic studies were performed both before and after the treatment of the potentialy doped CdSe nanocrystals with SILAR. Furthermore, EDX spectra have been recorded for samples after the doping procedure and SILAR. The results are shown below.

5.1 Europium

Firstly, we tried to incorporate Eu^{3+} in CdSe quantum dots. Figure 5.1 (left) shows the emission spectrum from (500-700 nm) of CdSe quantum dots after the doping process performed with europium (sample Eu D1). Figure 5.1 (right) shows the excitation (black) and emission (red) spectra of the sample (Eu DS1) after SILAR.

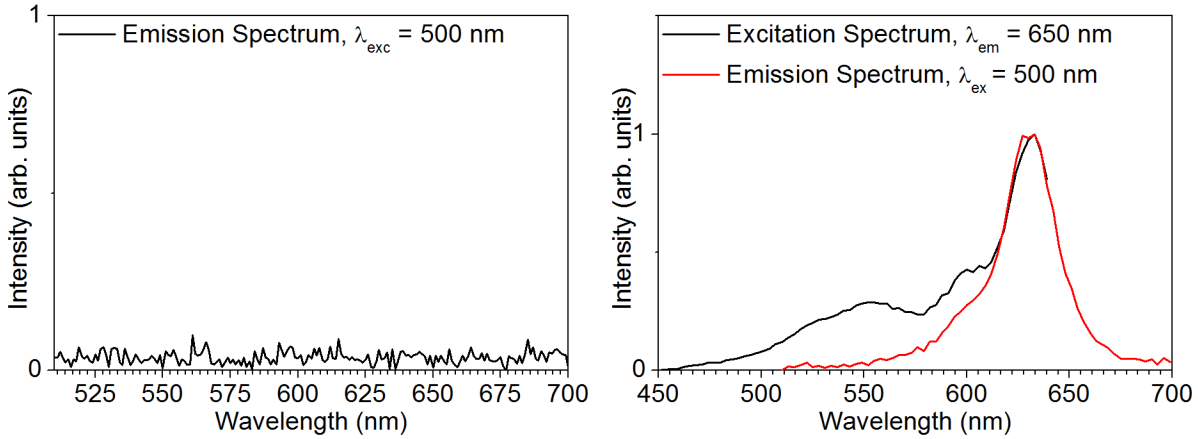

Figure 5.1: The emission spectrum from (500-700 nm) of CdSe quantum dots after the doping process performed with europium (left; sample Eu D1) and the excitation (black) and emission (red) spectra of the sample after SILAR (right; Eu DS1).

Clearly, the spectrum on the left shows no CdSe quantum dot emission. Although the sample (Eu D1) is coloured and the absorption spectrum resembles the characteristic CdSe absorption spectrum, no CdSe quantum dot emission is observed. The characteristic CdSe quantum dot emission and excitation returns after the overgrowth of CdSe by SILAR.

Figure 5.2 shows the emission spectrum of sample Eu DS1 for a region (800-1800 nm) where multiple europium peaks would be expected if europium incorporation is successful and host-dopant energy transfer occurs.

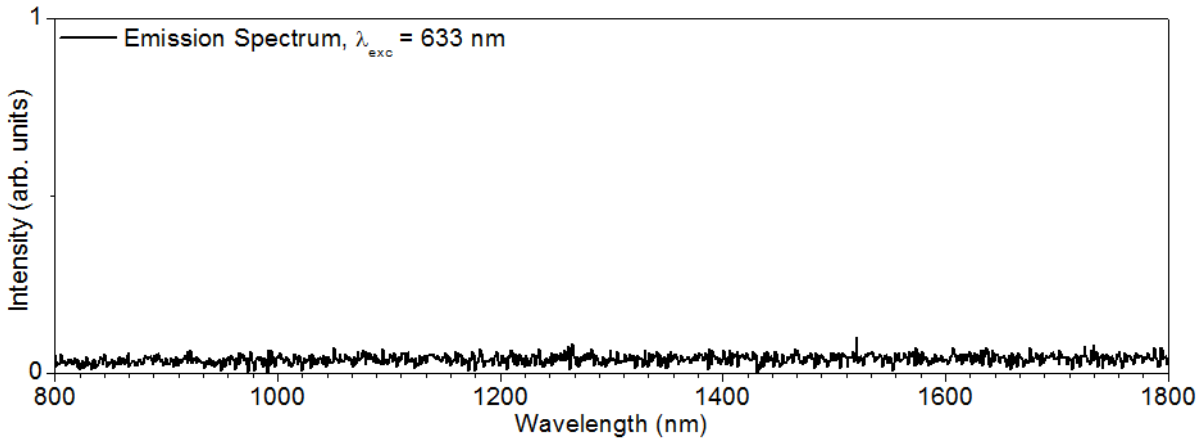

Figure 5.2: The emission spectrum of sample Eu DS1 from 800 to 1800 nm, where multiple europium peaks would be expected if europium incorporation is successful and host-dopant energy transfer occurs.

No (europium) emission is observed in the investigated region. This can be attributed to a lack of europium incorporated into the system, a lack of energy transfer between the host CdSe quantum dots and the dopant or due to alternate pathways for the relaxation of the europium in a non-radiative manner. Note that europium can also be excited in the energy range of the CdSe bandgap due to the transitations of the $^5D_0$ and $^5D_1$ states to the $^7F_0$ ground state.

In literature, Raola and coworkers[46] have shown the incorporation of europium inside CdSe although no spectroscopic data was presented. This might be a strong indication that europium doped CdSe quantum dots do not show any europium emission.

To determine if the europium is present in the CdSe quantum dots, several EDX spectra were recorded and one of these is shown in Figure 5.3.

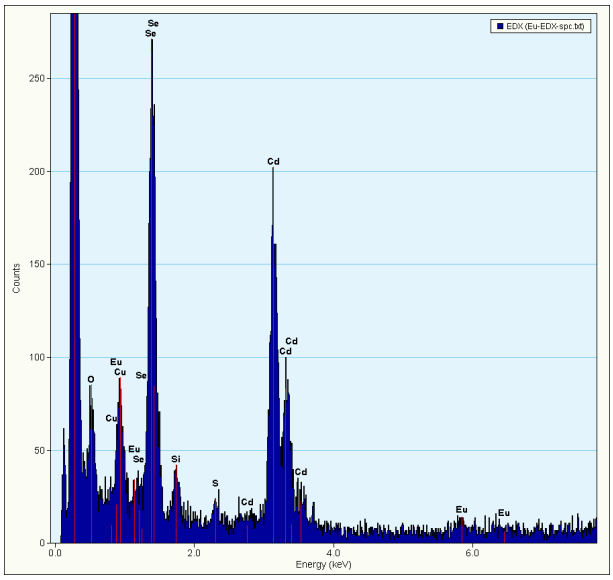

Figure 5.3: An EDX spectrum of the sample treated with europium and SILAR. Although low in intensity characteristic europium peaks are present around 6.0 keV.

In the EDX spectrum it can be seen that several characteristic europium peaks are present around 6.0 keV, although the intensity of the signal is weak. By integrating the signal of europium, selenium and cadmium an atomic ratio of 55:42:3 (selenium:cadmium:europium) was found, which corresponds to CdSe with a little bit of europium incorporated.

One explanation for the lack of europium emission is the presence of very efficient non-radiative pathways. Figure 2.5 shows that the europium has a high number of energy states (*e.g.* $^7F_6$ - $^7F_0$) which can result in more efficient quenching.

It might also be that the europium is still present in the solution as an organic complex. This would explain the presence of the europium in the EDX spectrum (although in lower amounts with respect to the ytterbium samples) and the absence of europium emission. The lack of europium emission can be explained by the lack of energy transfer from the CdSe and the efficient quenching of organic vibrations from the organic complex.

A third explanation is the fact that the temperature was not sufficient for the successful incorporation. For these experiments a new thermometer was used, which might have an offset compared to the old thermometer. It was already shown that the incorporation of the ytterbium dopant was temperature dependant and it could be that the temperature in these experiments were too low for sufficient incorporation. This would explain the lower amount of europium present in the sample compared to the ytterbium samples (3% instead of 8%).

5.2 Erbium

Another lanthanide which has been investigated, was erbium. Again, both spectrofluorometry and EDX were used to investigate the optical properties and the amount of dopant incorporated in the CdSe nanocrystals. EDX was performed on the sample prepared by doping and susequent SILAR adding three monolayers of CdSe. The optical properties were measured both before and after the treatment with SILAR.

Figure 5.4 shows the excitation spectrum (black) of CdSe quantum dot emission and the emission spectra from 450 - 1600 nm (red, green). In this region the CdSe quantum dot emission and several erbium emission peaks are expected.

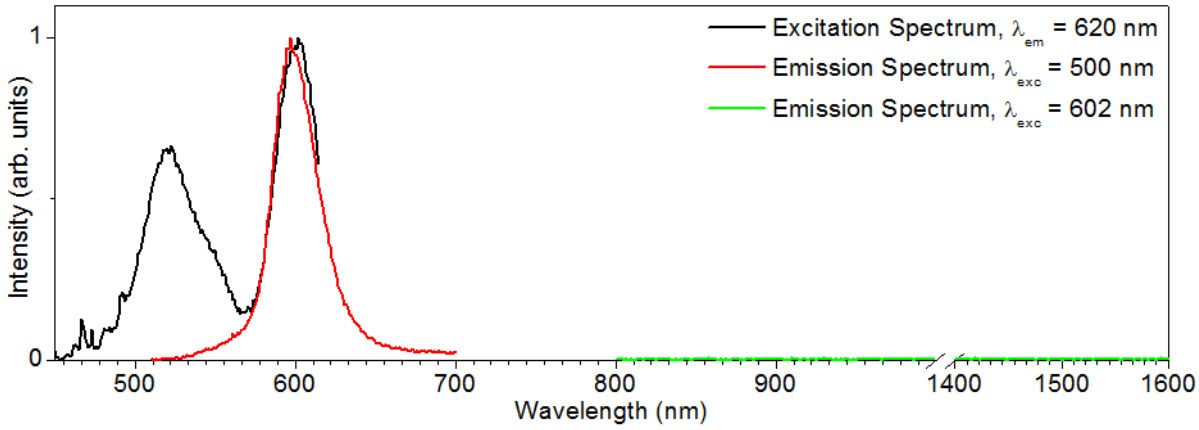

Figure 5.4: The excitation spectrum (black) of CdSe quantum dot emission and the emission spectra from 450 - 1600 nm (red, green).

From the spectra it can be seen that the CdSe emission is still present before SILAR, as opposed to the europium sample. In the sample before SILAR, no erbium emission is detected.

Figure 5.5 shows the same spectra but for the sample of potentially erbium doped quantum dots treated with SILAR adding three layers of CdSe.

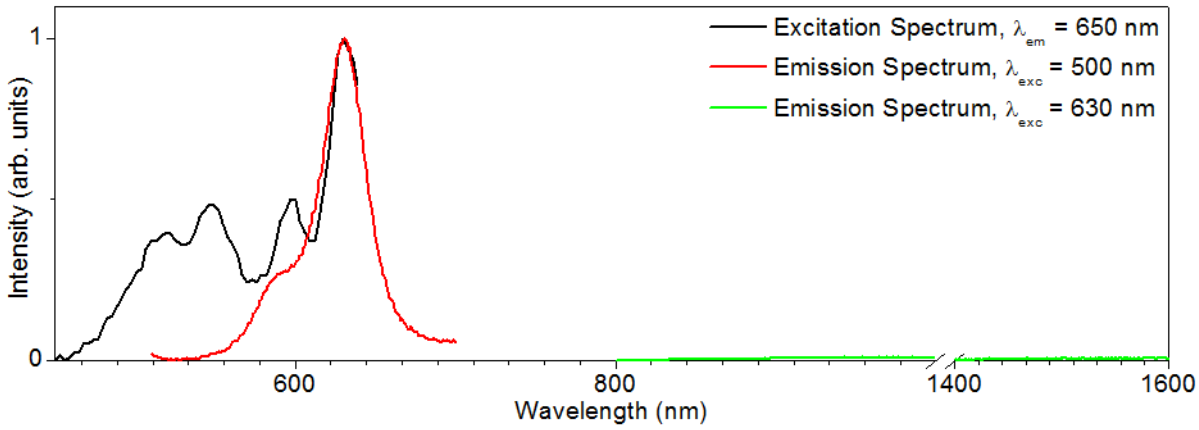

Figure 5.5: The emission (red) and excitation (black) spectra of CdSe and the (lack of) emission (green) of the erbium in the range of 600-1800 nm for the sample treated with SILAR adding three layers of CdSe.

Figure 5.5 shows no significant changes with respect to Figure 5.4 other than a redshift due to increasing size as a result of SILAR. From the spectroscopic measurements, no indications of successful incorporation of erbium has been observed.

To check the incorporation of the erbium in the CdSe quantum dots, an EDX spectrum were recorded. Figure 5.6 shows this EDX spectrum.

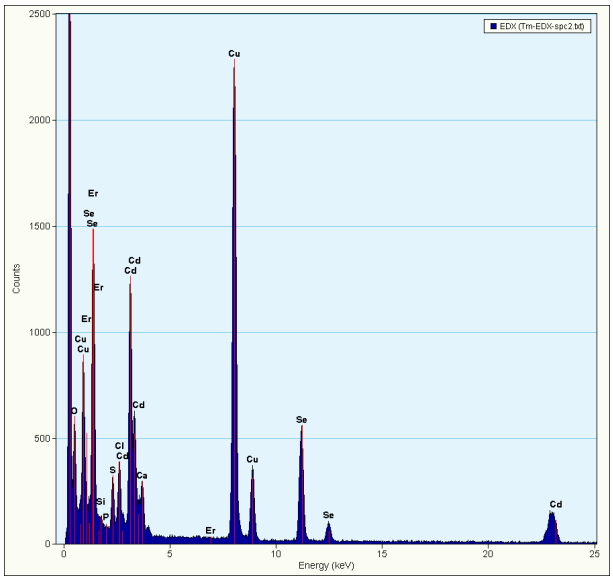

Figure 5.6: The EDX spectrum of the sample treated with an erbium precursor and SILAR. No erbium signal is found at the expected 6.5 keV.

No signal is found at the expected energy, which is roughly 6.5 keV (as shown in the figure). From these datasets it can be concluded that no succesful incorporation of the erbium has been achieved.

5.3 Thulium

Another lanthanide which has been investigated, was thulium. Again both spectrofluorometry and EDX were used to investigate the optical properties and the amount of dopant incorporated in the CdSe nanocrystals. EDX was performed on the sample prepared by doping and susbsequent SILAR, adding three monolayers of CdSe. The optical properties were measured both before and after SILAR.

Figure 5.7 shows the emission and excitation spectra of both the CdSe and the emission of the different wavelength ranges where thulium is expected to emit before SILAR.

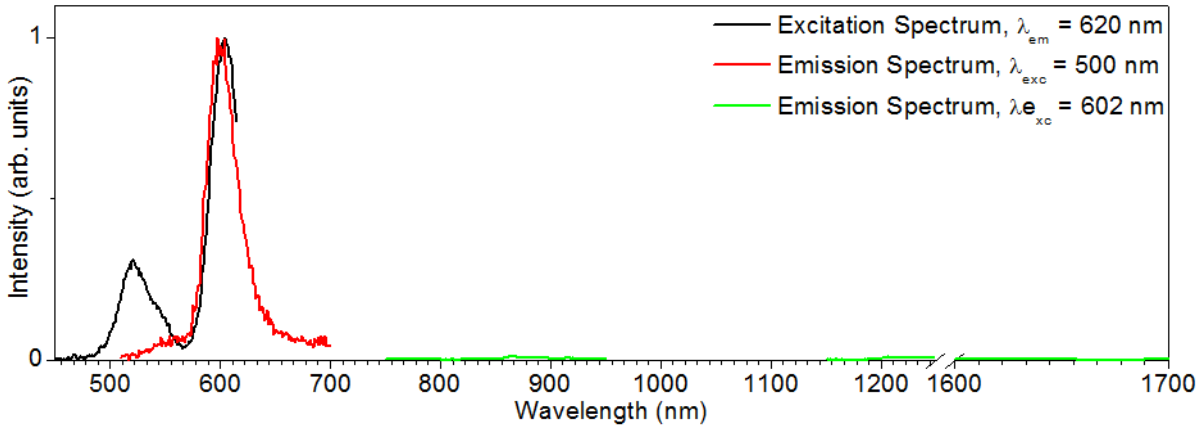

Figure 5.7: The emission (red) and excitation (black) spectra of CdSe and the (lack of) emission (green) of the thulium in the range of 600-1800 nm for the sample before SILAR.

From the spectra it can be seen that the CdSe emission and excitation is still present, as opposed to the results from the europium sample. Although no emission is detected between 1150 nm and 1250 nm and 1600 nm and 1700 nm, some emission although very weak has been seen around 850 nm. Although some emission is observed, it is not possible to say whether the emission is an artefact or real emission from the lanthanide.

The emission and excitation spectra of the sample treated with the thulium precursor and subsequent SILAR treatment adding three layers of CdSe will give more information about the emission found around 850 nm. Figure 5.8 shows these spectra.

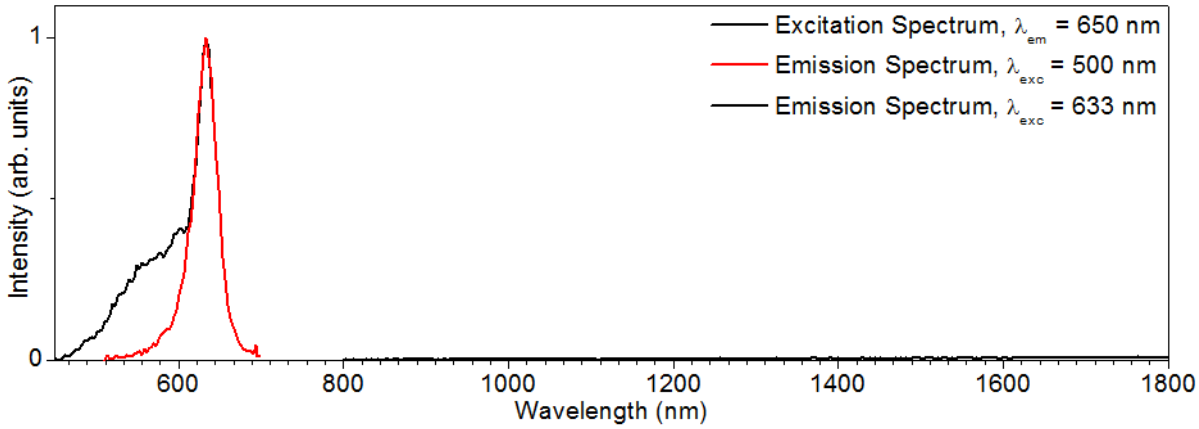

Figure 5.8: The emission (red) and excitation (black) spectra of CdSe and the (lack of) emission (green) of the thulium in the range of 600-1800 nm for the sample after SILAR, adding three layers of CdSe.

The peak observed before SILAR, has disappeared while the CdSe emission and excitation spectra have not changed significantly except for the redshift which is due to the increasing size. This suggests that either the SILAR experiment has removed the thulium from the surface, the thulium emission has been quenched by SILAR or that the emission observed before SILAR was some kind of artefact of

another source. To check the incorporation of the thulium in the CdSe quantum dots a EDX spectrum has been made and this spectrum is shown in Figure 5.9.

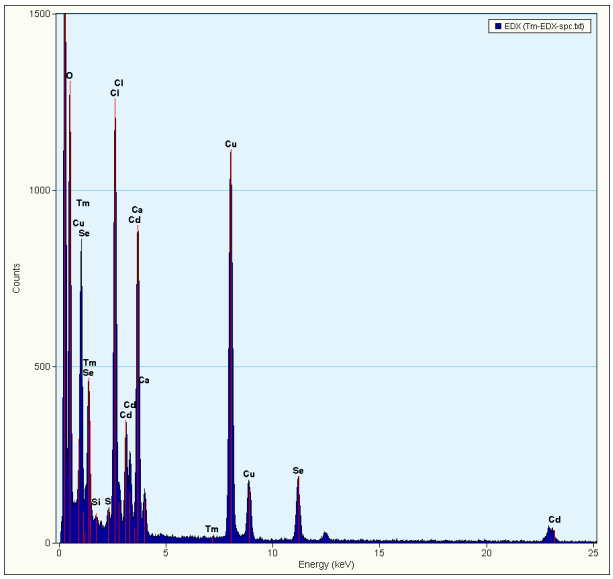

Figure 5.9: The EDX spectrum of the sample treated with an thulium precursor and SILAR. No thulium signal is found at the expected 7.5 keV.

No signal is found at the expected energy, which is roughly 7.5 keV (as shown in the figure). From these datasets it can be concluded that no successful incorporation of the thulium has been achieved. It is unlikely that the treatment with the SILAR method has removed the thulium from the surface, since this did not occur during the experiments with ytterbium incorporation.

Although the europium, erbium and thulium doping have been performed following the same procedure, not all doping experiments were successful. This might be due to a small discrepancy in the temperature since the samples were placed at different location of the heating block. If the doping experiment is very temperature dependent and if the temperature was higher (or lower) at the location of the europium sample it might explain the difference between the successful europium doping and the unsuccessful incorporation of the erbium and thulium.

Chapter 6

Lapis Philosophorum

During the course of this thesis a super promising lead has been found during the investigation of one of the samples using EDX. The TEM sample RG14 was prepared by deposition of a droplet of dispersion on a TEM-grid and this TEM-grid was further transferred towards the TEM using properly cleaned tweezers and a clean gridholder. The resulting TEM image and EDX spectrum are shown in Figure 6.1.

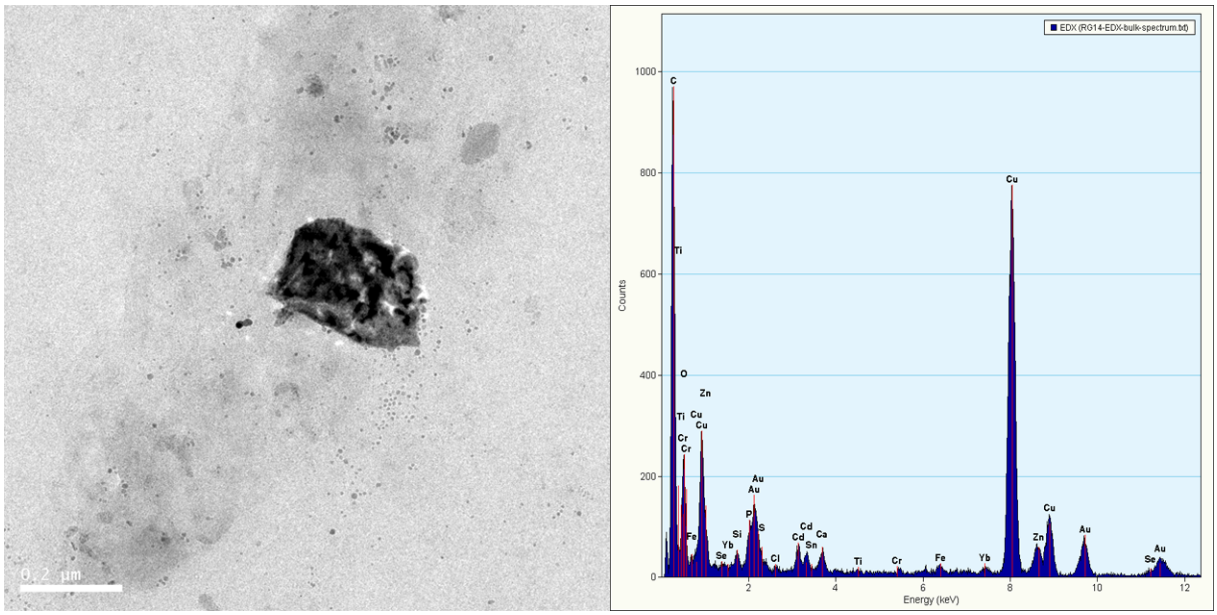

Figure 6.1: A TEM image of a large solid cluster surrounded by smaller nanoparticles (left) and the EDX spectrum of the imaged area (right).

During the preparation of sample RG14, in which CdSe:Yb^{3+} should be present in the presence of organic ligands, a yet unknown reaction has occurred resulting in a large solid particles which is roughly 200 nm. It is expected from the EDX spectrum that the chemical composition of the solid is mostly Zn, Cd and Sn based. The presence of these materials could be explained by the presence of a toxic cloud of all kinds of nasty chemicals present in the synthesis glovebox present at the CMI group. Since it is known that several students have worked with Zn, Cd and Sn based materials this assumption is justified.

The most promising results here however are the presence of chromium and gold in the EDX spectrum. We expect the large solid to be consistent with the Zn, Cd and Sn signals and that the large solid is capped with organic ligands to keep it dispersed in the organic solvents that we are working with. The small nanoparticles present around the large lump are roughly 5 nm in size and we are expecting these small particles to be the source of the gold and chromium. The following model is suggested for the formation of the gold and chromium nanoparticles.

During the first step of the reaction the hot injection of selenium to a cadmium rich phase leads to the formation of CdSe nanocrystals as described by Qu and Peng[17]. Subsequently some of the toxic nasty chemical cloud (TNCC) is dissolved in the liquid medium and the TNCC materials are clustering due to apolar solvent. A large portion of the CdSe nanocrystals migrate towards the cluster and reorganisation

takes place where the particles coalesce with the large cluster and the ligands are redistributed along the surface of the cluster which is increasing size. The driving force behind this phenomenon is the fact that the ligands available for stabilization of the surface is larger than the increase of surface due to coalescence with the nanocrystals. The resulting complex cluster is the lapis philisophorum, capable of performing chrysopoeia, in which base metals are converted to gold or silver according to Cleopatra the Alchemist[53],[54].

Although our results agree with the theory provided by Cleopatra *et al.* the presence of the chromium can not be explained. The results however have to be interpreted with a historical perspective since the knowledge in the time of Cleopatra (3rd or 4th century) was limited. This can be made clear by a sentence made famous by Led Zeppelin: "There's a lady who's sure all that glitters is gold". Since chromium is very reflective it could be that still in the seventies of the last century (the production date of Led Zeppelin IV, featuring the song Stairway to Heaven, was recorded between December 1970 and March 1971) people would still think of chromium and gold as the same material.

Knowing no difference between gold and chromium it might be that Cleopatra made a hasty generalization and we propose that the lapis philosphorum can perform chrysopoeia not only towards the noble metals gold and silver, but to more materials, for instance chromium. The possible transitions of metals are as of yet unknown and more research towards this topic will be addressed in further work.

Chapter 7

Discussions

7.1 Separated versus simultaneous doping and CdSe formation

As shown in the results, the cluster method for the incorporation of the ytterbium into CdSe nanocrystals did not succeed. In fact, only the experiments in which the CdSe is first synthesized and afterwards the lanthanide is introduced, show incorporation of the lanthanides into the CdSe material. This can be explained by nucleation and growth as explained in the theory. Due to the low affinity of lanthanides for the CdSe lattice (different valency, orientation number, etc.) the bulk term (Equation 7.1) will increase, leading to larger values for the critical radii of nuclei containing lanthanides ions.

$$\Delta G_{bulk} = -\frac{\frac{4}{3}\pi r^3}{v_0} kTln(\frac{S}{S_0}) \tag{7.1}$$

In this case the critical radius of lanthanide doped CdSe is larger than the critical radius of the CdSe nuclei, making the formation of CdSe nuclei the dominant process. Afterwards, during the growth phase, cadmium precursors have a much larger affinity than the lanthanide precursor, leading to the growth of the CdSe with additional cadmium and selenium. Only after the washing of the sample, in which case the excess cadmium precursor is removed, adding lanthanide precursors can lead to succesfull incorporation.

7.2 Lanthanide doped CdSe quantum dots

Not a lot is known about the mechanism of the energy transfer of the quantum dot towards the lanthanide dopant. From the spectroscopic measurements we know the energy difference between the conduction and valence band of the CdSe quantum dots (first excitonic absorption peak). Furthermore, the energy difference between the excited $^2F_{5/2}$ state and the ground state, $^2F_{7/2}$ of the ytterbium ion (ytterbium emission peak) has been investigated. The relative position of the energy levels of the lanthanides with respect to the CdSe VB and CB are however unknown. However, we expect that the $^2F_{5/2}$ and $^2F_{7/2}$ states are located in the bandgap. Figure 4.32 from the low temperature experiments, shows a broad peak arising from ca. 800-1100 nm. This peak is most likely due to trap state emission. However, it might be that the sufficient low temperature might give rise to the radiative relaxation from the CB to the $^2F_{5/2}$.

To explain the energy transfer, a two-step mechanism is proposed in which the trivalent ytterbium ion is reduced and oxidized. First the electron moves from the exciton to the Yb^{3+}, reducing it, resulting in Yb^{2+} which will have different energy levels and a different binding strength. In the second step the hole will be transferred to the Yb^{2+}, resulting in an excited ytterbium atom ($Yb^{3+,*}$), as illustrated in Figure 7.1[1].

[1] Courtesy of professor Rabouw

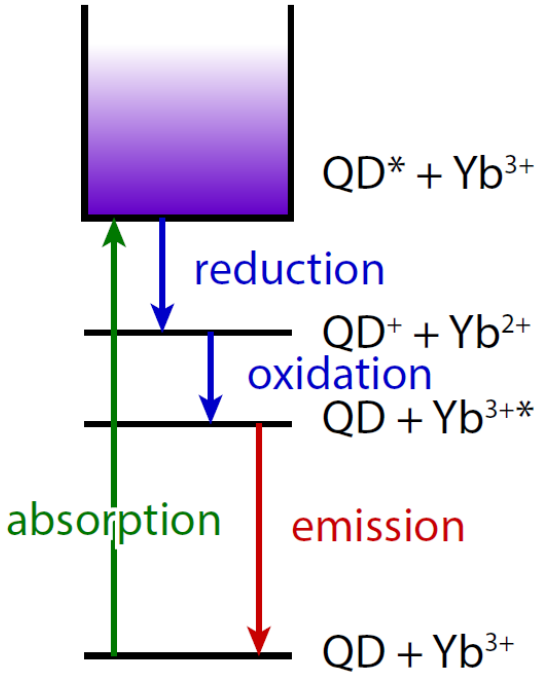

Figure 7.1: The proposed two-step mechanism for the energy transfer from CdSe quantum dots to the ytterbium dopant. In the first step the quantum dot gets excited and creates and exciton. Subsequently, the ytterbium gets reduced by the electron, then the ytterbium gets oxidized by the hole in the valence band resulting in an excited ytterbium state. Finally, the excited ytterbium relaxes, resulting in typical emission of 975-985 nm and 1030 nm.

As mentioned in the results it is very likely that the ytterbium is incorporated in the whole quantum dot ensemble. Since the radiative lifetime of quantum dots is around 10 ns and energy transfer rates are much faster (typically around 10-100 ps) it would be expected that all excitons will relax non-radiatively via the energy transfer towards the ytterbium and the quantum dot emission would be completely quenched. Although not expected, the CdSe emission is usually still detected for the ytterbium doped samples and this observation combined with the spectroscopic results have led to the model for the incorporation as depicted in Figure 7.2.

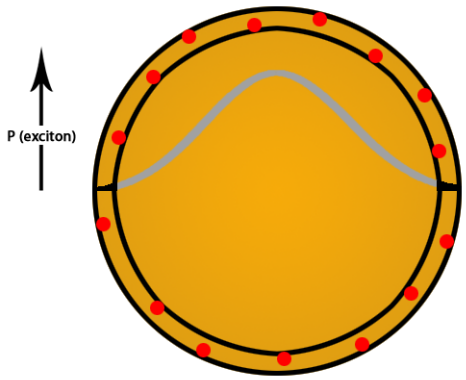

Figure 7.2: The proposed model for the CdSe:Yb^{3+} system. The probability of finding an exciton as a function of the distance from the quantum dot core. The area underneath the gray part of the Gaussian is the chance that no interaction between the dopant (red dots) and the exciton is present, the area under the black ends of the Gaussian correspond to the overlap of the exciton and the dopant.

The lifetime measurements, the experiments with the selenium after doping and the fact that TOP has such a large influence on the ytterbium emission indicate that the CdSe is not homogeneously doped with ytterbium, but that we have some kind of core/shell CdSe/YbSe heteronanoparticles. The fact that we still observe CdSe emission can be explained by this model. For the efficient energy transfer of the CdSe to the ytterbium we need to satisfy two conditions. The first condition is that the relaxation pathway via the ytterbium is much faster than the radiative relaxation by emitting a photon. The second condition is that the exciton wavefunction needs to have significant intensity at the ytterbium position. This overlap would be high in the case of homogeneously doped quantum dots and relatively low in the condition of the core/shell particle in which the exciton is localized in the CdSe 'core' and the ytterbium is present in the shell. The probability of finding the exciton at the surface of the quantum dot is much lower than finding the exciton at the centre of the quantum dot as shown in Figure 7.2. Due to the small overlap between the exciton and the dopant in the case of inhomogeneous doping there is still competition between the radiative decay and the relaxation due to energy transfer to the dopant and both CdSe and Yb^{3+} emission are present.

This model makes sense with respect to the experimental methods used to incorporate the ytterbium. Using the growth doping method, ytterbium is introduced to the quantum dots after the nucleation and growth. Although it might be possible to have diffusion of the ytterbium towards the centre of the quantum dot, it is most likely that the majority of the dopant will be near the quantum dot surface.

The amount of CdSe emission is different for different values and for some lanthanide doped samples the CdSe emission is completely quenched (*e.g.* Figure 5.1). For the ytterbium case this was found for a sample for which the doping synthesis was performed at elevated temperatures. The increase in temperature might have increased the amount of ytterbium incorporated in the final quantum dots but it is likely that the amount of surface defects and other trap states have increased as well. Due to the extra non-radiative pathways the CdSe emission is completely quenched.

In the case of europium doped samples, no CdSe emission is observed. This might be explained in the same fashion as the ytterbium doped samples although the CdSe emission quenching in europium doped samples seems larger (no CdSe emission has been observed at all in pre-SILAR europium doped samples). This might be due to the lower oxidation potential for europium with respect to ytterbium (Eu(II) to Eu (III) = 0.35 eV and Yb(II) to Yb(III) = 1.05 eV in water). In the proposed model, the dopant ion gets reduced and subsequently oxidized. The oxidation potential is a measure for how effective the dopant ion can be oxidized and thus a measure of how effective the energy transfer can occur. In the case of europium, this potential is lower, leading to a more efficient energy transfer process and to the complete quenching of the CdSe quantum dot emission in europium doped samples.

In both the ytterbium and europium cases the CdSe emission is restored after the addition over several layers of CdSe using the SILAR method. This is most likely due to the reconstruction of the surface by adding new layers of CdSe to remove surface defects. With less surface states the CdSe has less non-radiative relaxation pathways and the emission spectra are recovered.

Chapter 8

Conclusions

In this work a novel method has been developed for the incorporation of trivalent lanthanide ions in CdSe nanocrystals. Successful incorporation of the trivalent lanthanides was confirmed using spectroscopy and EDX. Although the method was optimised for the ytterbium incorporation, first indications have shown that other lanthanides can be incorporated in the same fashion. The preparation of CdSe nanocrystals with lanthanide dopants incorporated was done using a separated CdSe synthesis and subsequent doping experiment. Several key aspects for the doping method have been optimised. The effect of using different dopant precursors and the ratio with respect to the QDs was investigated first. From these experiments it was determined that the optimal ratio of Yb^{3+}:CdSe QDs was 30:1 when the ytterbium oleate precursor is used and 175:1 for the ytterbium acetate precursor. It was shown that the absence of TOP during both the doping method and the subsequent SILAR experiments was crucial for the successful incorporation of the ytterbium ions in the CdSe. SILAR was used to add extra layers of CdSe after the incorporation of the lanthanide ions and the first few layers of CdSe had a large effect on the lifetime of the ytterbium emission although the effect reached a plateau after several layers of CdSe. The optimal lifetime was already reached after roughly 2 extra layers of CdSe via the SILAR method. Time-resolved analysis of the ytterbium emission, which had a FWHM of around 2 nm, showed that the whole ensemble of quantum dots is doped with ytterbium.

Although no successful incorporation of thulium or erbium has been detected EDX confirms the succesful incorporation of europium in the CdSe quantum dots. The absence of CdSe emission from the europium doped sample and the recovery after addition of extra CdSe layers suggests that the europium is present. However no europium emission has been observed.

Chapter 9

Outlook

The results shown in this work have been able to answer many scientific question, although a lot of follow-up experiments can still be performed. Several of these ideas will be discussed below.

9.1 Further investigation of the proposed model

The proposed model allows us to explain the fact that we still see both the quantum dot emission and the ytterbium emission. Due to the low exciton wavefunction intensity at the ytterbium locations, the relaxation pathway via the ytterbium dopant is competative with the radiative relaxation of the CdSe quantum dots. The result is that both ytterbium and CdSe quantum dot emission is observed.

An interesting follow-up experiment would be to investigate the ytterbium and CdSe emission with respect to the starting size of the CdSe quantum dot. Using smaller initial CdSe quantum dots it is expected to have higher exciton wavefunction intensities at the ytterbium locations. This would result in more efficient energy transfer, leading to the energy transfer as the dominant relaxation pathway. In this case, the CdSe quantum dot emission would be completely quenched and the ytterbium emission would be more intense compared to the work performed here. Using an integrating sphere to determine the quantum yield, more quantitative data can be obtained to further investigate the efficiency of the energy transfer.

9.2 Temperature dependence of the doping synthesis

In the Results section of this thesis some work has been performed on the temperature dependence of the incorporation. From the results it was seen that the quality of ytterbium emission was higher at higher doping temperatures. Not only was the ytterbium emission more intense, the quantum dot emission peak was completely quenched, indicating more quenching of the reaction by ytterbium, both by energy transfer and additional trap states caused by ytterbium related defects. At lower temperatures the ytterbium emission was poorer compared to the standard temperature used throughout this work.

Further investigation of this temperature dependence would be very interesting. Using EDX a quantitative study can be performed which correlates the amount of dopant to the doping temperature and the effect on the dopant emission. Using higher temperatures might even promote diffusion of the dopant towards the inside of the quantum dot.

9.3 Incorporation of different lanthanides in CdSe

Due to the chemical similarities between the different lanthanides, it is expected that the doping behaviour of the different lanthanides is comparable. Although this work has focussed mostly on ytterbium, some evidence has been found of the successful incorporation of europium as well. Although the erbium and thulium incorporation has been studied briefly without results, more extensive research on the different lanthanides might yield a successful general method of incorporating trivalent lanthanide ions in CdSe quantum dots.

9.4 Incorporation of Yb^{3+} in other II-IV semiconductors

In this work the successful incorporation of trivalent ytterbium in CdSe has been observed and optimized with respect to several key parameters. An interesting follow-up experiment would be to check the incorporation method for other II-VI materials with the same crystal lattice (*e.g.* CdS) and different crystal lattices (*e.g.* CdTe). In this fashion the dependancy of the doping method with respect to the crystal lattice parameters can be investigated.

9.5 Incorporation of Yb^{3+} in III-V semiconductors

Although we have seen the incorporation of ytterbium work for II-VI materials, the trivalent lanthanide is expected to be incorporated easier into a III-V quantum dot (*e.g.* InP or GaAs) due to the similar charges. In the case of III-V quantum dots, cation exchange might be a possible method of incorporation, which might yield homogeneously doped quantum dots instead of the quasi core/shell heteroparticles created with the growth doping method with subsequent overgrowth.

9.6 Lapis Philisophorum

Although the lapis philisophorum research in this thesis already show some super promising results, the investigation into this system is still very limited. A lot of follow-up experiments can be devised leading towards a better understanding of the system. The synthesis should be made reproducible and a quantitative chemical analysis can be performed to figure out the crucial components of the system and the structure (perhaps some gold can be made and sold to acquire € 60,000 for an ICP-MS).

Chapter 10

Acknowledgments

During my master I have not only been able to perform my master's thesis at Condensed Matter and Interfaces, but I have had the privilege to be part of the CMI group. I really felt at home because of the great work environment in which work and fun are blended into a productive, educational and wonderfull experience. Of course, a lot of people have contributed to this great ambiance and I want to thank all these people for their enthusiasm.

The first three people I would like to thank are Joren Eilers, Rosa Martín-Rodríguez and Andries Meijerink. There is a reason your names are on the front of this work, since it would not have been possible to perform my work without your guidance. So in no specific order:

Rosa, thank you for your knowledge and your trust. I think a physicist and a chemist are a great combination. You gave me enough space to let me do my own thing in the gloveboxes and the labrooms. On the other hand, I can't even count the times you've helped me with either the spectrometer or the data that came out of it. You are a very intelligent and enthusiastic woman and you inspired me to do my best. And last but not least, thank you for making the borrels extra 'gezellig', you and Francesca made me laugh a lot!

Joren, thank you for your interest in my work and willfully taking over the supervisor job after Rosa left. You were able to answer every question I could throw at you, ranging from chemistry related topics to the best way to tackle a cabinet with an axe. Furthermore, I really liked the low threshold on a social level, resulting in drinks, barbecues and fun outside the lab. And most of all, thank you for leaving me in the illusion that you are a Viking who sails from Norway towards Utrecht everyday on a longboat.

If there ever was a stereotype of a professor, it's Andries. Already during my first year as a chemistry student, Andries made an impression on me by drawing random spectra from memory on the blackboard. A very dedicated teacher and a very interested supervisor. He gets a lot of respect from me because he is always busy and still he finds the time to explain things or discuss results. The only thing I have not yet been able to do, is play a game of klaverjassen with him. However, I mostly blame the random generator of Freddy for this situation. Hopefully in the near future, we can 'kaartje leggen'.

During my time at CMI, software was installed, computers worked, labs were kept cleanish, gloveboxes worked on as many occasions as possible and chemicals and liquid nitrogen were available. This is all the work of Stephan, Hans and Relinde. Thank you for the hard work and the fun times at the TEM, preparing the TEM grids or just have a nice talk during lunch breaks.

Last but not least I would like to thank all the bachelor and master students and the PhD candidates for their unparalleled effort to make the ambiance great! Whether it was klaverjassen during lunch breaks, whining about klaverjassen during lunch breaks, klaverjassen during work time, whining about work times during work time and sometimes even discussing work related stuff. Especially Annelies, Quinten, Jasper, Stephan, Josine, Jantina, Peter, Jaco, Joca, Leon, Robin (lees; Robbin), Anne, Tim, Eline, Susan, Carlo, Elleke, Francesca, prof. Van der Stam, prof. Rabouw, prof. De Jong3 and everyone else I forgot to mention here.

Bibliography

[1] M. Faraday. On the color of colloidal gold. *Phil. Trans. R. Soc. London*, 147:145–181, 1857.

[2] Charles Kittel. *Introduction To Solid State Physics*. -, 8th edition, 2005.

[3] N. Bijbelgenootschap. *Geïllustreerde Gezinsbijbel Genesis 1.3*. Nederlands Bijbelgenootschap, 1951.

[4] T. H. Maiman. Stimulated Optical Radiation in Ruby. *Nature*, 187(4736):493–494, August 1960.

[5] S. Mackowski, T. Gurung, T. a. Nguyen, H. E. Jackson, L. M. Smith, G. Karczewski, and J. Kossut. Optically-induced magnetization of CdMnTe self-assembled quantum dots. *Applied Physics Letters*, 84(17):3337, 2004.

[6] C. Strümpel, M. McCann, G. Beaucarne, V. Arkhipov, A. Slaoui, V. Švrček, C. del Cañizo, and I. Tobias. Modifying the solar spectrum to enhance silicon solar cell efficiency: An overview of available materials. *Solar Energy Materials and Solar Cells*, 91(4):238–249, February 2007.

[7] J. M. Klostranec and W. C. W. Chan. Quantum Dots in Biological and Biomedical Research: Recent Progress and Present Challenges. *Advanced Materials*, 18(15):1953–1964, August 2006.

[8] M. Bruchez. Semiconductor Nanocrystals as Fluorescent Biological Labels. *Science*, 281(5385):2013–2016, September 1998.

[9] Cécile Bouet, Benoit Mahler, Brice Nadal, Benjamin Abecassis, Mickael D. Tessier, Sandrine Ithurria, Xiangzhen Xu, and Benoit Dubertret. Two-Dimensional Growth of CdSe Nanocrystals, from Nanoplatelets to Nanosheets. *Chemistry of Materials*, 25(4):639–645, February 2013.

[10] Liberato Manna, Erik C Scher, A Paul Alivisatos, and Recei V August. Synthesis of Soluble and Processable Rod- , Arrow- , Teardrop- , and Tetrapod-Shaped CdSe Nanocrystals. *Journal of the American Chemical Society*, 122(27):12700–12706, 2000.

[11] X Peng, L Manna, W Yang, J Wickham, E Scher, A Kadavanich, and Ap Alivisatos. Shape control of CdSe nanocrystals. *Nature*, 404(6773):59–61, March 2000.

[12] Louis E Brus. On the development of bulk optical properties in small semiconductor crystallites. *Journal of Luminescence*, 31-32:381–384, December 1984.

[13] Louis E Brus. Electron-electron and electron-hole interactions in small semiconductor crystallites The size dependence of the lowest excited electronic state. *The Journal of Chemical Physics*, 80(9):4403, 1984.

[14] Celso de Mello Donegá. Synthesis and properties of colloidal heteronanocrystals. *Chemical Society reviews*, 40(3):1512–46, March 2011.

[15] Emil Roduner. Size matters: why nanomaterials are different. *Chemical Society reviews*, 35(7):583–92, July 2006.

[16] W William Yu, Lianhua Qu, Wenzhuo Guo, and Xiaogang Peng. Experimental Determination of the Extinction Coefficient of CdTe, CdSe, and CdS Nanocrystals. *Chemistry of Materials*, 15(14):2854–2860, July 2003.

[17] Lianhua Qu and Xiaogang Peng. Control of photoluminescence properties of CdSe nanocrystals in growth. *Journal of the American Chemical Society*, 124(9):2049–55, March 2002.

[18] Yongan Andrew Yang, Huimeng Wu, Kathryn R. Williams, and Y. Charles Cao. Synthesis of CdSe and CdTe Nanocrystals without Precursor Injection. *Angewandte Chemie*, 117(41):6870–6873, October 2005.

[19] Y.W. Heo, D.P. Norton, L.C. Tien, Y. Kwon, B.S. Kang, F. Ren, S.J. Pearton, and J.R. LaRoche. ZnO nanowire growth and devices. *Materials Science and Engineering: R: Reports*, 47(1-2):1–47, December 2004.

[20] Dmitri V Talapin, James H Nelson, Elena V Shevchenko, Shaul Aloni, Bryce Sadtler, and a Paul Alivisatos. Seeded growth of highly luminescent CdSe/CdS nanoheterostructures with rod and tetrapod morphologies. *Nano letters*, 7(10):2951–9, October 2007.

[21] Jonathan E Halpert, Venda J Porter, John P Zimmer, and Moungi G Bawendi. Synthesis of CdSe/CdTe nanobarbells. *Journal of the American Chemical Society*, 128(39):12590–1, October 2006.

[22] Michelle D Regulacio and Ming-Yong Han. Composition-tunable alloyed semiconductor nanocrystals. *Accounts of chemical research*, 43(5):621–30, May 2010.

[23] Luigi Carbone, Concetta Nobile, Milena De Giorgi, Fabio Della Sala, Giovanni Morello, Pierpaolo Pompa, Martin Hytch, Etienne Snoeck, Angela Fiore, Isabella R Franchini, Monica Nadasan, Albert F Silvestre, Letizia Chiodo, Stefan Kudera, Roberto Cingolani, Roman Krahne, and Liberato Manna. Synthesis and micrometer-scale assembly of colloidal CdSe/CdS nanorods prepared by a seeded growth approach. *Nano letters*, 7(10):2942–50, October 2007.

[24] Bob C Fitzmorris, Ying-Chih Pu, Jason K Cooper, Yi-Fang Lin, Yung-Jung Hsu, Yat Li, and Jin Z Zhang. Optical properties and exciton dynamics of alloyed core/shell/shell Cd(1-x)Zn(x)Se/ZnSe/ZnS quantum dots. *ACS applied materials & interfaces*, 5(8):2893–900, April 2013.

[25] William A. Johnson and Robert F. Mehl. Reaction kinetics in processes of nucleation and growth. *Trans. Aime*, 135(8):396–415, 1939.

[26] Craig R. Bullen and Paul Mulvaney. Nucleation and Growth Kinetics of CdSe Nanocrystals in Octadecene. *Nano Letters*, 4(12):2303–2307, December 2004.

[27] Yongan Yang, Ou Chen, Alexander Angerhofer, and Y Charles Cao. On doping CdS/ZnS core/shell nanocrystals with Mn. *Journal of the American Chemical Society*, 130(46):15649–61, November 2008.

[28] Khalid M Hanif, Robert W Meulenberg, and Geoffrey F Strouse. Magnetic ordering in doped Cd(1-x)Co(x)Se diluted magnetic quantum dots. *Journal of the American Chemical Society*, 124(38):11495–502, September 2002.

[29] Santanu Roy, Christopher Tuinenga, Fadzai Fungura, Pinar Dagtepe, Viktor Chikan, and Jacek Jasinski. Progress toward Producing n-Type CdSe Quantum Dots: Tin and Indium Doped CdSe Quantum Dots. *The Journal of Physical Chemistry C*, 113(30):13008–13015, July 2009.

[30] Demetra a Chengelis, Adrienne M Yingling, Paul D Badger, Chad M Shade, and Stéphane Petoud. Incorporating lanthanide cations with cadmium selenide nanocrystals: a strategy to sensitize and protect Tb(III). *Journal of the American Chemical Society*, 127(48):16752–3, December 2005.

[31] Ung Thi Dieu Thuy, Axel Maurice, Nguyen Quang Liem, and Peter Reiss. Europium doped In(Zn)P/ZnS colloidal quantum dots. *Dalton transactions*, April 2013.

[32] Prasun Mukherjee, Robin F Sloan, Chad M Shade, David H Waldeck, and Ste Petoud. A Postsynthetic Modification of II-VI Semiconductor Nanoparticles to Create Tb 3+ and Eu 3+ Luminophores. *The Journal of Physical Chemistry C*, 2013.

[33] Brandon J. Beberwyck, Yogesh Surendranath, and a. Paul Alivisatos. Cation Exchange: A Versatile Tool for Nanomaterials Synthesis. *The Journal of Physical Chemistry C*, 117(39):19759–19770, October 2013.

[34] Daniel Bryan, Dana Schwartz, and Daniel Gamelin. The Influence of Dopants on the Nucleation of Semiconductor Nanocrystals from Homogeneous Solution. *Journal of Nanoscience and Nanotechnology*, 5(9):1472–1479, 2005.

[35] Jian Feng, Hui Zhu, and Xiurong Yang. A controllable growth-doping approach to synthesize bright white-light-emitting Cd:In2S3 nanocrystals. *Nanoscale*, 5(14):6318–6322, 2013.

[36] Nathan Grumbach, Anna Rubin-brusilovski, Georgy I Maikov, Evgeny Tilchin, and Efrat Lifshitz. Manipulation of Carrier âˆ’ Mn 2 + Exchange Interaction in CdTe / CdSe Colloidal Quantum Dots by Controlled Positioning of Mn 2 + Impurities. *J. Phys. Chem. C.*, 117(40):21021–21027, 2013.

[37] Nick S Norberg, Kevin R Kittilstved, James E Amonette, Ravi K Kukkadapu, Dana a Schwartz, and Daniel R Gamelin. Synthesis of colloidal Mn2+:ZnO quantum dots and high-TC ferromagnetic nanocrystalline thin films. *Journal of the American Chemical Society*, 126(30):9387–98, August 2004.

[38] Rosa Martín-Rodríguez, Robin Geitenbeek, and Andries Meijerink. Incorporation and Luminescence of Yb(3+) in CdSe Nanocrystals. *Journal of the American Chemical Society*, 135(37):13668–71, September 2013.

[39] Renguo Xie, Ute Kolb, Jixue Li, Thomas Basché, and Alf Mews. Synthesis and characterization of highly luminescent CdSe-core CdS/Zn0.5Cd0.5S/ZnS multishell nanocrystals. *Journal of the American Chemical Society*, 127(20):7480–8, May 2005.

[40] David W Piston and Gert-Jan Kremers. Fluorescent protein FRET: the good, the bad and the ugly. *Trends in biochemical sciences*, 32(9):407–14, September 2007.

[41] R. Martin-Rodriguez, R. Valiente, S. Polizzi, M. Bettinelli, A. Speghini, and F. Piccinelli. Upconversion Luminescence in Nanocrystals of Gd 3 Ga 5 O 12 and Y 3 Al 5 O 12 Doped with Tb 3+ -Yb 3+ and Eu 3+ -Yb 3+. *The Journal of Physical Chemistry C*, 113(28):12195–12200, July 2009.

[42] François Auzel. Upconversion and anti-Stokes processes with f and d ions in solids. *Chemical reviews*, 104(1):139–73, January 2004.

[43] Celso de Mello Donegá, Stephen G. Hickey, Sander F. Wuister, Daniël Vanmaekelbergh, and Andries Meijerink. Single-Step Synthesis to Control the Photoluminescence Quantum Yield and Size Dispersion of CdSe Nanocrystals. *The Journal of Physical Chemistry B*, 107(2):489–496, January 2003.

[44] Urte Hotje, Christoph Rose, and Michael Binnewies. Lattice constants and molar volume in the system ZnS, ZnSe, CdS, CdSe. *Solid State Sciences*, 5(9):1259–1262, September 2003.

[45] Sandip Das and Krishna C. Mandal. Optical downconversion in rare earth (Tb3+ and Yb3+) doped CdS nanocrystals. *Materials Letters*, 66(1):46–49, January 2012.

[46] Orlando E. Raola and Geoffrey F. Strouse. Synthesis and Characterization of Eu-Doped Cadmium Selenide Nanocrystals. *Nano Letters*, 2(12):1443–1447, December 2002.

[47] R. H. Fewster and F. J. Bryant. The parameters of ytterbium implantation in CdS, ZnS and ZnSe. *Philosophical Magazine*, 28(6):1225–1239, December 1973.

[48] F. J. Bryant. Ion implanation in group II-VI compounds. *Progress in Crystal Growth and Characterization*, 6(2):191–263, January 1983.

[49] Jun Dong, Michael Bass, Yanli Mao, Peizhen Deng, and Fuxi Gan. Dependence of the Yb3+ emission cross section and lifetime on temperature and concentration in yttrium aluminum garnet. *Journal of the Optical Society of America B*, 20(9):1975, 2003.

[50] By Gerald A Hebbink, Jan W Stouwdam, David N Reinhoudt, and Frank C J M Van Veggel. Lanthanide(III)-doped nanoparticles that emit in the near-infrared. *Advanced Materials*, 14(16):1147–1150, 2002.

[51] Song Dang, Jiang-Bo Yu, Xiao-Fei Wang, Zhi-Yong Guo, Li-Ning Sun, Rui-Ping Deng, Jing Feng, Wei-Qiang Fan, and Hong-Jie Zhang. A study on the NIR-luminescence emitted from ternary lanthanide [Er(III), Nd(III) and Yb(III)] complexes containing fluorinated-ligand and 4,5-diazafluoren-9-one. *Journal of Photochemistry and Photobiology A: Chemistry*, 214(2-3):152–160, August 2010.

[52] Yanjun Hou, Jing Shi, Wenyi Chu, and Zhizhong Sun. Synthesis, Crystal Structure, and Near-IR Luminescent Properties of Lanthanide Bis(β-diketonate) Complexes. *European Journal of Inorganic Chemistry*, 2013(17):3063–3069, June 2013.

[53] Raphael Patai. *The Jewish Alchemists: A History and Source Book*. Princeton University Press, 1994.

[54] Stanton J. Linden. *The alchemy reader: from Hermes Trismegistus to Isaac Newton*. Cambridge University Press, 2003.

Appendices

Appendix A

Summary samples of doping method

A.0.1 Ytterbium

Sample	QDs (nmol)	$Yb(Ac)_3{}^a$ (mmol)	$Yb(Oa)_3{}^b$ (mmol)	Se (mmol)	Ratio Yb^{3+}:QDs
A1	140	0,26	-	0,25	1875
B1	140	0,26	-	0,25	1875
C1	140	0,26	-	0,25	1875
D1	140	0,26	-	0,25	1875
DOP1	140	0,26	-	0,25	1875
DOP2	140	0,18	-	0,18	1313
DOP3	140	0,11	-	0,1	750
DOP4	140	0,026	-	0,025	188
DOP5	140	0,026	-	0,025	188
DOP6	140	0,053	-	0,05	375
DOP7	140	0,026	-	0,025	188
DOP8	140	0,053	-	0,05	375
DOP9	140	0,013	-	0,025	94
DOP10	140	0,0053	-	0,005	38
DOP11	140	-	0,019	0,025	136
DOP12	140	0,026	-	-	188
RG1-12	140	-	0,0027	0.025 (TOPSe)	19
RG13	100	-	0,0027	0,025	27
RG14	100	-	0,0027	0,025	27
D Yb1	100	-	0,0031	0,031	31
D Yb2	100	-	0,0031	0,031	31

Table A.1: A summary of all the samples created with the dopant method for ytterbium doped quantum dots (QDs), including the amount of quantum dots, ytterbium acetate[a], ytterbium oleate[b] and selenium added and the ratio between the quantum dots and the dopant.

A.0.2 Other lanthanides

Sample	QDs (nmol)	$Ln(OA)_3$ (mmol)	Se (mmol)	Ratio Ln^{3+}:QDs
Er D1	140	3,8	3,8	38
Er D2	140	3,8	3,8	38
Er D3	100	4	4	40
Eu D1	140	4	4	30
Tm D1	140	4	4	30
Tm D2	100	4,5	4,5	45
Tm D3	100	4,5	4,5	45

Table A.2: A summary of all the samples created with the dopant method for europium, erbium and thulium doped quantum dots (QDs), including the amount of quantum dots, lanthanide oleate, selenium added and the ratio between the quantum dots and the dopant.

Appendix B

Summary samples SILAR method

B.0.3 Ytterbium

Sample	Se added after doping?	# Cd additions	# Se additions	Starting Ion	Se or TOPSe
DS1	No	3	3	Cd	Se
DS2	No	3	3	Cd	Se
DS3	No	3	3	Cd	Se
DS4	No	3	3	Cd	Se
DS5	No	2	2	Cd	TOPSe
DS6	No	2	2	Cd	TOPSe
DS7	No	2	2	Cd	TOPSe
DS8	No	2	2	Cd	TOPSe
DS9	No	4	3	Cd	TOPSe
DS10	No	4	3	Se (excess)	TOPSe
DS11	No	4	3	Se	TOPSe
DS12	No	4	3	Se (excess)	TOPSe
DS13	Yes	4	4	Cd	TOPSe
DS14	Yes	4	4	Cd	TOPSe
RS1	Yes	1	1	Cd	Se
RS2	Yes	2	2	Cd	Se
RS3	Yes	3	3	Cd	Se
RS4	Yes	5	5	Cd	Se

Table B.1: A summary of the samples created using the SILAR technique after the doping of the samples with ytterbium, including the amount of precursor additions, starting ion and presence of TOP.

B.0.4 Other lanthanides

Sample	Se added after doping?	# Cd additions	# Se additions	Starting ion	Se or TopSe
DS Er1	Yes	3	3	Cd	Se
DS Er2	Yes	3	3	Cd	Se
DS Er3	Yes	3	3	Cd	Se
DS Eu1	Yes	3	3	Cd	Se
DS Tm1	Yes	3	3	Cd	Se

Table B.2: A summary of the samples created using the SILAR technique after the doping of the samples with europium, erbium and thulium, including the amount of precursor additions, starting ion and presence of TOP.